Surface Enhanced Raman Spectroscopy for Medical Diagnostics

1

Izabella J. Jahn, Andreea I. Radu, Karina Weber, Dana Cialla-May, and Juergen Popp

Contents

List of Abbreviations

1-DT	1-Decanethiol
4-MBA	4-Mercaptobenzoic acid
AA	Ascorbic acid
AD	Alzheimer's disease
AFM	Atomic force microscopy
AFP	Alpha-fetoprotein

I. J. Jahn · A. I. Radu
Leibniz Institute of Photonic Technology Jena, Jena, Germany

K. Weber · D. Cialla-May
Friedrich Schiller University Jena, Institute of Physical Chemistry and Abbe Center of Photonics, Jena, Germany

J. Popp (✉)
Institute of Photonic Technology, Jena, Germany

Institute of Physical Chemistry and Abbe Center of Photonics, Jena, Germany
e-mail: juergen.popp@ipht-jena.de

C. S. S. R. Kumar (ed.), *Nanotechnology Characterization Tools for Biosensing and Medical Diagnosis*, https://doi.org/10.1007/978-3-662-56333-5_1

AGC	Advanced gastric cancer
AIBN	Azobis(isobutyronitrile)
ATE	Telomeric repeat complementary oligonucleotide
AuFON	Gold film-over-nanospheres
Aβ	Amyloid β
BSA	Bovine serum albumin
Ce6	Chlorin e6
CEA	Carcinoembryonic antigen
CGM	Continuous glucose monitoring
CK-MB	Creatine kinase MB
CPBT	2-Cyano-2-propyl benzodithioate
CSF	Cerebrospinal fluid
cTnI	Troponin I
cTnT	Troponin T
CVD	Cardiovascular diseases
Cy5	Cyanine 5
DNA	Deoxyribonucleic acid
DT	Decanethiol
DTNB	5,5-Dithiobis(2-dinitrobenzoic acid)
DTTC	Diethylthiatricarbocyanine iodide
EBL	Electron beam lithography
ECG	Electrocardiogram
EDC	1-Ethyl-3-(3-dimethyl-aminopropyl)carbodiimide
EGA	Clarke error grid analysis
EGC	Early gastric cancer
EGFR	Epidermal growth factor receptor
ELISA	Enzyme-linked immunosorbent assay
G−	Gram negative
G+	Gram positive
GOx	Glucose oxidase
HBsAg	Hepatitis B virus antigen
HCPCF	Hollow core photonic crystal fiber
HeLa	Human cervical cells
HEMA	2-Hydroxyethyl methacrylate
HER2	Human epidermal growth factor receptor 2
HIV-1	Human immunodeficiency virus
HPLC	High-performance liquid chromatography
HPV	Human papillomavirus
IgG	Immunoglobulin G
iMS	Inverse molecular sentinel
ISO	International Organization Standard
ITO	Indium tin oxide
LA	Lipoic acid
LoC-SERS	Lab-on-a-chip SERS
LOD	Limit of detection

MBs	Magnetic nanobeads
MGITC	Malachite green isothiocyanate
MH	6-Mercapto-1-hexanol
MI	Myocardial infarction
miR21	Micro ribonucleic acid 21
miRNA	Micro ribonucleic acid
MNP	Magnetic nanoparticle
MPBA	Mercaptophenylboronic acid
mPEG-SH	*O*-[2-(3-Mercaptopropionylamino)ethyl]-*O′*-methylpolyethylene glycol
MPS	3-Methacryloxypropyltrimethoxysilane
MRI	Magnetic resonance imaging
mRNA	Messenger ribonucleic acid
MTC	Mycobacterium tuberculosis complex
MU	11-Mercapto-1-undecanol
MUA	11-Mercaptoundecanoic acid
NHS	N-Hydroxysuccinimide
NP	Nanoparticle
NPs	Nanoparticles
NT	Naphthalenethiol
OAD	Oblique angle deposition
OSCC	Oral squamous carcinoma
PBS	Phosphate-buffered saline
PBST	Phosphate-buffered saline tween-20
PCA	Principal component analysis
pCBAA	Zwitterionic poly(carboxybetaine acrylamide)
PCN	Pyocyanin
PCR	Polymerase chain reaction
PEG	Polyethylene glycol
PEG-SH	Thiolated PEG
PET	Positron emission tomography
PLS-DA	Partial least squares discriminant analysis
RBCs	Red blood cells
Rh6G	Rhodamine 6 G
SAM	Standard addition method
SERRS	Surface-enhanced resonance Raman spectroscopy
SERS	Surface-enhanced Raman spectroscopy
SESORS	Surface-enhanced spatially offset Raman spectroscopy
TAT	Turnaround time
TGFbRII	Transforming growth factor beta receptor II
TMB	3,3′,5, 5′-Tetramethylbenzidine
TPMT	Thiopurine s-methyltransferase
TS	Telomeres substrate
VAN	Vancomycin
VEGF	Vascular endothelial growth factor

1 Definition of the Topic

Medical diagnosis requires reliable identification of very low concentration of different biomarkers specific for medical conditions in a time-effective manner. In this chapter, we summarize the work reported on the application of surface-enhanced Raman spectroscopy for the detection and the identification of different biomarkers in body fluids, tissues, or in vivo.

2 Overview

Early disease diagnosis allows for better treatment options and leads to improved patient outcomes. This is because by delaying treatment the disease can also spread to otherwise healthy organs. The consequences of this can vary, depending on the specific medical condition (i.e., Alzheimer's disease, diabetes, cancer, etc.) and on the exact time of diagnosis.

One highly promising method for fast and reliable biomarker identification is surface-enhanced Raman spectroscopy (SERS). Depending on the particular medical diagnosis requirements, different SERS approaches can be considered. That is because, as it will be discussed in this chapter, many different SERS-active substrates are available, and they can be applied within different schemes. Specifically, functionalized SERS nanoparticles can have a high biocompatibility for in vivo measurements, while different microfluidic approaches can be considered for the analysis of body fluids.

The scientific interest for assessing the potential of SERS for medical analysis and diagnosis increased during recent years. This is also demonstrated by the multiple literature reports (scientific papers, communications, reviews, and book chapters) that test and push the limits of using SERS in medicine or report on new SERS-active substrates and platforms that are continuously developed for analyzing trace amount of analytes in body fluids and tissue [1–5]. However, SERS has not yet been established as a routine analytical tool for medical diagnosis. Moreover, clinical trials and development of analytical procedures are still required. The high potential and interest for development in this direction explains the high number of publications still being reported. The current chapter summarizes some of the most promising approaches introduced during the last 5 years. A wide panel of diseases is addressed, and the best-suited SERS-based approaches are discussed for each of the topics introduced.

3 Introduction

The latest developments in the health-care field have two directions: detection and diagnosis of disease and its treatment. They are of comparable importance when it comes to achieving positive patient outcomes. In particular, the fast and correct diagnosis of a medical condition leads to more appropriate treatment decisions and

to the establishment of a care plan at an early stage of the disease, increasing the chances of successfully fighting the disease [6]. Nevertheless, for example, the direct identification of viruses and bacteria can be challenging at times. In such situations disease-specific biomarkers are targeted instead. Biomarkers, or biological markers, have been defined several times in the literature, and they are mainly described as substances, structures, or processes that can be objectively measured in the body and can be used as indicators for normal biological processes, pathogenic processes, or pharmacological responses to a therapeutic intervention (i.e., deoxyribonucleic acid (DNA), messenger ribonucleic acid (mRNA), enzymes, metabolites, transcription factors, and cell surface receptors) [7]. Frequently, during the early stages of disease, biomarkers are present in low amounts, and their reliable detection is challenging. In clinical chemistry, the specific and sensitive detection of disease biomarkers, of drug levels in biological fluids, or the assessment of enzyme activities is carried out by a multitude of analytical methods, such as high-performance liquid chromatography [8–13], mass spectrometry [11, 14, 15], or immunoassays [16–21]. Since each method has its advantages and shortcomings, the scientific community is continuously searching for new, faster, and affordable tools.

Vibrational spectroscopy, particularly Raman spectroscopy, can provide molecular fingerprint information [22–24] and is suitable for investigating biological samples because of the low scattering cross section of water molecules. Consequently, no or little sample pre-processing steps are required prior to the analysis. However, owing to the inherently weak Raman effect, the identification of target molecules present at very low concentrations is challenging. This is especially important for the early diagnosis of medical conditions. Nevertheless, the sensitivity of Raman spectroscopy can be easily enhanced by several orders of magnitude by taking advantage of the plasmonic properties of nanostructured metallic particles and performing surface-enhanced Raman spectroscopy (SERS) measurements. The two underlying mechanisms of SERS, extensively described in the literature [25–29], are the electromagnetic and the chemical enhancement mechanisms. The first mechanism explains how the molecules situated in the proximity of metallic nanoparticles (NPs) experience a strong local electromagnetic field, referred to as localized plasmon polaritons. This is caused by the resonant interaction between an incident electromagnetic wave and the oscillating charge density of the NPs. As a consequence, both the electromagnetic radiation of the laser source incident on the molecules and the intensity of the Raman-scattered photons will be enhanced. As the plasmon resonance condition for a spherical NP, $\epsilon(\lambda) = -2\epsilon_m$,[1] can be fulfilled only for materials with $\mathrm{Re}(\epsilon(\lambda)) < 0$ and $\mathrm{Im}(\epsilon(\lambda)) \approx 0$,[2] gold and silver are the most preferred metals for plasmonic nanostructure fabrication.

[1] $\epsilon(\lambda)$ is the wavelength-dependent dielectric function of the NP's material, and ϵ_m is the dielectric function of the surrounding medium.

[2] The dielectric function is a complex function with $\epsilon(\lambda) = \mathrm{Re}(\epsilon(\lambda)) + i \cdot \mathrm{Im}(\epsilon(\lambda))$, where $\mathrm{Re}(\epsilon(\lambda))$ is the real part and $\mathrm{Im}(\epsilon(\lambda))$ is the imaginary part.

The electromagnetic mechanism accounts for enhancement magnitudes up to 10^{11} [30]. However, enhancement factors of 10^{14}–10^{15} [31, 32] have been often reported in literature. This is due to the chemical enhancement mechanism to which three different processes have been suggested to contribute: (1) chemical interactions between the NP and the target molecule in the electronic ground state, (2) resonant excitation of the charge-transfer process between the target molecule and the NP, and (3) the resonance Raman enhancement. As the aim of this book chapter is to give a comprehensive overview of the SERS advancements in the field of medical diagnosis, a detailed description of the fundamental principles of the technique is beyond the purpose, and the reader is directed to the multiple extensive reviews and book chapters reported in the literature [25–29, 33, 34].

An important factor when performing SERS measurements is the choice of the SERS-active substrates to be used: planar substrates, NP suspension, core-shell structures, functionalized NPs, etc. Depending on the exact application, specific structures will be preferred. Moreover, the development of NPs that show a high biocompatibility while still maintaining their physical properties is often desirable in medical applications [35–37]. To this end, different functional layers are added to the NP to facilitate their delivery to a specific affected organ. Upon this, the destruction of the NP's core-shell structure can lead to the release of different filling materials [35], to a faster clearance of the NPs from the body, or to the induction of a highly localized electrical field in the close vicinity of the NP that increases the efficiency of in vivo biomarker detection.

In the following section, we will address some of the most relevant experimental details having a considerable impact on the outcome of the SERS measurement. Namely, details regarding Raman systems used for SERS measurements will be introduced; the commonly used SERS-active substrates and the different approaches used for SERS measurements will be summarized; the choice regarding the best-suited laser wavelength for the investigation of biological samples will be discussed; the synergy between SERS, immunoassays, and microfluidics will be presented; and finally some details regarding quantitative SERS measurements will be addressed.

4 Experimental and Instrumental Methodology

When performing SERS measurements, the experimenter is confronted with a series of measurement parameters to be considered and decided for. For example, reliable SERS results can be achieved only when the parameters of the Raman setup, the physicochemical properties of the targeted samples, the properties of SERS-active substrate, and the measurement design are all carefully considered and optimized. SERS spectra can be acquired with a large variety of commercial or in-house build Raman setups. Detectors and instrumentation in this field are in continuous development, and therefore, in the following, we will provide just a generalized view on Raman (micro)spectroscopy, highlighting some of the major factors relevant for SERS measurements. For a more detailed overview, the reader is directed to the multiple book chapters reported in the literature [38–40].

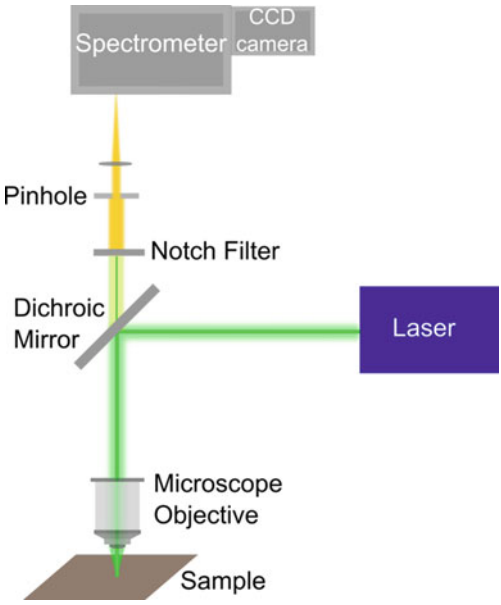

Fig. 1.1 Scheme of a confocal Raman microscope

Although the Raman effect was discovered by C. V. Raman already in 1928, only 30 years later, with the development of lasers, Raman experiments gained popularity. The introduction of charge-coupled devices (CCD) with high quantum efficiency and the establishment of confocal micro-Raman spectroscopy have further sparked the interest of scientists for this technique. For example, in Fig. 1.1 one of the many existing Raman setups is depicted. Here, a laser source provides the monochromatic light required to induce the inelastic light scattering events yielding a Raman spectrum. The excitation laser is coupled into the Raman microscope via a dichroic mirror. This element acts as a long pass filter, and it reflects with high efficiency the laser excitation light, whereas the backscattered Stokes-shifted Raman photons will be transmitted. If, however, the detection of the anti-Stokes Raman photons is desired, the setup must be equipped with a holographic beam splitter that will act as a notch filter. Further on, after the monochromatic light is reflected by the dichroic mirror, it is focused on the surface of the sample via a microscope objective. Here, the backscattered light is collected via the same objective, and it is transmitted via the dichroic mirror. The currently available coating technologies applied on dichroic mirrors reach a reflection of the elastically scattered photons of up to 95%, and thus, for a more efficient suppression of the Rayleigh line, an additional edge/notch filter is also implemented. This reduces the laser light intensity by around six orders of magnitude. The resulting filtered light crosses through a pinhole, which, if present, yields a confocal collection and reduces the background signal of the sample. Finally, the light is coupled into a spectrometer, where by the aid of gratings the beam is dispersed onto the CCD detector by deflecting each wavelength at a slightly different angle.

When deciding on the particularities of the experiment, the user can freely opt for a number of the above-enumerated components such as the excitation source to which the researcher should match the dichroic mirror and notch filter, the used microscope objective, as well as the size of the pinhole and the type of grating. Below, we will address the particularities of each of these parameters.

Generally, in order to obtain intense Raman spectra, lasers with short emission wavelengths (UV, blue, or green) are preferred as the Raman-scattering intensity is proportional to the fourth power of the frequency of the exciting laser radiation. Nonetheless, many samples show strong fluorescence when excited with these lasers and the detection of the Raman-scattered photons is inhibited. This is especially valid for biological samples, as it will be discussed in the following sections, and thus, often a red or near-infrared laser (emission above 600 nm) is preferred. Furthermore, for SERS spectroscopy, one has also to consider the localized plasmon polariton resonances of the employed SERS-active substrates in order to make use of the electromagnetic enhancement mechanism. Generally, for silver spheres blue/green laser lines are chosen, whereas for gold, wavelengths above 600 nm are applied. This can be explained by considering the dielectric function of the two metals, and it was described, among others, by, i.e., Le Ru et al. [33].

Besides carefully choosing the excitation wavelength, one has to pay attention also to the excitation power. Although the Raman intensity is proportional to the power of the used laser, limitations brought by the thermal damage of the sample have to be considered. In Raman experiments, the excitation power can vary from microwatts to several hundreds of milliwatts depending on the thermal conductivity and absorption of the sample and the measurement conditions (point scan, line scan, light sheet illumination, etc.). For SERS measurements, the applied laser power will vary also based on the employed SERS-active substrate. When measurements are performed on planar plasmonic substrates under dry conditions, laser powers in the ~20–500 microwatt range are used in order to avoid the local heating and damage of both the nanostructure and molecule. If these substrates are measured while they are incubated in the sample solution, the laser power can be increased up to 5–10 mW due to the increased heat dissipation in the presence of a liquid. For measurements carried out with microfluidic platforms, thanks to the dynamic flow, the laser intensity can be increased considerably as no sample degradation is expected.

Microscope objectives play also a key role in maximizing collection efficiency and spatial resolution. For applications where both parameters are crucial for optimal results, objectives with a high numerical aperture (above 0.8) have to be selected. Nevertheless, these objectives have generally a low working distance (at most 2–3 mm) and a reduced collection depth. Therefore, if the surface of the sample to be measured presents high roughness, information might be lost during measurements due to getting out of focus or the objective might be irreversibly contaminated due to touching the sample surface. Furthermore, one must also pay attention to the choice of the right objective for the intended excitation laser as the antireflection coatings can present different transmission characteristics for different frequencies.

Lastly, a grating with a higher number of grooves per mm (e.g., 1800 l/mm) will yield a spectrum with a high resolution (~2 cm^{-1}) but with a lower spectral range,

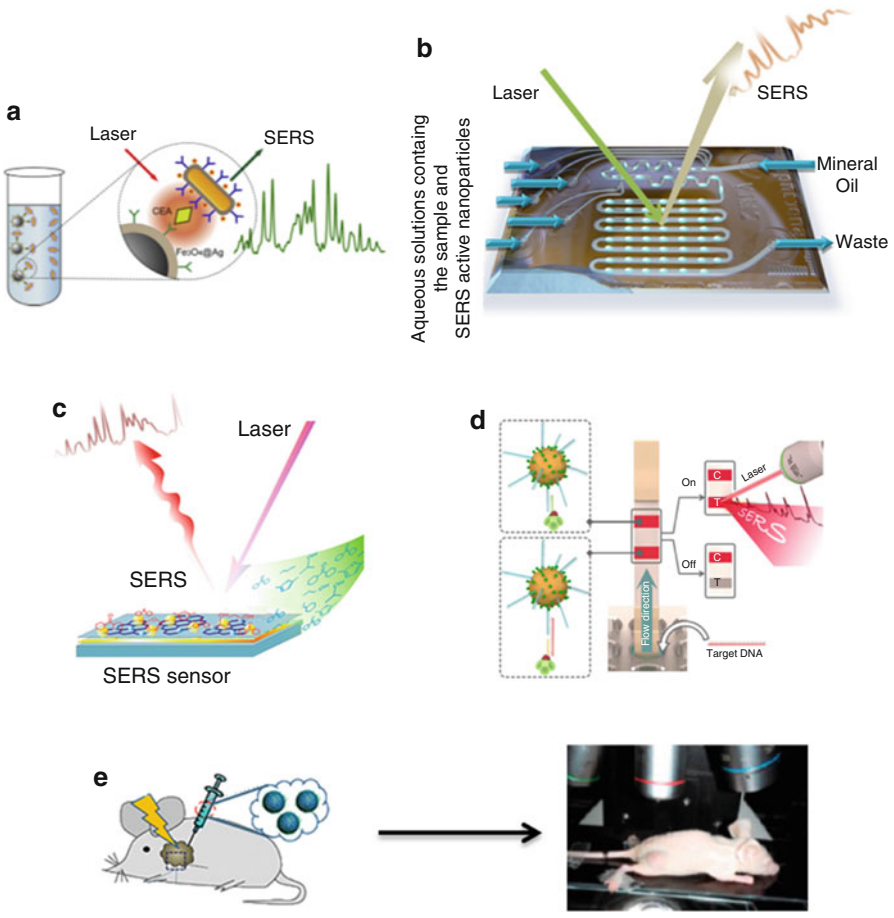

Fig. 1.2 Selected representations of the different encountered SERS measurement configurations: cuvette measurement (**a** – adapted from Rong et al. [41] with permission from Elsevier. Copyright © 2016 Elsevier); microfluidic platform measurement (**b** – adapted with permission from Hidi et al. [42]. Copyright © 2016, American Chemical Society); flat substrate-based SERS measurement (**c** – adapted with permission from Chen et al. [43]. Copyright © 2016, American Chemical Society); immunoassay-based SERS measurement (**d** – adapted from Fu et al. [44]. Copyright © 2015 Elsevier B.V., with permission from Elsevier); SERS measurement performed through the skin upon injection of the nanoparticles in laboratory mice (**e** – left image adapted with permission from Lin et al. [35]. Copyright © 2013, American Chemical Society; right image adapted with permission from Zeng et al. [37]. Copyright © 2015, American Chemical Society)

whereas a grating with, e.g., 600 l/mm will yield a lower resolution (~6–10 cm^{-1}), but it covers the whole Stokes Raman spectral range.

Overall, the excitation wavelength and power, the microscope objective, and the grating will strongly influence the outcome of the SERS measurements. Nevertheless, the choice of the SERS-active substrates and the measurement approach (see Fig. 1.2) will have also a key role. As summarized in several reviews [45–47], a large

variety of SERS-active substrates are available. As already mentioned in the previous section, the coinage metals, such as silver and gold, are the most often encountered materials for plasmonic structure fabrication. Depending on the preparation procedure, the SERS-active substrates can be classified into bottom-up, self-organizing, and top-down substrates [45–48]. Among the metal nanostructures fabricated by bottom-up procedures, there are metal colloids [49, 50], core-shell nanoparticles and structures, [35] seed-mediated growth structures [51, 52], and others. A large variety of such substrates have been fabricated owing to the relatively easy preparation protocols, the high diversity of sizes and geometries that can be developed, and the ease of use while performing the measurements. However, most of these NPs are suspended in an aqueous solution, restricting their application for fat soluble analytes. For such analytes, additional preparation steps can follow, resulting in the attachment of functional groups on the surface of the NPs, the formation of core-shell structures, or the addition of protective layers on the surface of the NPs. Still, this further increases the complexity of the preparation protocol and the time and the costs of the substrate preparation. The second category of SERS-active substrates mentioned are self-organizing substrates, which include self-assembled colloidal nanoparticle [53] clusters and arrays as well as template-based self-assembled planar nanostructures [52, 54, 55]. Finally, the top-down substrates are prepared by using a template produced by electron beam lithography (EBL) [56, 57], lift-off processes [58], and ion beam etching processes as part of lithographic methods [59]. Compared with the bottom-up procedures, the top-down substrates are less cost-effective, and the preparation protocol is more complex, but the resulting substrates have a more homogeneous size distribution and are highly reproducible and structured. Additionally, the substrates' templates can often be prepared in advance, and the final layer of the coinage metal (i.e., Ag, Au, Cu, or Pt) can be deposited on the substrate short before the actual SERS measurement is performed.

Among the measurement approaches, cuvette-based SERS measurements are the most widely spread ones. Here, the colloidal nanoparticles in aqueous suspension are mixed with the targeted analyte solved also in an aqueous solvent. Commonly, in order to efficiently enhance the Raman signal, an electrolyte is also added, which has the role to aggregate the nanoparticles and to create "hot spots." The order of mixing these three components, the ratio in which they are mixed, the type of electrolyte used, and the time lapse between mixing and measurements will highly influence the recorded SERS signal. Unfortunately, there exists no golden rule which guarantees the best results, and for each targeted molecule, the procedure is commonly optimized by the trial and error method. During the SERS measurements, objectives with a long working distance are preferred as this avoids the unwanted dipping of the microscope objective in the sample, and it offers information from a larger collection volume. The incident laser power can have values of above 1 mW up to tens of milliwatts due to the presence of the aqueous environment, and the excitation laser is focused on the water-air interface or short below it as this avoids the reabsorption of the Raman-scattered light by the sample.

If the targeted analytes are hydrophilic, scientists usually choose planar SERS-active substrates. The deposition of the analytes is done either by the drop-and-dry

approach or by incubating the substrate in the sample solution for a given time. For the first case, due to the coffee-ring effect, heterogeneous molecule layers will be obtained, while in the second case, the incubation time will strongly influence the outcome. Furthermore, in the second case, the scientist might opt to measure the substrate after it was air-dried or when it is still dipped in the solution. In all cases, most commonly Raman scans are performed in order to avoid the local heating and degradation of both the analyte and the plasmonic structure. Under dry conditions, laser powers lower than 1 mW are preferred, and objectives with a high numerical aperture are selected. These two procedures, cuvette and scanning the surface of the planar substrate, are suitable for the determination of biomarkers in body fluids. For the in vivo applications, nanoparticles are injected into the tissue of interest, or substrates are implanted below the skin and approaches like spatially offset SERS microscopy is performed.

Reproducible and automated measurement conditions are essential characteristics for the successful integration of new analytical methods in routine analysis. As mentioned above, SERS measurements with NPs in colloidal solutions are generally carried out in cuvettes, whereas in the case of the planar substrates, the analyte molecules are deposited on the metallic surface either via drop and dry or incubation. Neither of these two approaches offers the possibility to perform automated measurements, and both methods are subject to human errors. The combination of SERS with microfluidics, however, has been very promising at overcoming these limitations, and it opened a door toward a plethora of biomedical applications [60–68]. Notably, by employing microfluidics, the required reagent volumes can be considerably reduced, chemical reactions can be observed at the microscale, and sample preparation and measurements are integrated in the same platform. Among the optical methods that have been applied to record signals from such volume-reduced samples, SERS is favored because of its high sensitivity.

On the basis of literature, microfluidic platforms can be divided into two main categories: flow-through or continuous flow platforms [69–88] and segmented or droplet-based platforms [42, 68, 89–95]. In the first approach, planar substrates prepared via top-down processes can be integrated into the channel system, colloidal NPs can be injected via one of the inlet ports, or SERS-active substrates can be produced in situ. In these platforms, solvent evaporation is inhibited, the coffee-ring effect occurring in the open platforms is avoided, and the diffusion of the target molecules toward the metallic surface can be improved via, e.g., electrokinetic [96] or hydrodynamic focusing [97]. However, because the sample is permanently wetting the channel walls of the microfluidic platform, the so-called memory effect can appear, where the channel surface of the channels becomes enriched with the samples over time and the reliability of the SERS measurements can be compromised. This is one of the reasons leading to the development of droplet-based microfluidic platforms. In these platforms, cross contamination can be significantly inhibited by ensuring no or very low cross talk between the different liquid compartments by dispensing the sample and colloidal NPs into individual droplets surrounded by an immiscible liquid phase. These droplets can be trapped, sorted, mixed, or split, based on the specific experimental requirements. As droplet

formation is controlled by high precision pump systems, the method will suffer less from human-induced errors, and the SERS signals will offer reliable results.

With this approach, two of the main limitations of the SERS technique, reproducibility and automation, can be overcome. However, this is not sufficient for the selective detection of molecules in complex matrices. Generally, the SERS-active substrates will enhance the signal of any Raman-active molecule situated in their proximity. Consequently, the molecules of a complex matrix and the target molecules will compete for free binding sites on the metallic surface, and the successful detection of the molecule of interest can be inhibited. For example, when a biomarker must be detected in human blood, proteins, red blood cells, and other large molecules will block the nanostructured metallic surface. Thus, the distance between the target molecule and the enhanced electromagnetic field will be too large for the molecule to still experience the SERS effect. Increased selectivity of the metallic surface is present only toward those molecules that have functional groups with high chemical affinity for the respective metal. Namely, thiol groups, the lone pair electrons of oxygen and nitrogen atoms, and π electrons of aromatic rings show high affinity toward gold and silver. To increase the selectivity of the SERS substrates for the targeted molecules, immunoassay-based SERS platforms have been developed. The working principle of an immunoassay is based on the antigen-antibody binding reaction. The technique gains its high specificity and sensitivity from three important properties of antibodies: (1) the ability to bind to both natural and synthetic molecules, (2) specific binding, and (3) binding strength [98–101]. Immunometric assays, such as the enzyme-linked immunosorbent assay (ELISA), use two different specific antibodies that form a sandwich around the target of interest, and they are suitable for the detection of molecules with large molecular weight, such as proteins or peptides. For the low molecular weight substances, the competition design is preferred. Here, the target molecule competes with a fixed amount of tracer (labeled molecule) for a limited number of antibodies. The affinity of the target molecule for the antibody is higher than that of the tracer. Therefore, when the target molecule is present in the sample, fewer tracers will bind to the antibody than in the absence of such a molecule. Finally, after the successful formation of immunocomplexes, SERS can be used to detect the signal. Commonly, Raman reporter molecules with well-defined and strong Raman signatures are embedded in the SERS tags, and their signal rather than that of the target molecule is measured. In the following section, the reader will find many examples of the successful detection of biomarkers by means of SERS-based immunoassay platforms.

For most medical diagnosis purposes, qualitative results are not sufficient for confirming the presence of a medical condition. However, quantitative SERS measurements are still very challenging even after more than 40 years from the first reported enhanced Raman signals of pyridine on roughened metallic surfaces [102]. This stems from the fact that SERS is a surface-sensitive technique. Only the Raman signal of the molecules in the first layers on the metallic surface will be considerably enhanced. Thus, the dynamic range of the method is limited, and very seldom it extends over more than one or two orders of magnitude. At high

concentrations of the target molecules, the so-called saturation or poisoning effect appears due to the evanescent character of the local electromagnetic field. Furthermore, using the traditional quantification method based on previously established calibration curves will fail because of the batch-to-batch variation in the quality of the SERS-active substrates and because of the high chemical variability of the biological samples. Nevertheless, most of the reported SERS-based immunoassay platforms, owing to their selective binding, offer reliable quantitative measurements, while for the microfluidic SERS platforms, the standard addition was implemented to improve quantitative measurements of molecules [89]. However, most studies in the literature show results measured in a single run, and they do not address the quantification of the target molecules in clinical samples, where the concentration is unknown. Therefore, before SERS can be considered as a tool for clinical diagnosis, this challenge has to be met.

In conclusion, due to the high variety of available SERS-active substrates, the choice of the best-suited substrate is never trivial and highly depends on the specific application. A top-down substrate with a highly homogenous surface would generally present a uniform enhancement over the surface, making it easily suited for applications that require quantification and high reproducibility (e.g., cell measurements). On the other hand, a substrate with less uniform enhancement would often present hot spots with higher enhancements, which would make the substrate better suited for applications connected to single-molecule detection or microfluidic system measurements [46, 103]. Finally, functionalized colloids are easily distributed in the organism, taken up by cells, or dispersed on tissues, making them a generally good choice for in vivo medical applications. Nevertheless, in this situation, the problem of ensuring the formation of hot spots remains, and different solutions have been reported in the literature as it will be discussed below.

5 Key Research Findings

5.1 Aging-Associated Diseases

5.1.1 Neurodegenerative Diseases

Life expectancy has risen dramatically during the last century, leading to an increase in the proportion of the elderly population. This, given the progressive degeneration of the structure and function of the nervous system during aging, has increased the incidence of neurodegenerative disorders. Alzheimer's disease (AD) is the most prevalent form of late-life mental failure in humans. Since 2010, multiple SERS studies of AD have been conducted, and their results will be the subject of the present section of the chapter. However, before discussing the findings in the field, a brief summary of key factors related to AD will be presented in the following paragraphs. For an extensive discussion of AD pathology, the reader is referred to the multiple excellent review papers and books published on this topic [104–114].

AD is associated with progressive memory impairment, disordered cognitive function, and altered behavior, including paranoia, delusions, and loss of social

appropriateness, accompanied by progressive decline in language function [104–108]. The study of AD pathogenesis generated long discussions in the medical community. Nowadays, it is commonly accepted that the two main pathological hallmarks of the disease are extracellular neuritic plaques and intracellular neurofibrillary tangles. The neuritic plaques are microscopic foci of extracellular depositions consisting of amyloid β (Aβ) proteins [104]. Aβ is a 39–43-residue-long polypeptide generated through cleavage of the amyloid precursor protein by β- and γ-secretase [115]. The Aβ species associated with AD are composed of 40 or 42 residues. Aβ (1-40) has a higher concentration in AD patients, although the neurotoxicity of Aβ (1-42) is much more pronounced owing to its greater tendency to form aggregates in vivo. The question of whether the insoluble Aβ fibrils and monomeric Aβ proteins are less pathogenic than soluble, nonfibrillar assemblies (dimers, trimers, or larger oligomers) has generated an intense debate [110–112]. In addition to amyloid plaques, the AD brain contains also large, non-membrane-bound bundles of abnormal fibers composed of the microtubule-associated protein tau [113, 114] with abnormal posttranslational modifications, including phosphorylation and acetylation [116, 117]. In AD, more than 20 residues become phosphorylated, whereas in the healthy brain, 8–10 of these residues are heterogeneously phosphorylated and, therefore, do not bind to microtubules. As a consequence, dendritic spines in the AD brain become enriched in the tau protein, which might interfere with neurotransmission [118].

These two pathologies can occur independently of each other. Neurofibrillary tangles have been observed in other neurodegenerative disorders that are not associated with amyloid plaques. Similarly, Aβ aggregates were observed in brains of cognitively normal-aged individuals in the virtual absence of tangles [104]. Therefore, the gold standard for AD diagnosis to date is postmortem neuropathological confirmation. However, it is commonly accepted that the neurological changes leading to AD begin to develop decades before the earliest clinical symptoms occur. Biomarker detection has been proposed to be used for early diagnosis. The five most widely studied biomarkers of AD are decreased Aβ (1-42) concentrations in the cerebrospinal fluid (CSF), increased CSF tau levels, decreased fluorodeoxyglucose uptake assessed by positron emission tomography (PET) imaging, PET amyloid imaging, and structural magnetic resonance imaging (MRI) measurements of cerebral atrophy [105].

Aβ monomers and oligomers have been detected by electrochemical, surface plasmon resonance, colorimetric, resonance light scattering, and fluorescent sensors, as well as by ELISA and with large-scale instrumentation such as mass spectrometry [115, 119–122]. However, there is no gold standard for these assays, and the research community is strongly driven by this unmet challenge. As already described in the experimental section, the combination of SERS with immunoassays yields a platform with high specificity, sensitivity, and selectivity. Multiple groups have taken advantage of this detection principle and reported on the successful determination of Aβ and tau proteins in phosphate-buffered saline (PBS) and in artificially spiked whole-blood samples. In Fig. 1.3, an easy and straightforward approach to detect Aβ (1-40) is illustrated [123]. The platform is based on capturing Aβ (1-40) antigens by

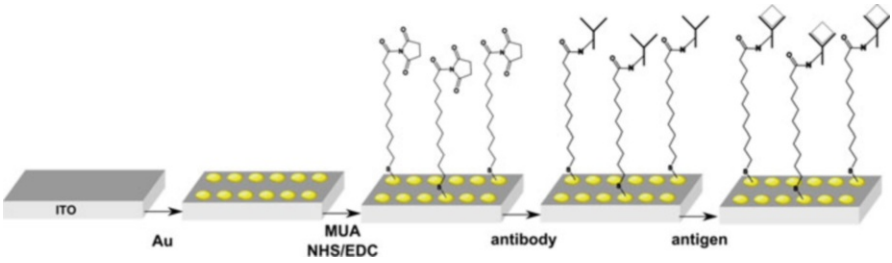

Fig. 1.3 Schematics of the SERS-based immunoassay used for Aβ (1-40) detection described by El-Said et al. [123]

antibodies immobilized on an N-hydroxysuccinimide (NHS)- and 1-ethyl-3-(3-dimethyl-aminopropyl)carbodiimide (EDC)-activated 11-mercaptoundecanoic acid (MUA) layer linked to electrochemically deposited Au NPs. This immunoassay was used for the detection and quantification of Aβ (1-40) based on its SERS spectrum, at concentrations between 100 fg/ml and 1 μg/ml in PBS, with a linear dynamic range of 100 fg/ml–1 ng/ml.

Tau, the biomarker indicating the formation of neurofibrillary tangles in the human brain, has also been successfully quantified in PBS solution by a homogenous sandwich assay combined with SERS [124]. For this, the authors used monoclonal anti-tau antibody-functionalized hybrid magnetic nanoparticle (MNP) probes and polyclonal anti-tau antibodies immobilized on gold NPs as SERS tags. Figure 1.4 illustrates schematically the working principle of the assay. In the first step, silica-coated, oleic acid-stabilized maghemite (γ-Fe_2O_3) NPs were prepared. To prevent self-polymerization of the MNPs, 3-methacryloxypropyltrimethoxysilane (MPS) in the presence of hydroquinone as a catalyzer was deposited on their surface. The MPS-modified MNPs were then coated with the chain transfer agent 2-cyano-2-propyl benzodithioate (CPBT) and azobis(isobutyronitrile) (AIBN). Grafted hybrid MNPs were obtained via the surface-mediated reversible addition-fragmentation chain transfer polymerization of 2-hydroxyethyl methacrylate (HEMA) from CPBT-modified MNPs poly(HEMA). This was followed by the cleavage of the poly(HEMA) grafted chains from the hybrid MNPs, the removal of dithiobenzoate end groups, and the addition of the monoclonal anti-tau antibody. These hybrid MNPs have a diameter of ~70 nm. As SERS tags, gold NPs with a diameter of 15 ± 8 nm, modified with a self-assembled monolayer of 5,5-dithiobis (2-dinitrobenzoic acid) (DTNB) and followed by the attachment of the polyclonal anti-tau antibody, were used. A polyclonal antibody was chosen to amplify the low signal from the target tau, as polyclonal anti-tau antibodies can recognize multiple epitopes on tau molecules. As a result, sandwich complex aggregation is induced.

To detect the tau protein, the hybrid MNPs, functionalized with the monoclonal anti-tau antibody, were added to the sample solutions. After 30 min, the resultant tau conjugated MNPs were isolated with a magnet, washed, and added to the solution containing the SERS tags. After another 30 min, the resultant sandwich complex was isolated with a magnet and SERS measurements were performed. The MNPs are not

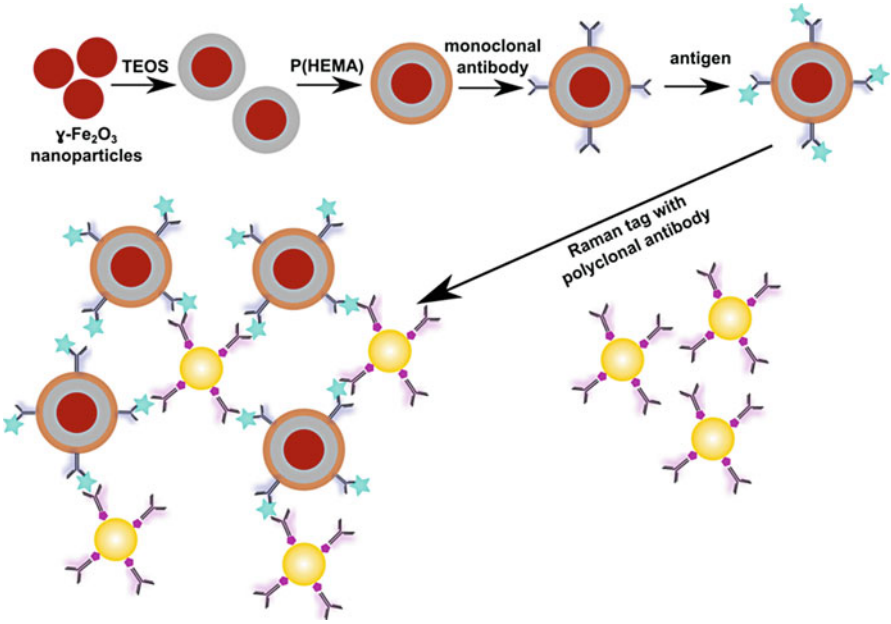

Fig. 1.4 Scheme of the preparation of sandwich assay for tau protein detection described by Zeng in et al. [124]

SERS active, and therefore, there is no plasmonic coupling between them and the SERS tags. However, it is very likely that hot spots can be generated between adjacent polyclonal anti-tau antibody-functionalized Au NPs. This is clearly supported by the appearance of Raman bands in the SERS spectrum associated with the vibrational modes of DNTB (Fig. 1.5a). Under these conditions, it is expected that by increasing the amount of tau proteins conjugated with the hybrid MNPs, the number of captured polyclonal antibody-conjugated Au NPs will also increase. The sensitivity of this immunoassay SERS platform is illustrated in Fig. 1.5b. An excellent linear response was obtained for tau concentrations between 25 fM and 500 nM. Furthermore, the cross-specificity of the assay was also tested using a solution containing equal amounts of tau, bovine serum albumin (BSA), and immunoglobulin G (IgG). As it can be seen in Fig. 1.5c, the SERS intensity obtained from the response of the mixture was strongly similar to that obtained from the sample containing only tau in solution. Therefore, BSA and IgG had no strong influence on the performance of the assay, confirming its high specificity for the tau protein.

Ideally, the assays intended to diagnose a medical condition should measure multiple indicators of the disease in biological fluids in order to avoid false-positive results. In the case of AD, this is especially important, because common dementia cases can be easily misdiagnosed as AD. Therefore, although the two assays presented above offer high sensitivity and specificity for the detection of Aβ (1-40) and tau in PBS, an assay offering multiplex measurements in biological fluids

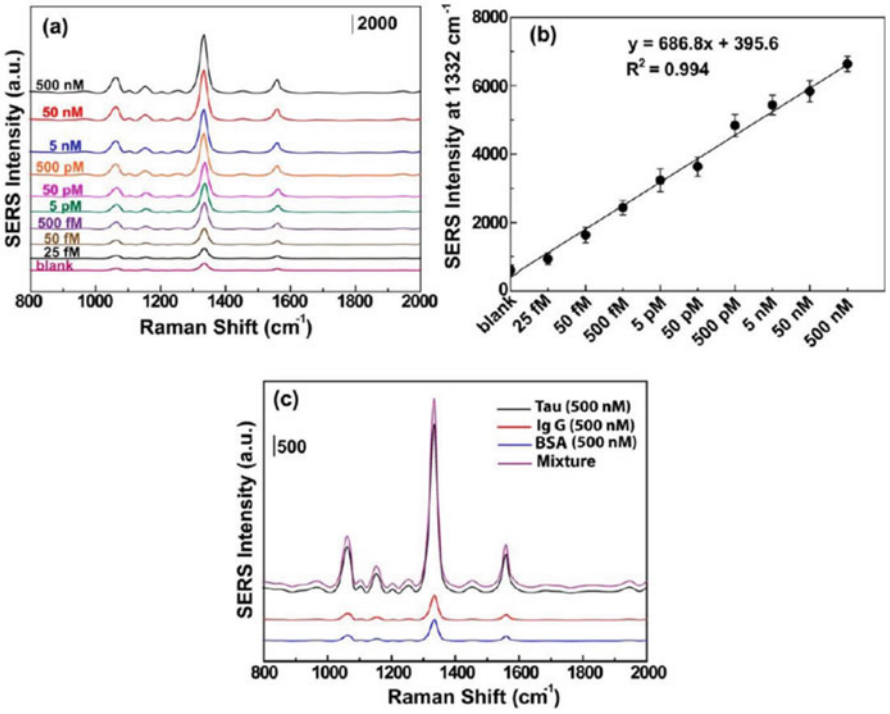

Fig. 1.5 (**a**) SERS spectra at different tau concentrations showing the Raman bands characteristic for the DNTB molecule. (**b**) Concentration-response curve of the tau assay. For each concentration four different reading of the SERS intensity was performed. (**c**) SERS spectra demonstrating the specificity of the sandwich assay for the tau protein (Adapted with permission from Zengin et al. [124]. Copyright © 2013, American Chemical Society)

is desired. Additionally, whole blood would be an attractive alternative to CSF as a biological fluid of clinical interest for biomarker detection, because it allows less expensive and invasive measurements, suitable for repeated, routine examinations. However, the Aβ (1-42) levels in plasma (~20 pg/ml) are considerably lower than those in CSF (800 pg/ml) [125, 126]; furthermore, plasma is a much more complex matrix, as it contains high amounts of different proteins, and Aβ in plasma can also be derived from peripheral tissues and not only from the brain [127]. In the case of tau, its plasma levels were ~8 pg/ml, whereas its levels in CSF were ten times higher. Furthermore, to have elevated tau protein levels in the plasma, substantial axonal injury is required; thus, high levels of tau in the plasma is a late marker of AD [128].

Keeping in mind the need for multiplex detection platforms and the low concentrations of Aβ (1-42) and tau protein in plasma, Demeritte and coworkers developed a large-scale, chemically stable, bioconjugated, multifunctional, hybrid graphene oxide platform for the separation and identification of trace levels (femtogram) of the two AD biomarkers in whole blood [129]. Their nanoplatform conjugated with anti-tau and anti-Aβ antibodies is based on magnetic core-plasmonic shell nanoparticles

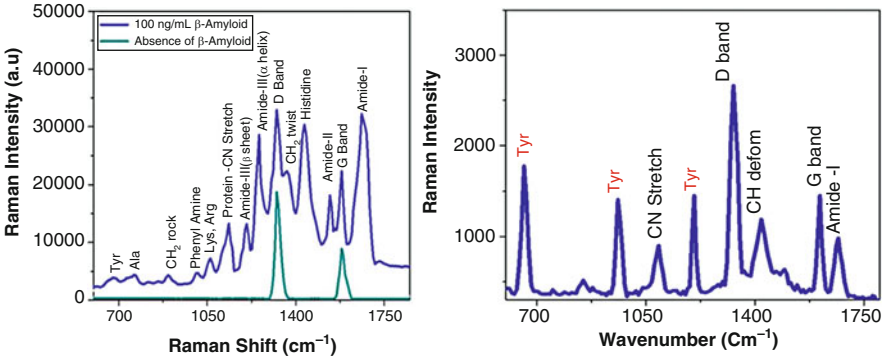

Fig. 1.6 SERS spectrum of Aβ (1-42) and tau protein measured with magnetic core-plasmonic shell NPs attached to 2D hybrid graphene oxide platforms (Adapted with permission from Demeritte et al. [129]. Copyright © 2015, American Chemical Society)

attached to 2D hybrid graphene oxide. Here, as also in the former report, the authors took advantage of the magnetic properties of their particles in order to separate them from the complex matrix and avoid autofluorescence background signals originating from blood cells. The large surface area of the graphene oxide supports high adsorption of the target molecules, and it also facilitates stable hot-spot creation between the core-shell particles. The selective capture efficiency of the assay was confirmed by using an ELISA kit, and it was estimated to be 98% for Aβ (1-42) and 97% for tau. In contrast to the previous case, SERS protein detection was performed label-free, based on their intrinsic Raman vibrational modes. The SERS spectra of Aβ (1-42) and tau are shown in Fig. 1.6, together with the background signal from the nanoplatform. In the latter case, the Raman bands were assigned to the D and G bands of graphene oxide. The SERS spectrum of Aβ (1-42) shows sharp bands assigned to the amide I, amide II, and amide III groups. The position of the amide III band is especially important, as it gives information about the structure of the protein. When the protein adopts an α-helical structure, it is shifted to high wavenumbers (~1300 cm^{-1}), whereas with β-sheet conformations, it is shifted toward the low wavenumbers (~1220 cm^{-1}). In addition to the amide bands, histidine residues, phenylalanine, and tyrosine molecules contribute to the Raman spectrum of Aβ (1-42). In the case of tau, the vibrational modes of tyrosine are strongly contributing to the Raman spectrum. Owing to the absence of amide II and amide III bands in the spectrum of tau, the two molecules can be easily discriminated based on their SERS spectrum. The sensitivity of the assay was 500 fg/ml for Aβ (1-42), with a linear dynamic range up to 1 pg/ml. For the case of tau, SERS signals were present at 100 fg/ml, but the authors do not offer information regarding the linear range.

The three examples described above demonstrate the high potential of immunoassay SERS platforms for the detection of AD biomarkers with very high sensitivity. However, SERS spectroscopy is not limited to the detection of molecules, but it can also offer valuable information about the structure and conformation of the

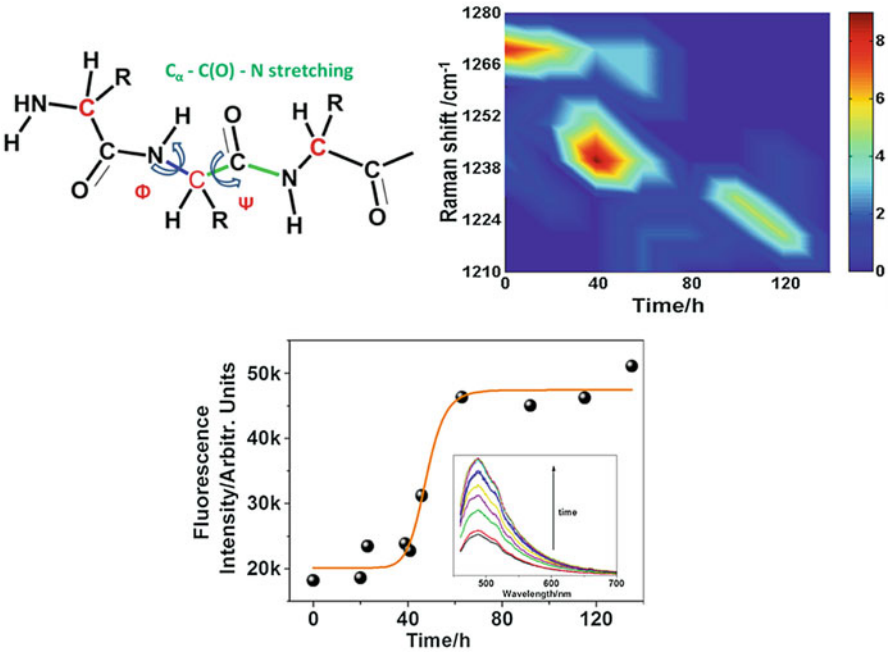

Fig. 1.7 Model of peptide secondary structure and predominately contributed Raman signal associated with the C_α–H bending motion mode. Characterization of Ab (1-42) peptide Am III frequency, with simultaneously ThT assay fluorescence measurement of Aβ (1-42) (Adapted from Wang et al. [132] with permission from Wiley)

molecules. Although this does not have a diagnostic value per se, it is often important to gather additional information of the detected molecules.

In the case of Aβ, it has been proposed that small oligomers, profibrils, Aβ-derived diffusible ligands, and heterogeneous globular species are more neurotoxic than the fibrils in late aggregation stages [130, 131]. To investigate the aggregation pathway, it is crucial to identify the conformation of the proteins accumulated in the different aggregation stages. As already mentioned above, the position of the Raman mode ascribed to the amide III vibration is sensitive to the conformation of the protein (α-helical or β-sheet). Consequently, the C_α-H and N-H bending motions of secondary structure elements, defined by the Ψ and Φ Ramachandran angles (Fig. 1.7), will be affected by the aggregation stage of the protein. In a SERS study carried out with Ag NPs coated with a silica shell, the authors were able to monitor the conformational changes occurring during aggregation by correlating the SERS measurements with the results of a thioflavin T fluorescence assay, the gold standard for assessing Aβ aggregation, and atomic force microscopy [132]. The SERS results are nicely summarized in Fig. 1.7. In the 3D plot, the Raman shift of the amide III band is shown as a function of the incubation time with Aβ (1-42) monomer in PBS at 37 °C. These results show that as the incubation time increases, the center of the Raman band shifts from higher to

lower wavenumbers. At time points below 20 h, the position of the band suggests that the structure of the protein might be flexible to form different hydrogen bonds between C_α-H and N-H. This hypothesis was confirmed by fluorescence measurements, showing no significant changes in the fluorescence intensity at times below 20 h, indicating that Aβ is still not aggregated or has only elementary aggregation forms. For incubation times at the range of 20–80 h, the fluorescence emission of thioflavin T increased exponentially, suggesting Aβ (1-42) aggregation, accompanied by the formation of β-sheet hydrophobic cores. The apparent heterogeneity of the Raman signal suggests that the aggregation process is not homogenous. After 80 h, the aggregation process reaches equilibrium and the Raman band is shifted to 1220 cm^{-1}. In conclusion, SERS is a powerful tool for structure investigation, and it is much more sensitive than classical fluorescence measurements.

5.1.2 Cardiovascular Diseases

Approximately half of the deaths in the western world are caused by cardiovascular diseases (CVD) and particularly by myocardial infarction (MI). The early diagnosis of MI will have a high impact on the health of the patients, as MI causes irreversible heart damage, and it will also significantly decrease the financial burden placed on clinical resources. MI diagnosis is performed by electrocardiogram (ECG) measurements combined with the determination of the level of cardiac specific biomarkers in patient blood [133, 134]. Troponin I (cTnI), troponin T (cTnT), myoglobin, and creatine kinase MB (CK-MB) are the most commonly monitored MI biomarkers. Myoglobin elevation above the clinical cutoff value of 70–200 ng/ml in the first 1–3 h is considered to be one of the earliest signs of MI. However, myoglobin is released by both skeletal and cardiac muscle injury, and, thus, it has low specificity [134]. CK-MB increases above the clinical cutoff value of 10 U/l 3–4 h after MI, and it is considered of medium specificity for the clinical condition [134]. For the confirmation of cardiomyocyte damage, cTnI and cTnT are considered to be the gold standard [135, 136]. The troponin complex is responsible for skeletal and cardiac muscle contraction. After myocardial damage, the individual proteins of the complex are released in the bloodstream. Nevertheless, up to 6 h have to pass since the first physical symptoms appeared to reach a concentration level above the cutoff value of 0.01–0.1 ng/ml. Based on these facts, it becomes clear that once again, as in the case of AD, it is desirable to determine the presence of more than just one biomarker to avoiding false-positive diagnoses. Optical (intensity readout, luminescence, surface plasmon resonance, SERS), electrochemical (amperometric, potentiometric, impedimetric), and paramagnetic particle-based immunosensors have been widely employed for this purpose [133, 134, 137–141].

The high sensitivity of SERS was the driving force for the development of various assays for cardiac biomarker detection. Myoglobin concentrations as low as 10 ng/ml were detected in PBS and in human urine, with a linear dynamic range of 10 ng/ml–5 μg/ml, by employing a template-free, one-step synthesis for the plasmonic structure [142]. However, the employed Ag nano-pinetree film-modified ITO substrates are not selective for myoglobin and are most probably not suitable for the detection of the molecule in blood.

ELISA assays are routinely performed for molecule detection with high specificity and sensitivity. The recently developed assays use fluorogenic, electrochemiluminescent, and real-time polymerase chain reaction to generate quantifiable signals. SERS was also considered as a signal readout method, and it was successfully applied for the quantification of the cTnT biomarker at concentrations of 2–320 pg/ml. For this, the target molecule at different concentrations was incubated in antibody-coated microplates, followed by the addition of an anti-cTnT-horseradish peroxidase conjugate, chromogen A (3,3′,5, 5′-tetramethylbenzidine (TMB)) and chromogen B (H_2O_2). As a result of the enzymatic reaction, TMB^{2+} was obtained, and it was found that its SERS intensities decreased upon decreasing the concentration of the antigen (cTnT) present in the sample.

International guidelines for cardiac biomarker detection recommend a turnaround time (TAT) of less than 1 h from the moment the patient is admitted to the hospital. A competitive immunoassay for the simultaneous detection of two cardiac biomarkers in human blood, cTnI and CK-MB, was proven to deliver results in less than 15 min, requiring a minimum sample consumption of 10 μl [143]. In this assay, monoclonal antibodies against cTnI and CK-MB were conjugated to magnetic beads, and the target antigens were immobilized on the surface of SERS tags. Therefore, the free target antigens in the sample would compete with the antigen-conjugated SERS tags for the binding sites on the surface of the magnetic particles. After binding for 7 min, the immunocomplexes were captured with a magnetic bar, and the Raman signals of the remaining SERS tags in the supernatant were measured. As reporter molecules, malachite green isothiocyanate was used for cTnI and X-rhodamine-5-(and-6)-isothiocyanate for CK-MB. The cross-reactivity between cTnI and CK-MB was also evaluated for a concentration range between 10 pg/ml and 1 μg/ml. The SERS spectra of the two reporter molecules exhibited well-separated Raman bands. Therefore, multiplex detection could be easily carried out. The clinical application of the competitive immunoassay-based SERS platform was evaluated by determining the two biomarkers in 18 blood samples collected from patients and comparing the results with data measured by a commercial assay. For the quantitative determination of the target molecules, SERS calibration curves were generated from cTnI and CK-MB dissolved in PBS. The limit of detection was 42.5 pg/ml and 33.7 pg/ml for CK-MB and cTnI, respectively. By applying the Bland-Altman and Passing-Bablok regression analysis, it was demonstrated that the differences between the results of the SERS assay and the commercial assay were in the 95% limit of agreement range. Thus, the authors were successful in developing an immunosensor with fast TAT and high specificity and with a considerably higher sensitivity than the commercially available platform.

5.1.3 Diabetes Mellitus

Glucose levels in the human body are regulated by the ability of insulin, secreted by the pancreas, to promote glucose uptake in the peripheral tissues and to suppress hepatic glucose production [144]. Type I diabetes mellitus, also referred to as juvenile diabetes, is caused by insulinopenia, and it affects 5–10% of all diagnosed patients. Type II diabetes, with a prevalence outreaching 90%, is described as an

insulin resistance. The onset of type II diabetes happens at adult age when the pancreas is not able to produce excess insulin to overcome the resistance, and its incidence increases with age. There is no established cure for this medical condition, although the state of the patients can be considerably improved by responsible glucose level monitoring. An impressive variety of glucose sensors are on the market, including point-sample and continuous monitoring devices [145–147]. Although glucose monitoring is not a diagnostic procedure per se, we consider that the high number of publications reporting SERS-based sensors for glucose monitoring [148–173] requires a separate section for highlighting the major findings in the field.

Glucose molecules do not naturally absorb onto metallic surfaces; hence different strategies had to be developed in order to detect them. The enzyme glucose oxidase (GOx) catalyzes the oxidation of glucose, generating H_2O_2 and gluconic acid. Consequently, the pH value of the microenvironment is changing. Several researchers took advantage of this reaction and developed sensors based on it. GOx was deposited on SERS-active microneedles used for in vivo glucose sensing [159]. Specifically, 0.2 mm stainless-steel acupuncture needles were covered with gold nanoshells and a microporous polystyrene layer. As the SERS reporter molecule, 4-mercaptobenzoic acid (4-MBA) was deposited before GOx was added on the surface. When the sensor was immersed in an environment containing glucose, the integrated GOx molecules could convert the target molecule to gluconic acid, which would cause a pH change. Consequently, owing to the pH-sensitive SERS signal of 4-MBA, the concentration of glucose could be indirectly assessed. This sensor showed satisfactory linear response for glucose concentrations between 2.7 and 8 mM in water. By taking into account that the normal blood glucose levels in humans are in the range of 3–6 mM [174], the sensor would allow the quantification of blood glucose at normal levels, but hypo- and hyperglycemic states cannot be quantified. In the same study, the in vivo performance of the multifunctional acupuncture needle was demonstrated on a male New Zealand rabbit. For this, the glucose-responsive multifunctional acupuncture needles were inserted in the rabbit tendon and ear vein for 30 s. The signal from different needles was measured before and after the injection of a glucose solution (5 ml, 0.75 g) via the ear vein. At the same time, reference values were measured using a commercial glucometer. Unfortunately, the authors do not provide a quantitative estimation of the glucose levels in the rabbit; however, the 4-MBA signal decreased upon increasing glucose concentration. Overall, this technique is very promising, and with further work, it could compete with other commercial devices.

Boronic acid covalently binds saccharides via the diol moieties [175]. Thus, many glucometers rely on this recognition reaction for the detection of glucose levels. In the SERS studies different isomers of mercaptophenylboronic acid (MPBA) have been widely used for capturing glucose, and also as Raman reporters for quantification purposes [153, 155, 158, 169–171]. Glucose recovery levels of 84–110% in undiluted human urine were reported by employing a nanosensor based on 4-MPBA decorated Ag NPs [171]. The working principle of the sensor relies on the aggregation of the Ag NPs induced by the 2:1 4-MPBA/glucose bonding ratio. Glucose

contains two pairs of adjacent hydroxyl groups that could bind to two 4-MPBA-modified Ag NPs. This glucose sensor showed a response time of 12 min, and its selectivity over mannose, galactose, sucrose, and fructose was also demonstrated. Two-component (4-MPBA and 1-decanethiol (1-DT)) self-assembled monolayers, serving as molecular recognition and penetration agents, have also been employed in a paper membrane-based SERS sensor [155]. Owing to the nitrocellulose layer, blood cells and proteins were captured on the surface of the membrane, and only the small molecules reached through capillary forces the sensing site. The assay time was 5 min and a glucose recovery rate of 88% was reached. The limit of detection was estimated to be 0.1 mM and the linear range 0.5–10 mM. To increase the selectivity of the glucose sensing platforms, scaffolds incorporating two boronic acid groups have also been considered [153]. Direct and selective SERS detection under physiological conditions was carried out using a gold film-over-nanosphere (AuFON) substrate, functionalized with bisboronic acid receptors incorporating two 4-amino-3-fluorophenylboronic acid units. By employing monobornic acid, the glucose molecules will be in the close proximity of the metallic surface, sensing the high electromagnetic field. On the basis of their results, the authors concluded that a bisboronic acid analogue with seven atoms separating the amide carbonyls of the receptor units showed the highest selectivity and affinity for glucose. By applying multivariate statistical analysis, a clear distinction between hypoglycemic, normal, and hyperglycemic levels was achieved.

All sensors described above rely on point measurements, where the patients are requested to test their glucose levels multiple times per day. In this manner, hypo- and hyperglycemic episodes can be hardly detected, as they might occur randomly during the day. Continuous monitoring of glucose levels is therefore highly desired for the well-being of the patients. Multiple continuous glucose monitoring (CGM) devices are already on the market. However, they can generally function up to 7 days, they require multiple calibrations, and the product description recommends the patients to verify with a regular glucometer the actual glucose levels before taking measures. At the Van Duyne laboratory, a transcutaneous glucose sensing platform relying on surface-enhanced spatially offset Raman spectroscopy (SESORS) was developed, which could reliably sense glucose in vivo in rats for more than 17 days [151, 152]. While in normal Raman measurements the excitation and signal collection sites coincide, there is an offset between the two processes in SORS. In this way, the Raman signal from the underlying layers in the investigated samples will not be overwhelmed by the signals from the surface. Thus, SERS signals originating from the transcutaneous sensors can be easily collected. Decanethiol (DT)/6-mercapto-1-hexanol (MH) self-assembled monolayers partition and localize the glucose molecules on the AgFON surface. Based on space-filling computer models, the authors suggest that dynamic pockets capturing glucose are formed from the long DT chains and the short MH chains. The reliability and accuracy of new glucose sensors are generally assessed by the Clarke error grid analysis (EGA), illustrated in Fig. 1.8. The grid is divided into five zones (A–E), with measured concentrations by a reference method on the x-axis and predicted concentrations by the new method on the y-axis. The zones have the following

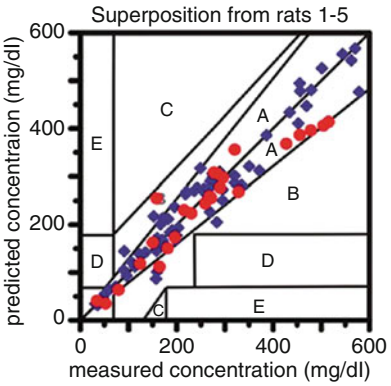

Fig. 1.8 In vivo transcutaneous SESORS glucose calibration (blue ♦) and validation (red •) data sets on five rats (Adapted with permission from Ma et al. [152]. Copyright © 2011, American Chemical Society)

significance: (A) clinically accurate measurements and treatment, (B) benign errors or no action, (C) unnecessary action, (D) lack of action, and (E) actions that are opposite to those that are clinically necessary.

Therefore, data acquired with the new method has to fall into the A and B zones in order to pass the accuracy test. Based on the plots presented in this study, this transcutaneous sensor detected hypoglycemia with an accuracy exceeding the current International Organization Standard (ISO/DIS 15197) requirements, with only one calibration in a time period of 17 days.

5.2 Cancer Diagnostics

Another important cause of a high number of deaths worldwide is cancer and cancer-related diseases. As nicely introduced in many review articles [176–178], the term cancer encompasses a large family of diseases, all characterized by uncontrolled cell growth that can potentially spread to other parts of the organism as well. Consequently, the diseases develop fast and are often diagnosed at a rather late(r) stage. Additionally, there is limited access to standard and efficient treatment, and cancer removal surgeries depend strongly on the proper assessment of the tumor borders in the affected tissue. Accordingly, cancer survival rates tend to be low, with the exact rates depending on the specific region of the world, the type of cancer, the age of the affected person, and the stage of the cancer spread [179]. To improve this, different techniques have been applied to achieve fast and reliable cancer diagnosis at an early stage, including polymerase chain reaction (PCR), ELISA, electrophoresis, SERS, micro-cantilevers, colorimetric assay, electrochemical assay, and fluorescence methods [176–178]. Each of these techniques relies on the specific identification of different cancer biomarkers present in tumor tissues, cells, or body fluids [176, 180]. Nevertheless, due to the high diversity of cancer-related diseases and

the particularities of its detection at different organs, often, detection of more than one biomarkers is required to assess whether an individual has cancer. DNA, mRNA, enzymes, metabolites, transcription factors, and cell surface receptors are some of the biomarkers used for cancer diagnosis [176, 179].

Proteins and related biomarkers released from cells and organs have been used for the detection and monitoring of cancer [181–184]. The available SERS studies for the ex vivo (cell, tissues, and body fluid measurements) identification of cancer often relies on the recognition of such biomarkers, and promising results have been reported for their ex vivo detection in cell culture [185–194]. Nevertheless, a more clinically relevant approach would rely on body fluid measurements. However, the concentration of protein biomarkers in serum during early cancer stages can be as low as 10^{-16}–10^{-12} M, making their detection rather challenging [181]. Since SERS is a molecular fingerprinting technique that can identify target molecules at very low concentrations, different SERS-based approaches have been tested to achieve this goal. Among the most straightforward approaches, SERS NPs in the form of commercially available colloids [195] or colloids prepared according to easy preparation protocols [50] were mixed with blood or serum samples, dropped on glass slides, and measured by Raman spectroscopy [195–197]. However, due to the low specificity of label-free SERS NPs, the results obtained by this procedure only partly correlated to the gold standard analysis (i.e., high-performance liquid chromatography – HPLC) [195]. Nevertheless, upon functionalization of these nanostructures, their specificity for specific cancer biomarkers increased, leading to better diagnostic results [198, 199]. In addition to pure Au or Ag nanostructures [50, 182, 195, 198], core-shell NPs have also been reported in the literature for cancer detection applications: Fe_3O_4/Au/Ag [41, 199], Au@Ag [41], or Au @ polyethylene glycol(PEG) – Au@PEG [182]. For each of these structures, specific tags were used for distinct cancer types, making the overall SERS substrate preparation protocols not universally applicable. For example, a surface-enhanced resonance Raman spectroscopy (SERRS) sensor based on sandwich immunocomplexes consisting of a mixture of Fe_3O_4@Ag NPs conjugated with capture antibody through an amidation reaction, and Au@Ag NPs conjugated with antibody using an HS-PEG-COOH/Tween 20-assisted method was tested for the detection of the colon cancer biomarker carcinoembryonic antigen (CEA) in clinical serum samples [41] (schematic representation in Fig. 1.9). For the preparation of the sandwich structure, a rather complicated and time-demanding procedure was followed. That is, the Fe_3O_4@Ag NPs were first incubated overnight in an ethanolic solution containing 10 μM MUA and 10 μM 11-mercapto-1-undecanol (MU). Then the carboxyl groups on the NP surface were activated by using a mixture of 1 mM and 5 mM sulfo-NHS, and the resulting NPs were incubated overnight in the presence of 10 μg of capture antibody. In the case of the Au@Ag NPs, upon washing three times with a buffer containing 1 μM HS-PEG-COOH and 0.01% Tween 20, the NPs were sonicated for 30 min in 25 μM diethylthiatricarbocyanine iodide (DTTC) to synthesize Raman-encoded NPs. Next, the particles were sonicated for another 30 min in 10 μL of a 1 mM mPEG-SH solution to increase their stability, suspended in a K_2CO_3 solution, vigorously mixed with 25 μM EDC and 25 μM sulfo-NHS for 15 min, and

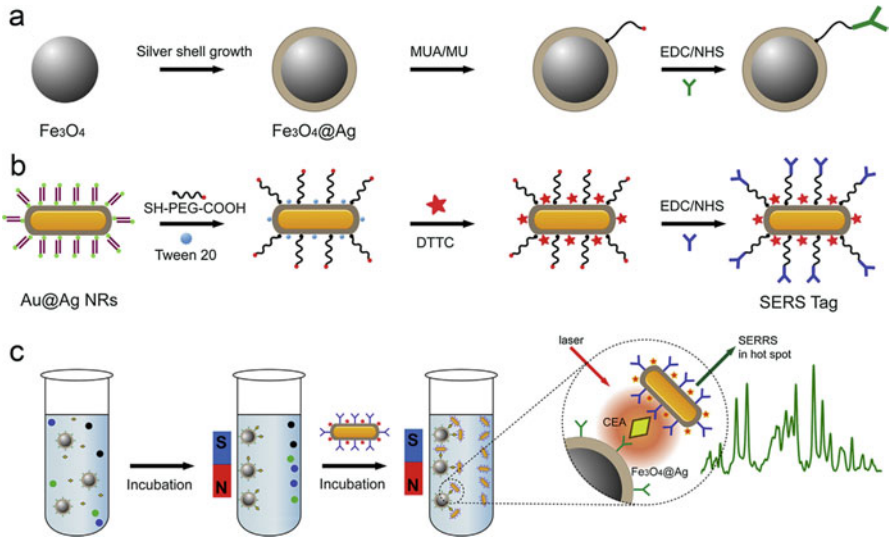

Fig. 1.9 Scheme of the preparation of sandwich assay for CEA protein detection (Reprinted from Rong et al. [41] with permission from Elsevier. Copyright © 2016 Elsevier)

re-suspended in a K_2CO_3 solution. Finally, the resulting activated NPs were incubated overnight in the presence of 10 μg of detection antibody. Thus, the preparation of the two different types of NPs required overnight incubation, making the overall NP preparation protocol rather time-consuming. However, once the NPs were available, the actual measurement protocol was rather simple. The magnetic NPs were first allowed to interact with the target solution for 30 min, and then the immune complexes were magnetically collected and washed. Subsequently, the DTTC-encoded Au@Ag were added and incubated for another 30 min. Finally, the formed sandwich complexes were washed with phosphate-buffered saline tween-20 (PBST), re-suspended in deionized water, and measured by SERS. Thus, the detection time required was approximately 1 h, which is fit for clinical application approaches.

Other commonly investigated biomarkers for cancer identification are DNA and mRNA. As in the previous case, both NP-based [200] and planar substrates-based [201] SERS immunosensors have been developed for their detection. For example, the detection of micro ribonucleic acid 21 (miR21) is often achieved by using labels such as cresyl fast violet T, Rhodamine B, Rhodamine 6G, and DTNB [201]. Nevertheless, it was recently shown [200] that by using an "OFF-to-ON" SERS inverse molecular sentinel (iMS) nanoprobe in a homogeneous assay for multiplexed detection of micro ribonucleic acid (miRNA) in a single sensing platform, no labeling is required. The starting point in the preparation of this detection scheme was the generation of Au nanostars based on a seed-mediated growth protocol introduced by Wang et al. [200], followed by Ag coating of these structures by adding 0.1 M $AgNO_3$ and 29% NH_4OH and allowing the chemicals to react for 5 min. Finally, the SERS iMS nanoprobes were produced by mixing 10 μl of a 10 μM stem-loop DNA

probe solution with 0.9 mL of 0.1 nM Ag-coated nanostars and 0.1 mL of a 2.5 mM $MgCl_2$ solution and incubating this mixture overnight at room temperature. The obtained structures were stabilized by a 30-min incubation with a 1 μM *O*-[2-(3-mercaptopropionylamino)ethyl]-*O*-methylpolyethylene glycol (mPEG-SH, 5000) solution. Following centrifugation and resuspension in Tris-HCl buffer (10 mM, pH 8.0) containing 0.01% Tween-20, the metallic surface of the nanostars was passivated with 0.1 mM MH. Subsequently, the SERS iMS nanoprobes were washed and redispersed in Tris-HCl-Tween-20 buffer. Finally, the iMS SERS signal was "turned OFF" by incubating the nanoprobes with 0.1 μM placeholder strands in PBS buffer solution containing 0.01% Tween-20 overnight at 37 °C. While performing the SERS measurements, the iMS SERS signal was "turned ON" when the structures sensed the presence of at least 1 μM miR-21 targets.

For each of the above mentioned biomarkers, SERS immunosensors are also available as planar substrates [43, 181, 184, 202–204] and within photonic crystal fiber probes [51, 182], for the detection of breast cancer biomarkers such as vascular endothelial growth factor (VEGF) [181], human epidermal growth factor receptor 2 (HER2) [184], and the wild-type and mutant mp53 protein [204] in patient blood plasma. An example of a hollow core photonic crystal fiber (HCPCF) probe used for multiplex detection of serological liver cancer biomarkers is illustrated in Fig. 1.10 [182]. Here, the fiber PCF was cut into 7 cm pieces cleaved at the ends, and its inner walls were coated with poly-L-lysine to induce active sites for the binding of the target biomarkers. The resulting fiber was then dipped in cell lysates from oral squamous carcinoma (OSCC) HER2 biomarker supernatant from Hep 3b cancer cell line for 3 min to allow for protein binding and was incubated at 4 °C for 2 h. After drying, a mixture of antibody-conjugated SERS nanotags was added into the fiber. In parallel, bio-conjugated SERS nanotags were prepared from commercially available NPs. For this, NPs were incubated with the following Raman reporter molecules: malachite green isothiocyanate (MGITC), naphthalenethiol (NT), or lipoic acid-modified cyanine 5 (Cy5), for 15 min, 1 h, or 15 min, respectively, in a ratio of 1:9. Subsequently, thiolated-carboxylated PEG (HS-PEG-CO_2H) was added and incubated for 20 min, followed by and incubation with thiolated PEG (PEG-SH) for 3 h. Upon activation of the carboxylic acid functional groups on the surface of these PEG-encapsulated NPs (by using EDC and sulfo-NHS), the resulting NPs were mixed with an additional antibody to achieve multiplexing: the alpha-fetoprotein (AFP) antibody was added to the activated Cy5 nanotag and the AIAT antibody to the MGITC nanotag. Finally, the resulting bioconjugated SERS nanotags were washed and bonded to the immobilized biomarkers in the fibers (see Fig. 1.10). In this study [182], the HCPCF was used both as a proof of concept, achieving the detection of HER2 in OSCC cancer cell lysate, and for the detection of two prominent hepatocellular carcinoma biomarkers, alpha-fetoprotein and alpha-1-anti-trypsin, in the Hep 3b cancer cell line. Furthermore, it was proposed that the HCPCF probe can be used for the analysis of saliva, tear, urine, and other body fluids for the early diagnosis of multiple diseases.

Other body fluids used for cancer biomarker detection include cervical fluids for the identification of the E7 gene of human papillomavirus (HPV) [202]; additionally,

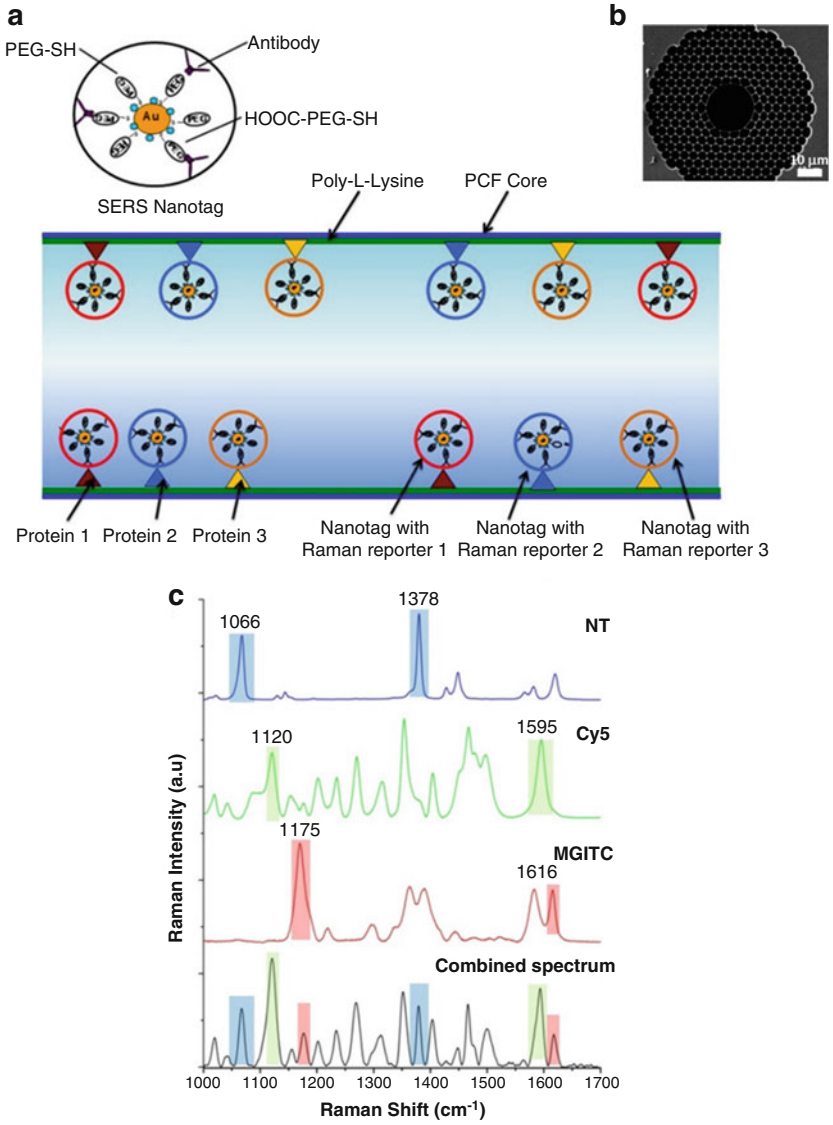

Fig. 1.10 Scheme of a hollow core photonic crystal fiber (HCPCF) probe used for multiplex detection of serological liver cancer biomarkers (**a**), SEM of the cross section of the HCPCF (**b**) and SERS spectra of individual SERS nanotags and their mixture used for the multiplexing measurements (**c**) (Adapted from Dinish et al. [182] with permission from John Wiley and Sons. Copyright © 2014 John Wiley and Sons)

breath analysis was also performed for the identification of volatile organic compound that can act as biomarkers for gastric cancer [43]. For the latter, a sensor was developed starting from a 7.5 cm clean glass, on which a 300-nm-thick Au layer was sputtered and 2 µL of a graphene oxide homogeneous solution was dropped and

dried. Following hydrazine vapor adsorption and reduction, the substrate was placed in N_2 for 30 min, and 1 μL of a 5 mM $AuCl_4^-$ solution was dried on the substrate, resulting in a Au NP distribution on the reduced graphene oxide film. The resulting SERS-active substrate was used for measurements of both simulated and real breath. To this end, the substrate was placed in a small vessel, and 50 μL liquid standard of each biomarker was added to the vessel without allowing any direct interaction between the substrate and the liquid to occur. The vessel was sealed and placed at 37 °C to allow for the liquid to vaporize and interact with the substrate, dry, and be measured. As illustrated in the simplified schematic in Fig. 1.11, statistical analysis was performed on the measured data and the results allowed for the differentiation of patients affected by early gastric cancer (EGC, stages I and II) from patients suffering from advanced gastric cancer (AGC, stages III and IV).

As is evident from the examples presented above, the drawback of these SERS-based analytical methodologies is the complexity of the protocol required for the preparation of the SERS-active substrates. Following NP preparation, functionalization and immobilization on a substrate are necessary, and the total time and complexity of the measurements increase. Nonetheless, once the SERS substrates are available, the measurements are easy to perform, and the results are available in a time-efficient manner. An alternative approach for the identification of cancer in tissues has also been reported in the literature [205–207], based on incubating the tissue with NP solutions, which does not require NP immobilization on any substrate. However, tissue measurements are by far the most invasive of the proposed methods, as the tissue must be removed from the patient before being investigated ex vivo by SERS. For the measurements, the tissue is first sliced into μm–mm thick sections [206, 207], then stained [206] or breaded [205] with NPs, and measured by mapping. It was found that upon incubation of the tissue with NPs, non-functionalized Au NPs form nano-clusters, which lead to increased Raman signals due to the formation of hot spots. On the contrary, encapsulated Au NPs (i.e., Au/SiO_2) and functionalized Au NPs are homogeneously spread over the tissue surface, increasing afferent specificity for the targeted biomarkers and lower Raman signals [205]. However, E. Cepeda-Pérez et al. [205] reported that in wet tissues, the Au/SiO_2 NPs used in their study formed aggregates in the vicinity of the biomolecules located on the tissue surface, leading to a further increase in Raman signals.

As an alternative to the abovementioned procedures, direct intra-tumoral injection of NPs (see schematic representation in Fig. 1.12) has also been used for cancer identification. Different approaches were considered here, starting from functionalization of commercially available NPs [36] and ending with the development of rather complex core-shell nanostructures [35, 208]. These complex core-shell nanostructures, depicted in Fig. 1.12, consist of Au vesicles encapsulating active compounds, such as chlorin e6 (Ce6). They were prepared starting from the generation of Au NPs by citrate reduction of $HAuCl_4$ in an aqueous phase. Subsequently, the Au NPs were dried on a glass substrate, followed by triggering the self-assembly of amphiphilic block copolymers by rehydrating of the thin Au NP film in water by sonication. Finally, Ce6 was encapsulated in the resulting Au NPs by rehydrating the structures with solutions having different concentrations of Ce6 during

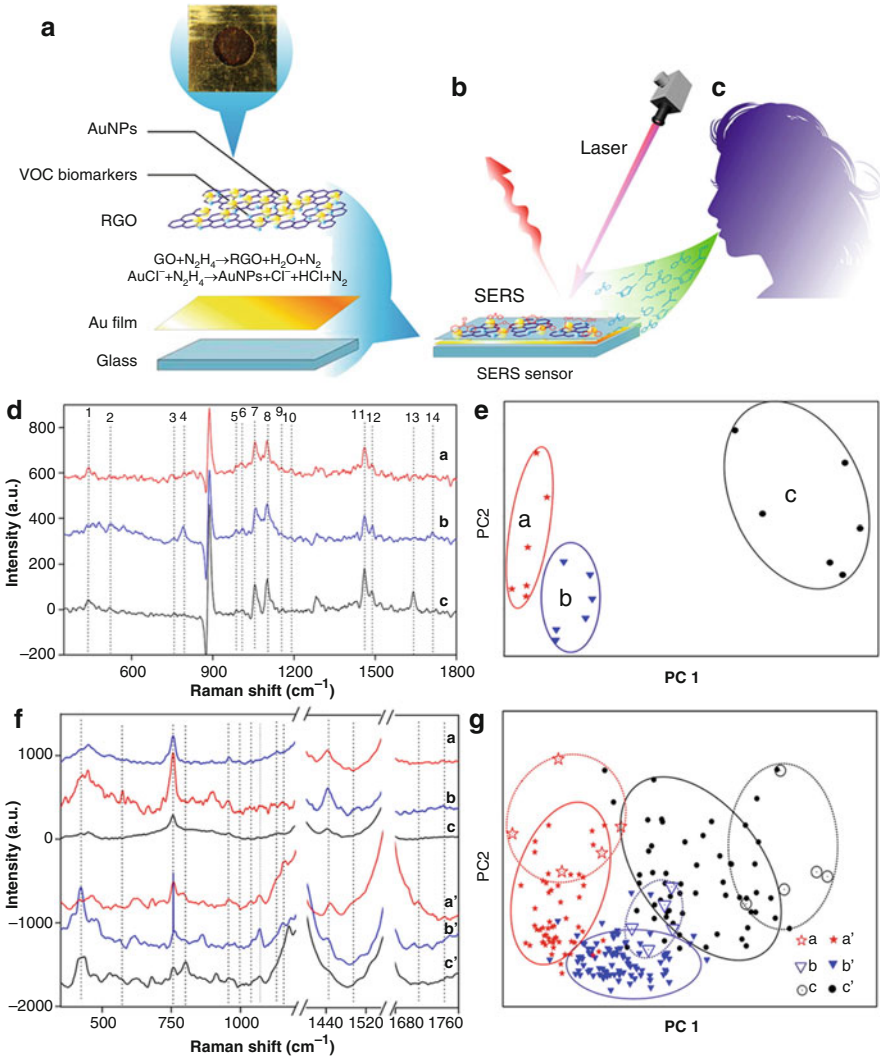

Fig. 1.11 Schematic representation of the SERS substrate preparation protocol (**a**), the SERS measurement procedure (**b**) of both simulated and real breath samples (**c**) and data analysis (**d**, **e**): the processed Raman spectra of the used biomarkers out of which 14 were associated to different vibrations that can be seen in the breath samples of healthy persons (*c*) and EGC (*b*) and AGC (*a*) patients (**d**); principal component analysis (PCA) of the data set of biomarker patterns of healthy persons (*c*) and EGC (*b*) and AGC (*a*) patients (**e**) obtained by using the mentioned bands; SERS spectra of simulated and real breath samples of healthy persons (*c*, *c*′) and EGC (*b*, *b*′) and AGC (*a*, *a*′) patients (**f**); PCA analysis of the data set of simulated and real breath samples of healthy persons (*c*, *c*′) and EGC (*b*, *b*′) and AGC (*a*, *a*′) patients (**g**) (Adapted with permission from Chen et al. [43]. Copyright © 2016, American Chemical Society)

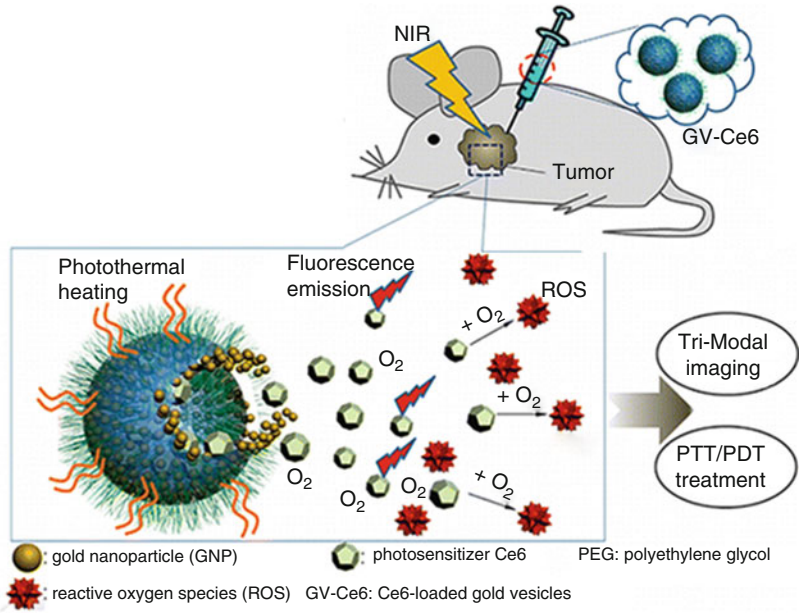

Fig. 1.12 Scheme of the preparation of sandwich assay for CEA protein detection (Adapted with permission from Lin et al. [35]. Copyright © 2013, American Chemical Society)

centrifugation of the mixtures. The resultant nanostructures were tested and characterized regarding their SERS, near-infrared spectroscopy, fluorescence, thermal, and photoacoustic properties. Moreover, it was found that laser irradiation causes them to break and to be easier cleared from the organism [208]. Additionally, during the experiments there was no significant inflammation observed in the heart, liver, spleen, lung, and kidneys, suggesting low cytotoxicity and high biocompatibility of the Au vesicles [208]. Therefore, these nanostructures are thought to represent a potentially interesting tool for cancer identification.

In a different study, the detection of the breast cancer-specific biomarkers epidermal growth factor receptor (EGFR), CD44, and transforming growth factor beta receptor II (TGFbRII) in mice was also reported [36]. To achieve this, three different reporter molecules were immobilized on the surface of commercially available 60 nm SERS NPs: malachite green isothiocyanate (MGITC), Rh6G, and Cy5. For this, solutions of 10 mM lipoic acid (LA) linker modified with Cy5, 10 mM malachite green isothiocyanate (MGITC), and 50 mM Rh6G were separately mixed with the AuNPs in a v/v ratio of x/x for 20 min. Subsequently, PEG encapsulation for antibody conjugation and protection of the nanotags was performed. Next, the carboxylic acid functional groups were activated on the surface of the resulting nanostructures by the EDC and sulfo-NHS coupling reaction. Finally, an anti-EGFR antibody was allowed to react with the activated Rh6G

nanotag, an anti-CD44 antibody with the malachite green isothiocyanate (MGITC) nanotag, and an anti-TGFbRII antibody with the Cy5 nanotag, for 2 h at 25 °C, and the samples were incubated overnight at 4 °C. Although the overall NP preparation was rather long (approximately 6 h of actual preparation time plus an overnight incubation at 4 °C), the achieved multiplexing efficiency makes the resulting NPs a potentially interesting structure. Moreover, the NP clearance by the liver and spleen was evaluated by monitoring the SERS signals in these organs for more than 72 h [36], and it was concluded that they are eliminated from the organism within 72 h from their intra-tumoral injection.

Regarding NP biocompatibility and clearance time in mice, the study of Zeng et al. [37] shows that the Ag@Au-DTTC nanostars prepared and used during the experiments had a negligible effect on tumor volume and overall body weight in mice for a period longer than 16 days (Fig. 1.13). Moreover, no inflammation in the heart, liver, spleen, lung, kidney, or intestine tissue was observed during the study. In this study, the NPs were injected through the tail vein and not directly at the tumor site. An additional study was carried out to compare the use of Ag@Au-DTTC nanostars, PBS, PBS + NIR, Ag@Au-DTTC, and Ag@Au-DTTC + NIR, and the results are summarized in Fig. 1.13. The NIR addition in the names of the different systems was used by the authors to denote that an 808 nm laser was applied for the excitation of the NPs instead of the 785 nm laser used in all other cases. Ag@Au-DTTC nanostars were prepared starting from simple, 20–30 nm Ag NPs by adding dropwise deionized water and 0.1 mM DTTC under stirring. This led to the formation of Ag-DTTC NPs, which were further mixed with 0.1 M HCl and 2.5 mM $HAuCl_4$ aqueous solutions. Then, 10 mM $AgNO_3$ and 100 mM ascorbic acid (AA) were added under vigorous stirring. Next, 0.1 mM DTTC was dropped into the NPs for the second time, while stirring, and the reaction was maintained for 10 min. Here, the addition of $AgNO_3$ was performed to generate anisotropic Au nanostars. Finally, the resulting Ag@Au-DTTC nanostars were modified with mPEG-SH by adding 2 mM mPEG-SH to the Ag@Au-DTTC nanostars under stirring and allowing them react for 30 min. Subsequently, the nanostarts were washed, redispersed in deionized water, and used for measurements.

While a few studies are introduced here, many others are available in the literature. Cancer detection is a high-interest topic, and much effort is directed toward developing methods for the reliable detection of cancer biomarkers present at low concentrations, especially at early stages of the disease.

5.3 Pathogen Detection

The early diagnosis of medical conditions caused by viruses and parasites is highly needed, especially in the cases where treatment administration during the early stage of the disease is crucial. For example, communal transmission of malaria and full recuperation of patients infected with the apicomplexan parasite *Plasmodium* species are guaranteed only when medication follows early detection. Hemozoin, a crystalline insoluble precipitate present in the red blood cells (RBCs), is considered to be a

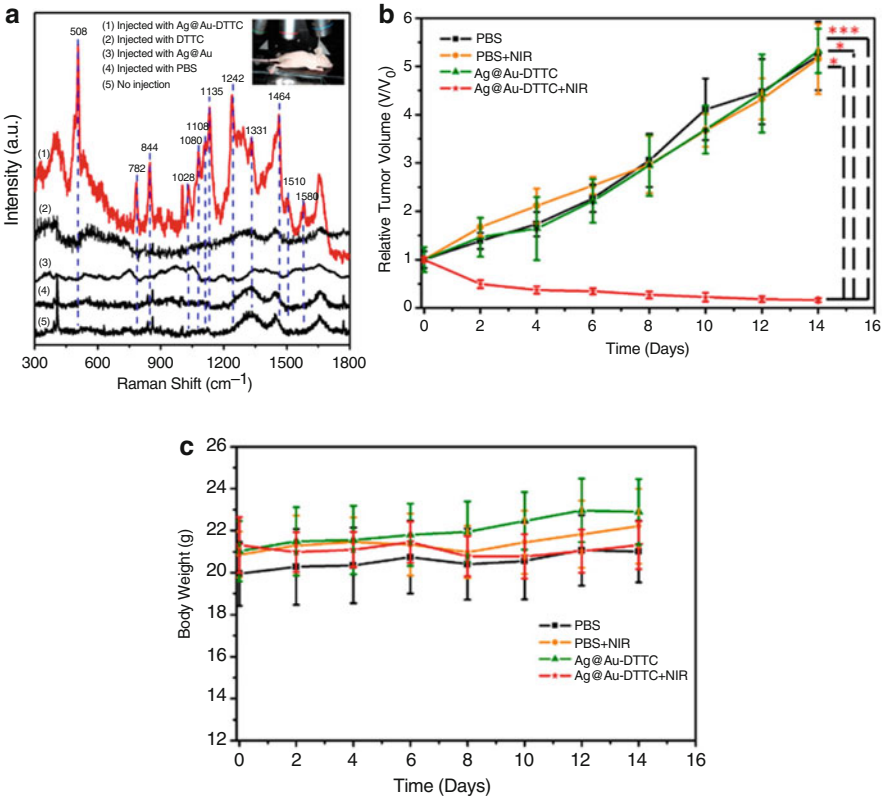

Fig. 1.13 In vivo SERS spectra of tumor-bearing mice in the control and injected with PBS buffer, Ag@Au, pure DTTC, and Ag@Au-DTTC nanostars under the excitation of a 785 nm laser (**a**); the change of relative tumor volume in different groups of PBS (under the excitation of a 785 nm laser), PBS + NIR (under the excitation of a 808 nm laser), Ag@Au-DTTC (under the excitation of a 785 nm laser), and Ag@Au-DTTC + NIR (under the excitation of a 808 nm laser) (**b**); the change of body weight in different groups of PBS, PBS + NIR, Ag@Au-DTTC, and Ag@Au-DTTC + NIR (**c**) (Adapted with permission from Zeng et al. [37]. Copyright © 2015, American Chemical Society)

biomarker for malaria diagnosis. The reference method for its detection is based on visual examination of light microscopy images of Giemsa-stained blood smears. However, a considerable amount of hemozoin precipitates have to be present in the sample in order to diagnose malaria with this method. Nevertheless, hemozoin is produced in the RBCs already during the earliest stages of the parasite lifecycle. In a period of 48 h, the parasite transitions from the merozoite stage to the ring and trophozoite stage, and then it matures to the schizont stage. During this time, the parasite digests up to 75% of the available hemoglobin, and it produces the crystalline, insoluble hemozoin. The compound is highly paramagnetic, and it has a strong Raman fingerprint, as it can be seen in Fig. 1.14. Because hemozoin is a product of hemoglobin digestion, most of the Raman bands are identical for the two molecules.

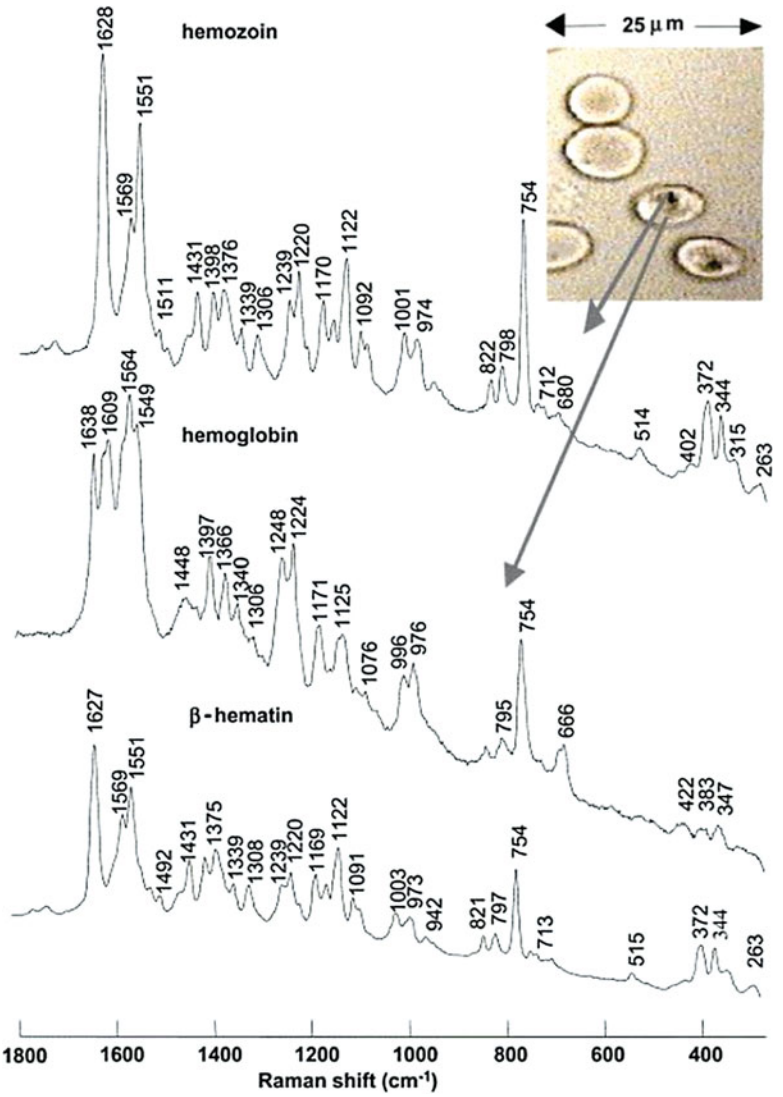

Fig. 1.14 Photomicrograph of *P. falciparum*-infected erythrocytes in the late trophozoite stage, showing vacuoles containing hemozoin. The Raman spectrum of β-hematin, a structurally identical, synthetic composite of hemozoin, is also depicted (Reprinted from Wood et al. [209] with permission from John Wiley and Sons. Copyright © 2003, American Chemical Society)

SERS, owing to its high sensitivity, can easily determine hemozoin at low concentrations, and multiple studies have reported the successful detection of the precipitates in lysed blood samples, infected RBC, or human blood, even at single parasite level [210–213]. For example, Garrett and coworkers used gold-coated butterfly wings for the detection of the malarial hemozoin pigment in the early

ring stage in lysed blood samples containing 0.005% and 0.0005% infected RBC [210]. However, because the surface of the substrate was not functionalized, hemozoin deposition from the cell lysate was random. The detection of the parasite at a concentration of 0.0005% infected RBC was achieved only by manually selecting the measurement spots on the SERS-active surface. This is a time-consuming approach, and it is not feasible for real-time measurements of a high number of samples. In another study, Chen et al. [211] performed detailed SERS investigations of normal and infected RBCs at different stages of infection. By using multivariate statistics based on principle component analysis, the authors were successful in discriminating between ring, trophozoite, and schizont stages of infected RBCs from normal RBCs. The changes observed in the SERS spectra were associated with changes of the cell membrane. Namely, during the life cycle of the parasite, the host cell plasma membrane displays a significantly decreased content of cholesterol and sphingomyelin, and an increased ratio of phospholipid to cholesterol, while a large number of proteins are exported. In this study, silver nanorods were fabricated via the oblique angle deposition method on glass microscope slides, and they were used for enhancing the weak Raman spectrum. In a recent study, Chen and coworkers reported a procedure confirming that the source of the measured SERS signal originated from a single parasite in the ring stage [212]. In order to do this, silver NPs were synthesized directly inside the parasites to ensure close proximity between the NPs and the target molecules and to avoid the necessity of lysing the parasites. Specifically, following lysis of blood cells from the infected sample, the lysate was re-suspended in $AgNO_3$ solution. Triton X-100 was mixed with hydroxylamine hydrochloride, and it was added dropwise to the $AgNO_3$ solution containing the sample. The resulting solution was smeared on glass slides covered with aluminum foil and measured with a Raman spectrometer. With the help of bright field microscopy images and the SERS spectra, the authors showed that the measurements were carried out on a single parasite level. On the basis of all the studies described above, it is clear that SERS is very promising for early malaria diagnosis. However, further work is required to design reliable platforms that can be affordable for developing countries.

Hepatitis B can lead to liver cirrhosis and hepatoma; during the last years, proteins, antibodies and antigens, and specific DNA sequences have been considered as hepatitis B biomarkers. As already demonstrated in the previous sections, the combination of immunoassays, microfluidics, and SERS yields fruitful synergy, and it was also applied for the detection of hepatitis B virus antigen (HBsAg) in human blood plasma [214]. In Fig. 1.15, the working principle of a microfluidic SERS-based immunoassay is depicted. GaN/Au-Ag was used as the capturing substrate. The substrate was modified with 6-amino-1-hexanethiol to form amino-terminated linkages. The thiolated metallic substrate was placed in the measuring chamber of the microfluidic chip fabricated on polycarbonate. A mixture of a hepatitis B virus monoclonal antibody (anti-HBsAg) and an activation solution was injected via one of the inlet ports. After 1 h, the remaining active surface was blocked by BSA, and the antibody-immobilized substrate was stored at 4 °C until the measurements were performed. The Raman reporter molecule, basic fuchsin, was designed to chemisorb

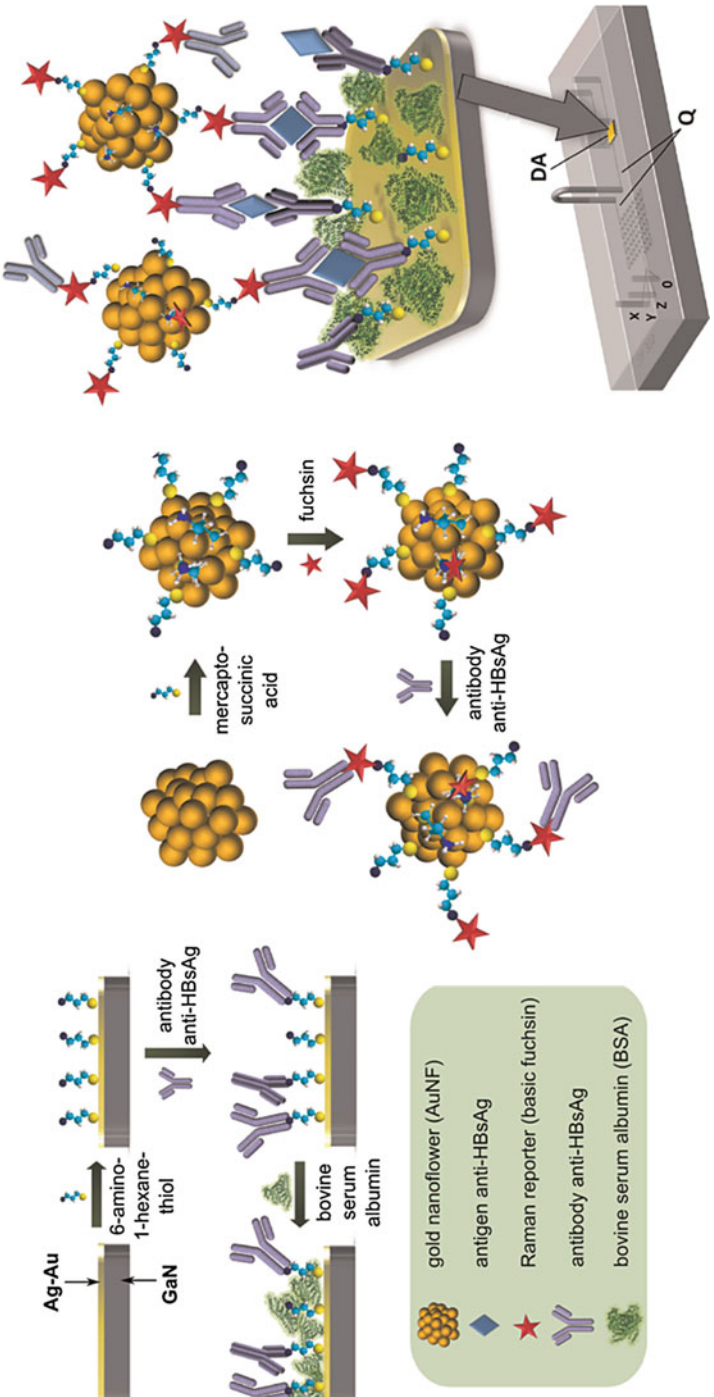

Fig. 1.15 Sequential steps for the formation of the microfluidic SERS-based immunoassay platform: capturing substrate preparation (GaN/Au-Ag modified with a thiol layer and anti-HBsAg), Raman reporter-labeled Au nanoflowers modified with anti-HBsAg, SERS detection of the sandwich interection, and integration of the assay within a microfluidic chip (Adapted from Kaminska et al. [214] with the permission of Elsevier. Copyright © 2014 Published by Elsevier)

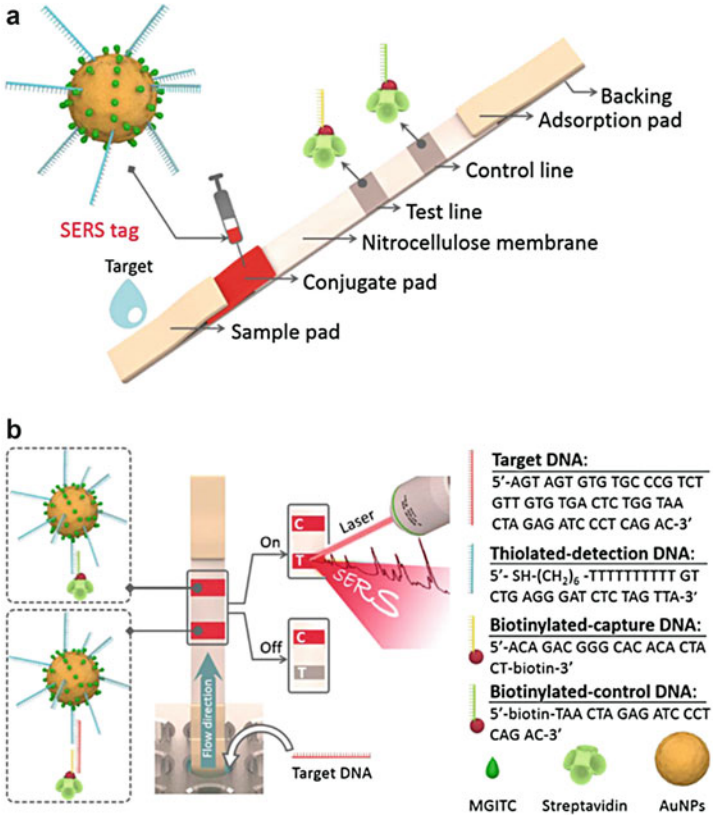

Fig. 1.16 SERS-based lateral flow assay for the quantification of HIV-1 DNA (Reprinted from Fu et al. [44]. Copyright © 2015 Elsevier B.V., with permission from Elsevier)

on thiol-modified gold nanoflowers and to covalently bind to the antibody via a terminal amino group. For the measurements, human blood samples from ten healthy volunteers were spiked with HBsAg in different concentrations. The samples were injected via the Y inlet, while the antibody-modified Raman reporter-labeled nanoflowers were supplied via the Z inlet of the microfluidic chip. After 3 min, the flows were stopped and for 30 min all reagents were incubated in the detection area of the microfluidic chip to generate the sandwich immunocomplex, which was then measured by Raman spectroscopy. A calibration curve was obtained from the SERS intensity of the Raman marker band of fuchsin. HBsAg was successfully detected at concentrations as low as 0.01 IU/ml (0.2 ng/ml corresponds to 0.05 IU/ml) with a relative standard deviation of less than 10%. In addition to this study, hepatitis B virus was also detected by employing plasmonic nanorice antennae on triangle nanoarrays [215] and spatially reinforced nano-cavity arrays [216]. A SERS-based lateral flow assay biosensor for the highly sensitive (down to 0.24 pg/ml) detection of human immunodeficiency virus (HIV-1) DNA was described by Fu and coworkers, and it is depicted in Fig. 1.16 [44]. The working principle of the platform

can be described as "DNA-conjugated Au NPs target DNA-capture DNA." Namely, on the nitrocellulose membrane, streptavidin-biotinylated capture DNA, which is complementary with a part of the target DNA, and streptavidin-biotinylated control DNA were immobilized at the test and control line, respectively. The control DNA was complementary with the detection DNA probe immobilized on the malachite green isothiocyanate (MGITC) functionalized Au NPs. The MGITC Au NPs were dispersed on the conjugated pad, which was designed to bind specifically the target DNA. The sample was applied on the sample pad and diffused toward the absorption pad due to capillary action. When the sample crossed over the conjugate pad, the target DNA, if it was present in the sample, and the detection DNA immobilized on the Au NPs hybridized to form a complex. The immunoassay complexes reaching the test line were captured by the DNA probe present there based on a second hybridization step between the target DNA and the capture DNA, yielding sandwich complexes. Finally, the excess DNA-conjugated Au NPs reached the control line and were captured by the probe DNA pre-immobilized on the strip. For quantitative analysis, SERS spectra were recorded at the test line with a bench top Raman spectrometer. The Raman characteristic bands of the Raman label molecule, MDITC, were considered for analytical performance assessment. The authors claim that a detection limit of 0.24 pg/ml was achieved based on the IUPAC regulations for LOD calculation. However, the lowest concentration that could be measured was 8 pg/ml, and it showed only low-intensity Raman bands. For an accurate estimation, measurements of solution with lower concentrations of HIV-1 DNA would be required. Furthermore, future experiments testing the feasibility of the platform to detect the target DNA in biological fluids instead of pure solvent are expected. As a simplified sample preparation protocol is of high interest for point-of-care applications, it will have a major impact on the commercialization of the device.

With more than 50 known species that can be easily spread through the air as aerosols, *Legionella* can rapidly infect a large number of people. As main clinical symptoms, acute fever appears after a short incubation period, followed by pneumonia symptoms. Therefore, rapid identification of *Legionella* is important. The study by Jing et al. [51] focuses on the discrimination between virulent and weak *Legionella* strains in five commercially available *Legionella* species (*ATCC33152 L. pneumophila*, strong virulence; *ATCC33156 L. pneumophila*, strong virulence; *ATCC43878 L. brunensis*, weak virulence; *ATCC35249 L. spiritensis*, weak virulence; and *ATCC35252 L. cherrii*, weak virulence) and three *L. pneumophila* strains (*strain 1*, strong virulence; *strain 2*, strong virulence; and *strain 3*, weak virulence) isolated from different samples. For this, the different *Legionella* strains were measured by SERS, using Au-tiopronin NPs. For the preparation of these NPs, Au NPs were first prepared by the standard citrate reduction method followed by seed growth by first mixing 0.24 ml of 15 nm Au NPs with 2.49 ml 10 mM $HAuCl_4 \cdot 3H_2O$ solution with stirring and then adding 100 ml 0.4 mM ascorbic acid at a 10 mL/min rate. Finally, excess tiopronin solution was added and allowed to react. The resulting NPs were washed and added to the *Legionella* colonies as follows: each grown colony was picked into a clean microslide onto which 5 μl NPs were added and incubated for 5–10 s before performing the SERS measurements. The results

obtained upon PCA analysis denote the potential of differentiating between *Legionella* species based on their virulence and support the notion that this technique could be further developed into an analytical tool for both environmental and medical applications.

Wu et al. [217] used a SERS Ag nanorod array substrate, fabricated by the oblique angle deposition (OAD) technique, to analyze and differentiate 27 different bacteria species, strains, and serotypes isolated from chicken carcass rinses (denoted USDACR in Fig. 1.17), patients from a medical center (denoted WRAMC in Fig. 1.17), and patients from an army medical center (denoted BAMC in Fig. 1.17. For the substrate fabrication, a glass slide was first cleaned and then positioned perpendicular to the incident vapor direction for the deposition of a 20 nm titanium film followed by a 200 nm silver film. The substrates were then rotated to an angle of 86° with respect to the incident vapor, resulting in the growth of Ag nanorods. Rods of two different thicknesses were created: 2000 nm for pristine Ag nanoroads and 800 nm for vancomycin (VAN) Ag nanoroads. Finally, the 800 nm Ag nanorods were immersed into a 1 mM vancomycin solution to achieve VAN functionalization of the 800 nm for VAN Ag nanorods. For the measurements, either a 2 ml droplet of a sample containing a single bacterial species was applied to the pristine Ag nanorod substrate or the VAN Ag nanorod substrate was immersed in 2 ml of the single-species bacterial culture for 2 h, rinsed with DI water, and measured. Upon statistical analysis of the data, different visualization procedures were tested. As shown in Fig. 1.17, it was possible to differentiate between gram-negative and gram-positive bacteria, but it was still challenging to differentiate between different serotypes of the same bacteria species.

The same SERS-active substrates were also used for the differentiation of patients infected with *Pseudomonas aeruginosa* (denoted PA+ in Fig. 1.18) and *Staphylococcus aureus* (denoted PA+/SA+ in Fig. 1.18) or patients that tested negative for *Pseudomonas aeruginosa* infections (denoted PA- in Fig. 1.18), by analyzing sputum samples [218]. Since the target analyte for *Pseudomonas aeruginosa* identification was the redox-active blue green pigment pyocyanin (PCN), PCN was extracted from sputum samples by mixing 100 μL of processed sputum with 50 μL of chloroform and then refrigerate the mixture for 2 min. Subsequently, the chloroform layer was transferred to a new tube, a 1 μl droplet of the sample was dropped on the SERS-active substrate, the contaminants on the substrate surface were removed using Ar^+ plasma generator, and the substrate was dried inside a plasma generator chamber and measured by SERS. The LOD for the SERS detection of PCN in aqueous solution was detected to be 5 ppm (2.38×10^{-8} M). This information was used together with the calibration curve obtained by measuring chloroform-treated sputum control samples spiked with different concentrations of PCN (reproduced in Fig. 1.18a) to predict the presence of *Pseudomonas aeruginosa* in patient sputum samples and to classify the patients based on this information. Upon measuring 15 patient sputum samples and using the mentioned calibration curve, it was found that the concentration of PCN ranges from 18.7 to 64.9 ppb in the PA+ samples, from 5.1 to 21.5 ppb in the PA+/SA+ samples, and from 1.1 to 2.9 ppb in the PA− samples (Fig. 1.18b). Considering that the LOD for detecting PCN was

A

Abbreviation	Bacteria species	Strains	Serotypes	Gram
AB1	*Acinetobacter baumannii*	ATCC 19606	N/A	–
AB2	*Acinetobacter baumannii*	ATTC BAA-1605	N/A	–
AB3	*Acinetobacter baumannii*	ATTC 17961	N/A	–
AB4	*Acinetobacter baumannii*	ATTC 19003	N/A	–
AB6	*Acinetobacter baumannii*	WRAMC #13	N/A	–
CK	*Citrobacter koseri*	USDACR	N/A	–
PP	*Pseudomonas putida*	USDACR	N/A	–
EC	*Escherichia coli*	USDACR	N/A	–
EF	*Enterococcus faecalis*	USDACR	N/A	+
ENC	*Enterobacter cloacae*	USDACR	N/A	–
KP1	*Klebsiella pneumoniae*	IA-525	N/A	–
KP2	*Klebsiella pneumoniae*	BAMC 07-18	N/A	–
KP3	*Klebsiella pneumoniae*	Xen-39	N/A	–
PA1	*Pseudomonas aeruginosa*	Xen-41	N/A	–
PA2	*Pseudomonas aeruginosa*	PA 01	N/A	–
SalE	*Salmonella entericat*	USDACR	Enteritidis	–
SalH	*Salmonella enterica*	USDACR	Heidelberg	–
SalI	*Salmonella enterica*	USDACR	Infantis	–
SalK	*Salmonella enterica*	USDACR	Kentucky	–
SalT	*Salmonella enterica*	USDACR	Typhimurium	–
SA1	*Staphylococcus aureus*	IQ 0070	N/A	+
SA2	*Staphylococcus aureus*	Xen 40	N/A	+
SA3	*Staphylococcus aureus*	ATCC 33591	N/A	+
SA4	*Staphylococcus aureus*	TCH 1516	N/A	+
SA5	*Staphylococcus aureus*	USDACR	N/A	+
SH	*Staphylococcus hyicus*	USDACR	N/A	+
SK	*Staphylococcus kloosii*	USDACR	N/A	+

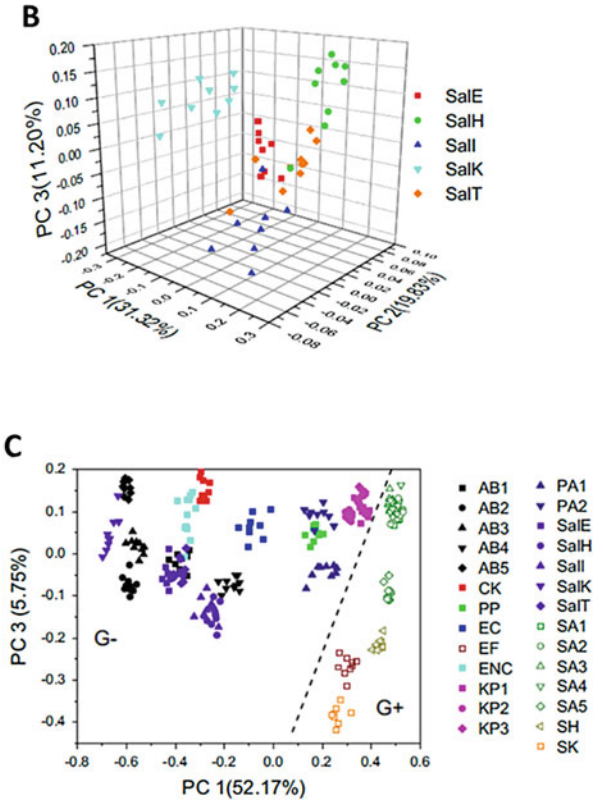

Fig. 1.17 (continued)

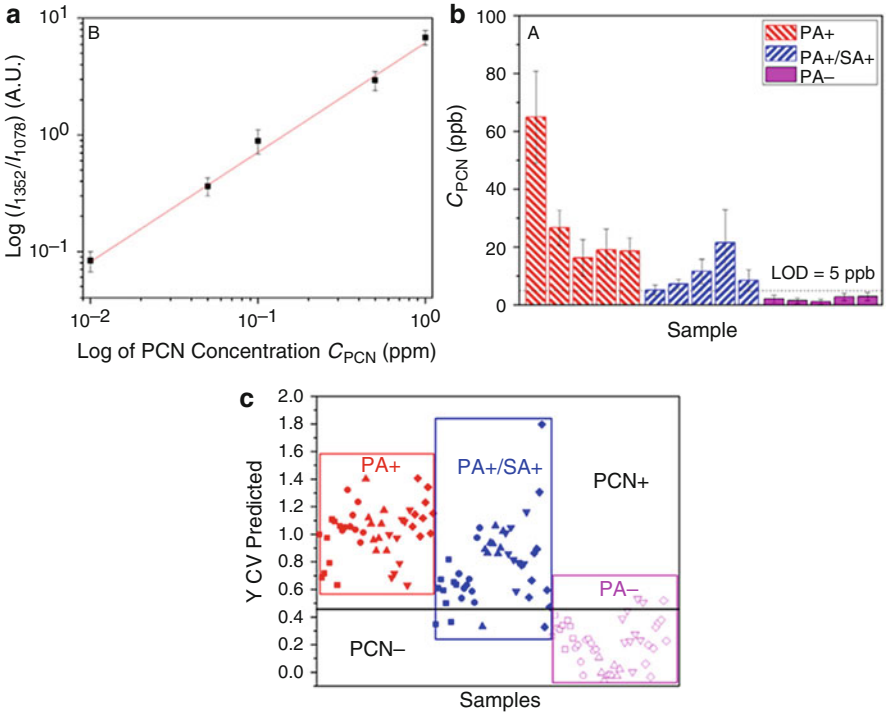

Fig. 1.18 Intensity ratio of two peaks belonging to PCN in the PCN-spiked sputum samples (**a**). Estimated PCN concentration in clinical sputum samples (**b**). PLS-DA plot of SERS spectra of the clinical sputum samples (**c**) (Reprinted from Wu et al. [218]. Copyright © 2014 Elsevier Inc., with permission from Elsevier)

5 ppm, the authors concluded that the patients in the PA− group were not infected by *Pseudomonas aeruginosa*. However, to better visualize and confirm this result, the authors also performed PLS-DA analysis on the measured data, and the results are also reproduced in Fig. 1.18c. Considering that by using the chloroform extraction procedure introduced by Wu et al. [218] the total experimental work time is approximately 5 min, this represents a promising analytical approach.

Rapid identification of bacteria has also been reported in the case of urinary tract infections and the detection of *E. Coli*, *Enterococcus faecalis*, *Staphylococcus*

Fig. 1.17 Bacteria species, strains, and serotypes isolated from chicken carcass rinses (denoted USDACR), from patients at a medical center (denoted WRAMC), and from patients at an army medical center (denoted BAMC) used during the measurements (**a**). 3D PCA score plot differentiation of five different serotypes of *Salmonella* species based on the chemometric analysis of the SERS spectra (**b**). Partial least squares discriminant analysis (PLS-DA) score plot: gram-positive (G+) bacteria are indicated as unfilled symbols, and the gram-negative (G-) bacteria are indicated as filled symbols (**c**) (Reprinted from Wu et al. [217]. Copyright © 2015 Elsevier B.V., with permission from Elsevier)

aureus, *Staphylococcus saprophyticus*, *Klebsiella pneumoniae*, *Staphylococcus haemolyticus*, and *Proteus mirabilis* [219]. In this case, however, a bacterial culture was required. The authors cultured the bacteria on nine different nutrient agar plates and incubated them for different times: 1, 2, 4, 6, 8, 10, 12, 18, and 24 h. At the end of each time frame, the bacteria were measured by SERS, using Ag NPs prepared according to a simple procedure introduced by Leopold and Lendl [50]. As already mentioned, it was found that a 1-h incubation was enough to discriminate between the different bacteria.

Differentiation of the *Mycobacterium tuberculosis* complex (MTC), including *M. tuberculosis*, *M. bovis BCG*, *M. canettii*, *M. abscessus*, and *M. szulgai*, was attempted using a bead-beating module in combination with a lab-on-a-chip SERS (LoC-SERS) system [90] and NPs prepared according to the Leopold-Lendl protocol [50]. In this study, it was found that *M. abscessus* and *M. szulgai* can be differentiated with an accuracy of 100%, whereas the bacteria in the MTC group (containing *M. bovis BCG*, *M. tb Beij*, *M. can*, and *M. tb H37Rv*) could only be differentiated as follows: *M. can* was separated from the others with an accuracy of 100%, while the separation of *M. bov BCG* and *M. tb H37Rv* only reached 75.3% by applying a principal component analysis-linear discriminant analysis (PCA-LDA) model.

As has been largely discussed in the literature, it is important to properly consider and plan the growth conditions [220] as well as the steps prior to the measurement [221] when working with cell and bacteria culture, since even small quantities of culture medium present in the sample during the SERS measurement can give rise to a strong SERS response [221] and also because more extreme culture growth conditions (i.e., starvation) can modify the main components of the cell wall. Indeed, according to a recently published study by Premasiri et al. [220], cell wall SERS spectra of bacteria that were starved before performing the measurements at 785 nm show that the cell wall is not dominated by peptidoglycan layer components such as *N*-acetyl-D-glucosamine, *N*-acetylmuramic acid, lipids, and proteins, which would be the normal cell wall composition suggested by the literature, but by molecular species such as purine phosphoribosyltransferases, enzymes that convert purine mononucleotides to purine bases. Moreover, according to this study, these purines are the result of metabolic degradation of nucleic acids and nucleotides (i.e., RNA, adenosine triphosphate, guanosine triphosphate, and other nucleotide containing molecules). They are produced when bacteria are placed in a nutrient-free environment [220]. In contrast, the cell wall SERS spectra of starved bacteria measured at 514/532 nm were nearly equivalent to those of flavin adenine dinucleotide [220]. Figure 1.19 reproduces some of the example figures presented by the authors. However, it is important to mention that the conditions of the SERS measurement play a very important role. For example, whether NPs can interact with any other part of the bacteria or whether they come in contact only with the cell wall will have an impact on the results. Also, it is important to notice whether the NPs are functionalized or not and how this induces a binding preference toward certain molecules of the cell wall. In the particular case presented above, an aggregated Au NP-covered SiO_2 SERS-active substrate was prepared by the hydrolysis of tetramethoxysilane in an acidic methanol solution of $HAuCl_4$ (containing methanol, water, and $Si(OCH_3)_4$).

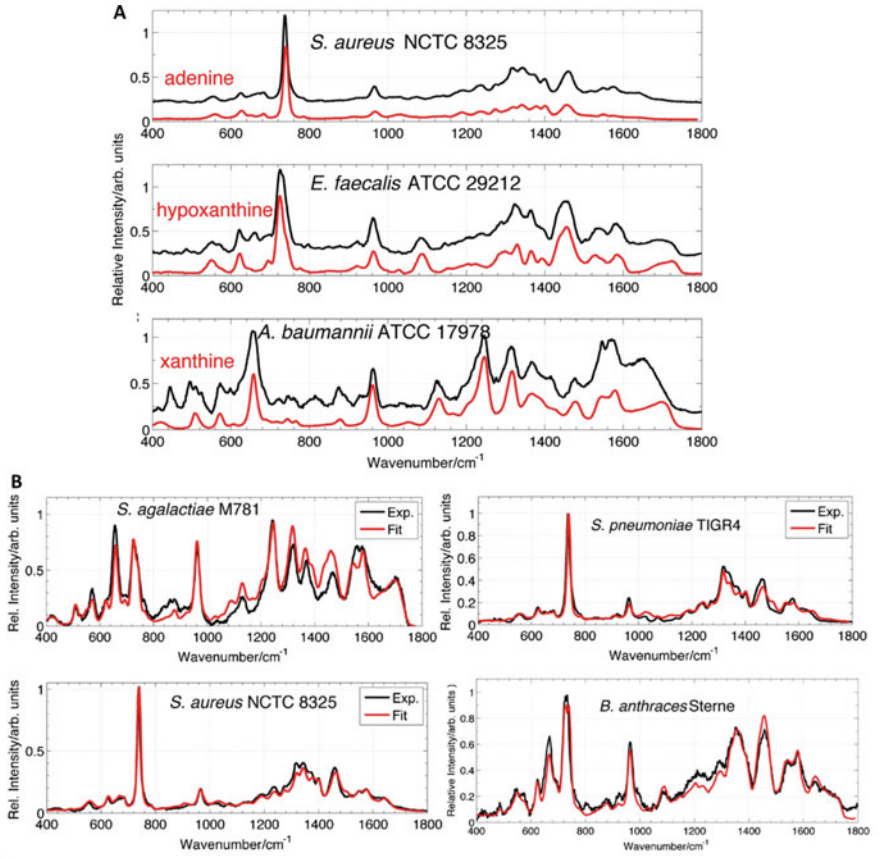

C

Organism	Source or reference	Adenine[a]	Hypoxanthine[a]	Xanthine[a]	Guanine[a]	Uric acid[a]	AMP[a]
Streptococcus agalactiae M781	ATCC	8/2	39/56	47/38	6/4	0	0
Streptococcus pneumonia TIGR4	[44]	65/62	0	3/8	0	0	32/30
Bacillus anthracis Sterne	Colorado Serum Company	27/9	45/71	0	28/20	0	0
Staphylococcus aureus NCTC 8325	[45]	75/69	0	0	8/16	0	17/15

AMP adenosine monophosphate

[a] The first number is the percent contribution of the purine component surface-enhanced Raman spectroscopy (SERS) spectrum normalized by the spectrum maximum the second number is the percent contribution scaled by the relative cross section of the purine component and is thus the relative number of purine component molecules accounting for the SERS signature

Fig. 1.19 Comparison of SERS spectra of bacterial species with model compounds (**a**). Empirically determined best fits (red) of the bacterial spectra (black) of some of the spectra shown in the left side graph of the figure (**b**). Best-fit-determined relative (%) purine contributions to the bacterial spectra on the graphs on the right upper side of the figure (**c**) (Premasiri et al. [220]. Copyright © Springer-Verlag Berlin Heidelberg 2016, with permission of Springer)

This resulted in the formation of metal-doped sol-gels, which were dried at room temperature before mixed with aqueous sodium borohydride and exposed to water-saturated air for 1 h. Subsequently, the solution was drained and the gel chips were covered with water and gently shaken for 30 min. Finally, the substrates were

incubated for 24 h in a diluted $NaBH_4$ solution for the slow growth of Au NPs. The resulting substrates were covered with a 1 μL bacteria loop and measured 2 min later [52, 220].

In the above paragraphs of this section, we presented the most promising findings on pathogen detection. Different SERS platforms were applied in these studies, starting with Leopold-Lendl colloids and microfluidic devices and reaching to SERS immunoassays and easy to prepare SERS planar substrates. Depending on the type of substrate, different measurement methods were also chosen. Both very simple measurement conditions, such as a simple mixing of the analyte with the pathogen suspension or dropping the analyte on planar substrates and measuring the resulting dried substrate, and more complicated approaches, such as microfluidic platforms, have been tested. Additionally, owing to the high resemblance of SERS spectra from pathogens belonging to the same species, statistical analysis is often required for reliable identification. Moreover, even though discrimination of pathogen species is often reported in the literature, separation of different strains belonging to one species is still challenging. However, there are numerous other reports proving the high potential of SERS for medical diagnosis of infectious diseases, and with further work carried out with clinical samples, SERS might yield a wide range of applications.

5.4 Other Fields of Application with Clinical Relevance

5.4.1 Therapeutic Drug Monitoring

The cost of medical treatments could be significantly lowered, while the patient outcome could be considerably improved, by the practice of personalized medicine. Therapeutic drug monitoring is of especially high value, as several drugs have a narrow therapeutic range and the concentration of the active agent in the human body strongly varies among individuals. Currently, different physiological indices (lipid concentrations, blood glucose, blood pressure) are routinely used to monitor the pharmacological response and determine the pharmacokinetic and pharmacodynamic characteristics of drugs. However, there are many drugs with insufficiently sensitive or no direct indicator of their therapeutic response. In these cases, therapeutic drug monitoring relies on measurements of the concentration of the prescribed xenobiotic that, with an appropriate interpretation, could directly influence the prescribing procedure and lead to the desired clinical outcome [222].

In clinical chemistry, the determination of drug levels in biological fluids is performed by methods based on chromatographic separation or immunological assays [98, 101, 223–230]. The first approach offers great specificity and sensitivity for, theoretically, all existing drugs, but it is mainly available in reference clinical laboratories and academic centers because of the high initial financial investment required. On the other hand, immunological assays (or immunoassays) are easy to integrate in a clinical setting, but they are available for only a limited number of drugs because they require specific antibodies. In recent years, multiple SERS studies for the determination of various drugs at clinically relevant concentrations in biological fluids were reported. Thanks to the high sensitivity of the method and

the narrow Raman bands, SERS is optimal for the determination of trace amounts of molecules in complex matrices. Although SERS cannot compete with chromatography for sensitivity and specificity in an academic lab setting, it finds its place in on-field applications and near-patient settings thanks to the development of high-performance portable and handheld Raman setups.

Anticancer drugs are notorious for their toxic effects when their concentration in the human body exceeds their therapeutic range. Methotrexate is generally administered at high doses (5000 mg/week) for cancer therapy. However, its action is not restricted only to cancerous cells, and a concomitant administration of leucovorin is recommended to avoid side effects. According to most medical guidelines, a plasma methotrexate concentration $\leq$0.2 μM allows the clinician to stop leucovorin administration [231]; 42 h after the start of methotrexate infusion, the target concentrations are $\leq$1 μM, while high-risk toxic effects are associated with concentrations $\geq$10 μM [232]. The direct, quantitative determination of methotrexate in diluted human serum samples spiked with different concentrations of the target drug was achieved by employing gold NP deposited on paper as SERS-active substrate [233, 234]. Specifically, a mixture of citrate-reduced gold NPs and sodium citrate, used as aggregation agent, was added to a glass vial containing a 1 cm^2 filter paper at the bottom. After 1 week, all particles were deposited on the surface of the paper. The supernatant was removed, and the paper was dried in air and stored in Milli-Q water. The relative standard deviation of the SERS signal from different analytes measured with substrates from different batches was 15%. Relative standard deviations of 10–20% are commonly reported in SERS studies and have their origin in the low homogeneity of hot spots on the solid SERS-active substrate and on the random orientation of the molecules on the metallic surface. Nevertheless, the SERS community is continuously aiming at improving this and increasing the reliability of the SERS measurements. For the determination of methotrexate with the abovementioned SERS-active substrate, calibration standards were prepared by spiking drug-free human serum with different amounts of methotrexate stock solutions. The final concentration of the drug in the fivefold diluted serum was 0.1–300 μM. The data were evaluated by employing chemometric methods, and the used model yielded a root mean square error of prediction of 31.57 μM, with an R^2 linear regression coefficient of 0.63. These values show that the method yields poor predictions, emphasizing the challenge of quantitative SERS measurements. Paclitaxel, another highly antineoplastic active drug against a wide spectrum of human malignancies, was also detected by SERS in blood plasma using microwave-treated gold film polystyrene beads [235]. Although the concentration window where the drug was detected was narrower than that of the previous case (10^{-8}–10^{-7} M), the accuracy was considerably higher (3.8×10^{-9} M). The authors attributed this great accuracy to the direct absorption of the molecule on the metallic surface owing to its high chemical affinity. However, as in the preceding case, the authors had to dilute the paclitaxel/blood mixture with ethanol to reduce strong matrix effects.

Clinical guidelines for antibiotic administration are most often derived from dose-establishing clinical trials carried out with healthy volunteers instead of patients. However, it was demonstrated that fix-dose administration will fail in the case of

patients in the intensive care unit [236]. Therefore, it is of high interest to determine the actual concentration of the active drug in the human body in order to guarantee treatment success and avoid the emergence of antibacterial resistances. The aminoglycoside tobramycin [237], the fluoroquinolone levofloxacin [42, 238], and nitroxoline [89] were successfully detected by SERS. A 1000-fold dilution of human serum samples spiked with tobramycin was required prior to SERS detection with Au NPs prepared according to the traditional citrate reduction protocol and modified with dithiobis-(2-nitrobenzoi acid) as a Raman reporter. Unfortunately, the authors did not carry out quantitative measurements, but the intense Raman spectrum recorded at 4 μM shows great promise for further studies.

SERS is a great analytical method owing to its specificity and sensitivity. However, it is challenging to achieve reproducible and automated measurement conditions. The synergy between microfluidic platforms and SERS can overcome this limitation, as demonstrated in numerous reports [60–68]. Hidi et al. took advantage of a droplet-based SERS microfluidic platform and conducted measurements on human urine samples collected from patients and healthy donors [42, 89]. As none of the donors had previously taken levofloxacin or nitroxoline, the two antibiotics were artificially added to the sample. In this way, the influence of the complex matrix on the SERS signal of the target molecules was carefully characterized. The authors first demonstrated that the two antibiotics can be successfully and reliably quantified in the complex matrix by employing silver NPs prepared at room temperature. Specifically, urinary levofloxacin concentrations in the range of 0.1–1 mM and urinary nitroxoline concentrations in the range of 3–42.8 μM were detected with a good linear response, covering the clinically relevant concentration window. The distinct detection regions for the two antibiotics were explained based on the different chemical affinity of the two molecules for the metallic surface. The detection limit for levofloxacin dissolved in high purity water was found to be 0.8 μM, whereas that for nitroxoline was 2.5 μM. The latter antibiotic showed a clear preference for binding on the metallic surface, as its detection limit was not significantly affected by the complex matrix, and this facilitated its detection.

Most of the reported SERS studies confirm that the technique can offer quantitative measurements under well-controlled, known conditions; however, very seldom the concentration of the target molecules is determined in patient samples containing an unknown amount of the molecules. This has numerous reasons. First, the chemical composition of the clinical samples varies strongly between patients, or even between samples collected from the same patient at different time points. Therefore, if no thorough sample cleanup procedure is applied, quantification based on previously established calibration curves will fail, as the SERS signal is very sensitive to the chemical species present in the sample. Second, the low batch-to-batch reproducibility of metallic NPs also inhibits the traditional quantification procedure, as signals measured with NPs of different batches cannot be reliably compared. To overcome these drawbacks, the SERS community directed its attention toward the standard addition method (SAM) [91, 239–242]. Here, all analytical measurements, including the calibration curve, are performed using the sample itself, and the slight variation between colloid batches will have no impact on the final results.

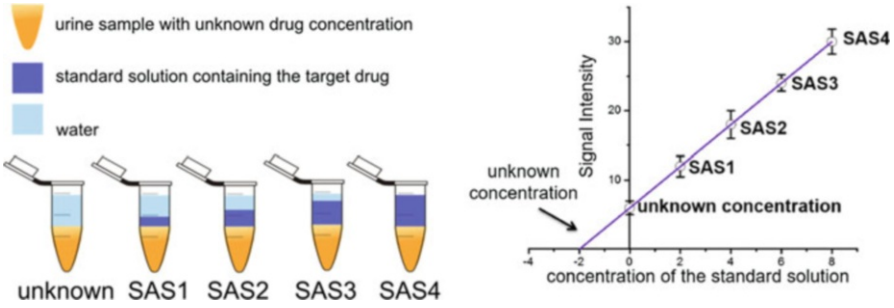

Fig. 1.20 The principle of the standard addition method: (1) equal amounts of the sample are pipetted into several volumetric flasks, (2) increasing volumes of the standard solution are added to each flask, and (3) the content of each flask is diluted with water to the same volume. The signal intensity for all flasks is measured and plotted. The intercept of the linear regression with the x-axis will give the concentration of the analyte in the unknown sample

The SAM experiments are carried out as follows: (1) equal amounts of the sample are pipetted into several volumetric flasks, (2) increasing volumes of standard are added to each flask, and (3) the content of each flask is diluted to the same volume (Fig. 1.20). Therefore, every flask contains the same concentration of the unknown sample and different concentrations of the standard solutions, which contain the same analyte as the one to be quantified. The number of flasks minus one represents the number of the standard addition steps (SAS). The signal intensity from all flasks is measured and plotted as shown in Fig. 1.20. The data are fitted by linear regression, and the x-axis intercept gives the analyte concentration in the unknown sample, which is the ratio between the intercept at $y = 0$ and the slope of the regression. By combining this method with microfluidic SERS measurements and multivariate statistical analysis, the authors were successful in determining the unknown concentration of nitroxoline in four simulated clinical samples. In the repots described above, sample dilution was carried out in order to reduce interference from the matrix molecules. Nevertheless, in a recent study, the β-blocker propranolol spiked into human serum, plasma, and urine was detected at physiologically relevant concentrations without the need for matrix dilution [243]. For this, the authors employed silver NPs synthesized according to the Lee-Meisel citrate reduction method and multivariate data analysis. In this study, stock solutions of the drug were prepared directly in the biological fluids, and serial dilutions of propranolol with each biological fluid of interest were then performed using these stock solutions in the range of 0–120 μM. In the case of the plasma samples, proteins were removed by centrifugation prior to the measurements. Metallic NPs were mixed with the samples in a 1:1 ratio, and 0.5 M sodium chloride was used as aggregation agent.

Principal component analysis of the SERS spectra demonstrated a clear differentiation between pure biofluids and biofluids spiked with varying concentrations of the target drug. To provide quantitative results, the authors used the partial least square regression method. The limit of detection for propranolol was estimated to be 0.45 μM, 0.53 μM, and 0.57 μM for serum, plasma, and urine, respectively. The

reported results showed a linear response in the 1–10 μM range for serum, 10–100 μM range for plasma, and 10–120 μM for urine. In conclusion, the authors were successful in detecting the target molecule in various biofluids with conventional silver NPs, demonstrating the high potential of SERS.

Finally, in two recent studies, approaches based on a vertical-flow paper system [244] and hierarchical zwitterion-modified SERS platforms [245] were reported and were used successfully for the detection of various drugs owing to the inhibition of substrate fouling by the components of the matrix. In the first approach, a sample droplet was applied to a membrane selected to trap serum components while transmitting the drug 5-fluorocytosine. An inkjet-fabricated paper-based SERS sensor was placed below the filtering membrane. In this way, large molecules from the serum were trapped, while the target molecule could interact with the metallic surface. The SERS signal was measured with a portable Raman spectrometer. This, and the fact that the no additional apparatus was required for sample cleanup, is very promising for bedside applications. However, it would be interesting to see the platform extend to whole-blood samples and to the determination of drug levels in clinical samples. Concerning the analytical performance of the platform for 5-fluorocytosine spiked into human serum, a limit of detection of 93 μM and linearity up to 1.16 mM were reported by the authors. An alternative strategy to avoid substrate fouling and to trap the target analytes was reported by Sun et al. [245]. In this study, the authors functionalized the optofluidic platform with two different layers. The role of the first layer was to capture the target molecule via functional thiols situated in the proximity of the SERS substrate. Thus, the surface could be enriched with substances exhibiting weak surface affinity, and the SERS signal could be enhanced. The second layer consisted of non-fouling zwitterionic poly(carboxybetaine acrylamide) (pCBAA) grafted via surface-initiated atom transfer radical polymerization, and it protected the metallic surface from the proteins in whole blood. This SERS platform could detect the anticancer drug doxorubicin when spiked into plasma sample. Doxorubicin is known to be deactivated upon protein binding; hence the detection of the free drug is of clinical interest. Owing to the presence of the polymer brush on the surface of the metallic substrate, only the unbound amount of doxorubicin could get into the close proximity of the hot spots. This phenomenon was confirmed by liquid chromatography-mass spectrometry measurements. Furthermore, doxorubicin measurements were proved to be reversible by carrying out experiments whereby drug-spiked plasma was injected into the optofluidic platform, followed by injection of pure plasma after 250 s. The continuously collected SERS spectra showed that doxorubicin detection was reversible with exponential response constants of 43 and 95 s for partitioning and departitioning, respectively. Furthermore, owing to the presence of thiol layers, the authors were successful in detecting the tricyclic antidepressant amitriptyline hydrochloride and antiseizure medications carbamazepine and phenytoin at 20 μM in spiked plasma. In conclusion, the same substrate could be used for multiple drug detection, which is a very promising approach. The scientific community is looking forward for further research developments to demonstrate the quantification power of the platform applied to clinical samples.

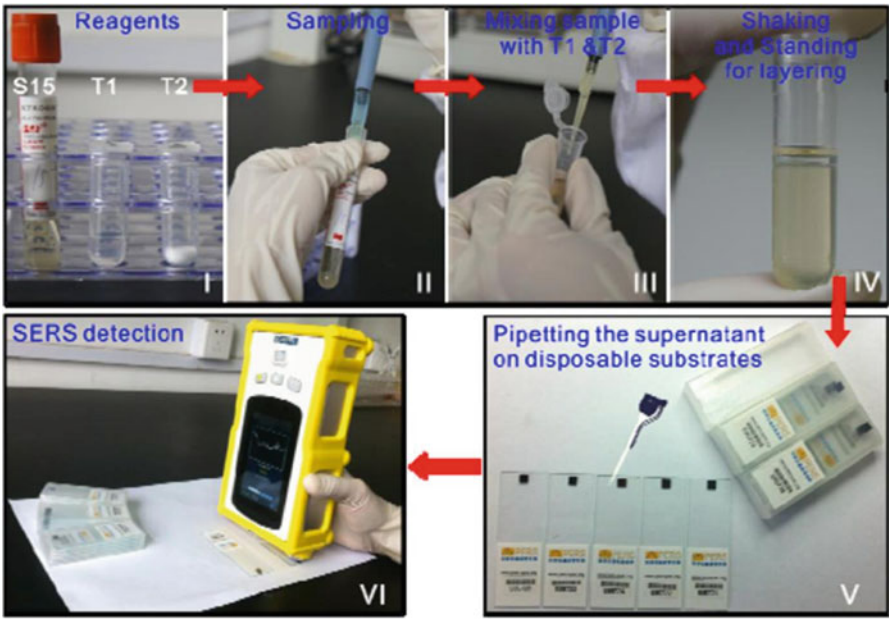

Fig. 1.21 Illustration of a portable kit for rapid SERS detection of drugs in real human urine: (*I*) the urine sample and reagents; (*II*) the sampling of certain amounts of urine; (*III*) the mixing of urine with T1 and T2; (*IV*) the layering of the mixture after fully shaking by hand; (*V*) 2 μL of the supernatant dropped and dried on 2D gold nanorods arrays, which were assembled on silicon wafer and deposited on glass slides; (*VI*) SERS detection with a handheld Raman device (Reprinted with permission from Han et al. [249]. Copyright (2015) American Chemical Society)

Although not exclusively related to the necessity of therapeutic drug monitoring, SERS was shown to be powerful also in the detection of illicit drugs. The system integration and miniaturization carried out in the last decade considerably increased the chances of Raman and SERS spectroscopy to be employed in the field of clinical forensics. Liu and coworkers published three consecutive studies during the last 3 years regarding the determination of amphetamines in human urine samples [246–249]. The group also developed a portable kit, shown in Fig. 1.21, to facilitate the multiplex determination of 3,4–methylenedioxymethamphetamine and methcathinone. The study was carried out with 30 volunteers providing urine samples. Briefly, the portable kit contains two sealed reagent containers, a standardized packet of highly reproducible gold nanorod 2D arrays on silicon wafers, and a handheld Raman device. Prior to the measurements, the human urine samples spiked with the drugs were subjected to a 3-min pretreatment. The obtained results were confirmed also by chromatographic measurements.

Overall, owing to the fingerprint specificity of Raman spectroscopy and the high sensitivity of SERS, the technique can determine therapeutic and illicit drugs at clinically relevant concentrations. However, work directed toward inhibiting the fouling of the SERS-active substrate and the specific capturing of the drugs still

needs to be performed before SERS can compete with the well-established reference methods currently used in clinical chemistry laboratories.

5.4.2 Enzyme Activity Assays

Enzymes regulate almost all metabolic processes in cells, and the assessment of their activity is crucial to either identify a special enzyme in order to prove its presence or absence in the sample or to quantify the amount of the enzyme in the sample [250]. SERS-based assays have been applied to assess the activity various enzymes, including telomerase [193, 251–253], thiopurine S-methyltransferase [254–256], and protease [257–261] activity.

Telomeres protect the ends of eukaryotic chromosomes by inhibiting the loss of base pair sequences and conserving the genetic information stored in the chromosomes [262]. Telomere activity is controlled by erosion during cell division and, in addition, determined by the telomerase activity. Telomerase or telomere terminal transferase elongates chromosomes by adding TTAGGG sequences to their ends. In normal somatic cells, this enzyme is highly suppressed; however, it was found that in more than 85% of cancerous cells, telomerase activity is enhanced. This leads to the so-called cell immortality and uncontrolled proliferation. Therefore, telomerase activity is considered an important biomarker for cancer diagnosis [263–265]. Zong and coworkers reported a dual-mode detection approach for assessing telomerase activity based on colorimetry and SERS [251]. Using telomeric elongation-assisted magnetic capturing of gold nanotags, a fast preliminary screening of the samples could be performed by the naked eye, using the colorimetric functionality, while SERS quantitative analysis could also be carried out. The platform employs two types of NPs: telomere substrate oligonucleotide (TS primer)-modified gold shell-coated magnetic nanobeads (MBs) as the capturing substrate and telomeric repeat complementary oligonucleotide (ATE)- and Raman reporter-conjugated gold NPs (Au-Tag). If the clinical sample possesses telomerase activity, then tandem telomeric repeats will be added to the TS primers on the surfaces of the MB@Au@TS particles. The elongated telomeric sequences will capture the Au-Tag NPs upon hybridization with ATE. This leads to a color change and enhancement of the SERS signal due to the aggregation of the magnetically separated NPs. If the sample does not present telomerase activity, the ATE-modified Au-Tag cannot hybridize with the MB@Au@TS, and neither a color change nor a SERS signal will be detected. Telomerase enzymes were extracted from human cervical cells (HeLa), human breast cancer cells (SKBR3, MCF7), and normal embryonic lung fibroblasts (MRC5). Quantitative analysis was carried out by diluting the cell extracts, and it was shown that telomerase activity of 1 cell/ml could be reliably detected.

Shi and coworkers recently published a very well-founded study regarding the detection of telomerase activity by SERS [193]. The authors first assessed the feasibility of their approach by performing quantitative measurements with crude telomerase extracts from HeLa cells. Then, they evaluated the selectivity of their method by measuring the telomerase activity in the cancer cell lines HeLa, HT29, and A549 and in the normal cell line HEK293. Furthermore, to test the capacity of

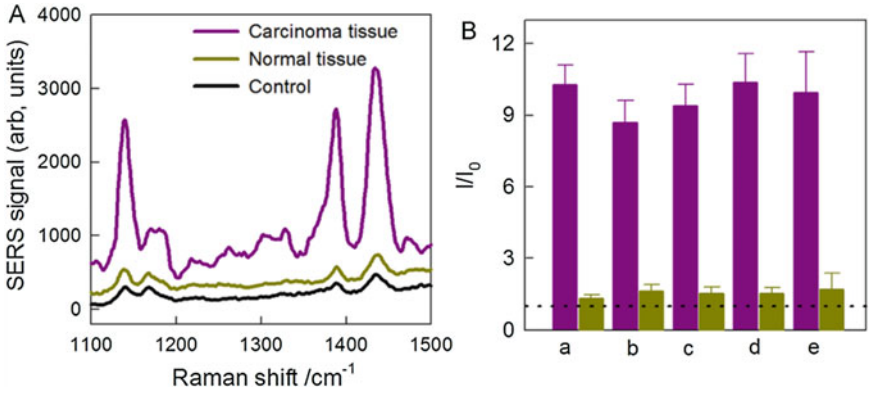

Fig. 1.22 Results of telomerase activity SERS-based platform carried out on colon cancer tissues. (**a**) SERS spectra of telomerase extracts of carcinoma tissue (purple), para-carcinoma normal tissue (green), and the heat-inactive control (black). The Raman bands originate from the vibrational modes of 4-amino-benzenethiol Raman reporter. (**b**) Histogram showing the results from five patients with colon cancer. Purple bar represents carcinoma tissue, while green bar represents para-carcinoma tissue (I_0 and I are the SERS intensities at 1440 cm^{-1} in the absence and presence of telomerase) (Reprinted from Shi et al. [193]. Copyright © 2015 Elsevier B.V. with permission from Elsevier)

their platform for ultra-early diagnosis of malignant disease, they mixed normal HEK293 cells and HeLa cells in four different ratios. Additionally, samples from colon cancer patients were also investigated, and their results were validated by the gold standard method (see Fig. 1.22). In total, five samples from patients were investigated. Finally, a telomerase inhibition assay was also carried out. For these studies, quadratic SERS signal amplification via telomerase-triggered silver NP assembly combined with ions-mediated cascade amplification was used. Namely, silica microbeads were conjugated with the telomerase substrate primer via the streptavidin-biotin binding reaction. In the presence of telomerase activity in the sample, the primer will be extended via the TTAGGG repeat units. Sulfhydryl-labeled single-stranded DNA served as the capture probe, and by hybridizing with the extended part of TSP, a long double-stranded DNA would form. This would provide numerous sulfhydryl groups for subsequent Ag NP conjugation via Ag-S bonds. This assembly works as the primary amplification element. Subsequently, the conjugated silver NPs were dissolved into Ag^+ upon the addition of H_2O_2. Ag^+ induced the aggregation of 4-amino-benzenthiol-modified gold NPs, creating highly active SERS hot spots. Based on the results presented in this study, the platform could offer reliable and valuable information for early cancer diagnosis.

In addition to telomerase activity, abnormal expression of certain proteases has also been related to the presence of cancer or Alzheimer's disease [266, 267]. Yazgan and coworkers investigated two different SERS-based platforms for the quantification of protease activity [258]. Spherical and rod-shaped gold NPs were used as SERS-active substrates, while the molecule DTNB was employed as a Raman

reporter. The first analysis platform used gold-coated glass slides conjugated with 11-MUA (11-mercaptoundeconic acid) as a support material. When the sample possessing protease activity was incubated on the surface of the platform, the covalently immobilized Raman-labeled SERS probe was released from the surface via the hydrolytic reaction catalyzed by the protease. Therefore, the SERS signal of the DTNB molecule was negatively correlated with the enzyme concentration in the sample. The second analysis platform used casein- or BSA-modified polystyrene microtiter plates, coated with the labeled SERS probe. Upon hydrolytic activity, the Raman probe with the peptide fraction was released from the surface and transferred to the supernatant. The SERS signal measured in the aliquoted supernatant positively correlated with the enzyme concentration. The platform with rodlike NPs on gold-coated glass slides yielded the best results. Namely, a linear correlation between protease activity and SERS signal in the range of 0.1–2 mU/ml and LOD and LOQ of 0.43 and 0.3 mU/ml, respectively. At the end of their study, the authors successfully quantified the protease activity in a commercial enzyme preparation. A second research group employed a novel "turn-on" SERS strategy based on non-cross-linking aggregation of gold NPs [257]. Specifically, by first stabilizing 4-MBA-modified Au NPs with a short peptide substrate, their aggregation was inhibited owing to their low isoelectric point. However, in the presence of a protease, this peptide was cleaved and the gold NPs formed hot spots, considerably enhancing the SERS signal of the reporter. Trypsin and thrombin were used as protease models, considering their importance in clinical diagnosis, and diluted human serum samples as matrix. The limit of detection was 85 fM for trypsin, and the experiments showed good selectivity over other proteases.

As described in the previous section, therapeutic drug monitoring is crucial for positive patient outcome. The pharmacokinetic and pharmacodynamic activity of drugs is often governed by the metabolic characteristics of the individual patient. In particular, the genetic differences in metabolic enzymes, such as thiopurine s-methyltransferase (TPMT), in humans have a major impact on the therapeutic response of drugs. This is the case for the immunosuppressive drug 6-mercaptopurine, which is deactivated in the presence of high TPMT activity, reducing the amount of parental drug available to form the active metabolite. Therefore, determination of TPMT activity in each patient before treatment is required in order to improve the therapeutic response. März et al. performed lab-on-a-chip SERS measurements on lysed red blood cells to assay TPMT activity [254], whereas Han et al. investigated the conversion of 6-mercaptopurine to 6-mercaptopurine-ribose in living cells by label-free SERS imaging [256]. In the first report, TPMT activity was assessed based on the methylation of 6-mercaptopurine to 6-methylmercaptopurine in lysed red blood cells. The parental drug and the metabolite developed specific Raman signatures based on which the two molecules could be clearly discriminated using linear discriminant analysis (LDA) (see Fig. 1.23). Furthermore, confirmation of TPMT activity in lysed red blood cells was obtained using a support vector machine classifier. The resulting accuracies were above 92%.

In the second study, the different orientation of 6-mercaptopurine and 6-mercaptopurine-ribose on the surface of the SERS-active Au@Ag NPs also generated

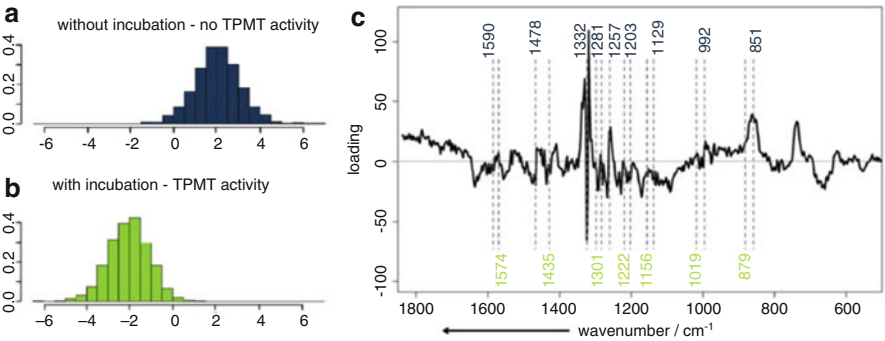

Fig. 1.23 LDA model of incubated test blood sample and test blood samples without incubation. (**a**, **b**) Histograms of LDA values of spectra from each group. (**c**) LDA loading with assignment of bands appearing in SERS spectrum of 6-mercaptopurine (blue) and 6-methylmercaptopurine (green) (März et al. [254]. Copyright © Springer-Verlag 2011, with permission of Springer)

specific Raman spectra. In this study, the authors used a straightforward ratio of two marker Raman bands to follow drug uptake and intracellular distribution, as well as metabolism. For these tests, the concentrated Au@Ag NPs were incubated with different concentrations of 6-mercaptopurine. After the removal of the free drug by centrifugation, the drug-conjugated NPs were re-suspended in culture media and incubated for 5 h with human lung adenocarcinoma cells. After washing steps to remove the loosely attached NPs, measurements were carried out at 0, 2, 4, 6, 8, 10, 16, 20, and 24 h. The authors noticed that owing to the uneven distribution of the parental drug in the cells, the transformation ratio of 6-mercaptopurine to 6-mercaptopurine-ribose was less at sites of high concentration, and it reduced at sites of low concentration. This and other SERS studies [268–285] on drug metabolism pathways can offer valuable information for drug development.

Overall, SERS offers multiple ways to monitor and assess enzymatic activity that can have a crucial impact on, i.e., cancer diagnosis, drug uptake, and drug metabolism. This is very important for improving patient outcomes and to reduce the costs associated with medical treatments.

6 Conclusions and Future Perspectives

The studies described in this chapter are just a small fraction of the publications related to SERS as an analytical method for medical diagnosis and were selected based on their significance. However, we are convinced that we did not manage to fully cover all the developments in the field, and we ask our readers who are interested in this topic to use this book chapter as a starting point for their research.

SERS was discovered more than 40 years ago. During these years, it transitioned from fundamental studies where metal-molecule interactions were investigated, such as food and environmental safety, to medical diagnosis. As demonstrated in this

chapter, SERS can be used for biomarker detection for Alzheimer's disease, myocardial infarction, diabetes, various types of cancer, and malaria, and it can offer information for therapeutic drug monitoring and enzyme activities. Despite the large number of publications, SERS is still not commercially available and is mainly used in academic research laboratories. There are multiple reasons behind this. One of the challenges is related to the preparation of SERS-active substrate. As described in the previous sections, most of the time, preparation of these substrates is labor-intensive. Additionally, their shelf life is seldom tested and needs to be considered for future studies and applications. Ideally, these platforms must offer high stability over time, reliable SERS enhancement, ease of use, and cost-efficiency. This is especially important for medical diagnosis, where a large number of samples is expected to be analyzed in a short time in non-laboratory environments, such as during field screening. Once the challenge with the platform is overcome, it could be easily combined with the existing high-performance portable Raman spectrometers. But before clinical applications, researchers must present proof that SERS brings considerable improvements as compared with chromatographic separation-based methods or traditional immunoassays. The topic is extremely interesting, and the work of researchers in the next years will demonstrate whether SERS could replace the reference methods in the clinical chemistry laboratories.

References

1. Lane LA, Qian X, Nie S (2015) SERS nanoparticles in medicine: from label-free detection to spectroscopic tagging. Chem Rev 115(19):10489–10529
2. Nima ZA et al (2014) Applications of surface-enhanced Raman scattering in advanced bio-medical technologies and diagnostics. Drug Metab Rev 46(2):155–175
3. Vo-Dinh T, Wang H-N, Scaffidi J (2010) Plasmonic nanoprobes for SERS biosensing and bioimaging. J Biophotonics 3(0):89–102
4. Wong Chi L, Dinish US, Olivo M (2015) Recent advances in SPR and SERS for sensitive translational medical diagnostics. Photonics Lasers Med 4:119–149
5. Prochazka M (2016) Medical applications of SERS. In: Prochazka M (ed) Surface-enhanced Raman spectroscopy: bioanalytical, biomolecular and medical applications. Springer International Publishing, Cham, pp 149–211
6. Recknagel P et al (2012) Liver dysfunction and phosphatidylinositol-3-kinase signalling in early sepsis: experimental studies in rodent models of peritonitis. PLoS Med 9(11):e1001338
7. Strimbu K, Tavel JA (2010) What are biomarkers? Curr Opin HIV AIDS 5(6):463–466
8. Zeng X et al (2011) Lung cancer serum biomarker discovery using label-free liquid chromatography-tandem mass spectrometry. J Thorac Oncol 6(4):725–734
9. Murph M et al (2007) Liquid chromatography mass spectrometry for quantifying plasma lysophospholipids: potential biomarkers for cancer diagnosis. In: Methods in enzymology. Academic, San Diego, pp 1–25
10. Sato Y et al (2012) Identification of a new plasma biomarker of Alzheimer's disease using metabolomics technology. J Lipid Res 53(3):567–576
11. McShane AJ, Bunch DR, Wang S (2016) Therapeutic drug monitoring of immunosuppressants by liquid chromatography–mass spectrometry. Clin Chim Acta 454:1–5

12. Baldelli S et al (2005) High-performance liquid chromatography with ultraviolet detection for therapeutic drug monitoring of everolimus. J Chromatogr B 816(1–2):99–105
13. Deters M, Kaever V, Kirchner GI (2003) Liquid chromatography/mass spectrometry for therapeutic drug monitoring of immunosuppressants. Anal Chim Acta 492(1–2):133–145
14. Peltier J et al (2016) Quantitative proteomic analysis exploring progression of colorectal cancer: modulation of the serpin family. J Proteome 148:139–148
15. Liu Y, Qing H, Deng Y (2014) Biomarkers in Alzheimer's disease analysis by mass spectrometry-based proteomics. Int J Mol Sci 15(5):7865–7882
16. Gan SD, Patel KR (2013) Enzyme immunoassay and enzyme-linked immunosorbent assay. J Investig Dermatol 133(9):1–3
17. Sun S-H et al (2015) Immunoassays for the cancer biomarker CA125 based on a large-birefringence nematic liquid-crystal mixture. Biomed Opt Express 6(1):245–256
18. Liu X et al (2008) A one-step homogeneous immunoassay for cancer biomarker detection using gold nanoparticle probes coupled with dynamic light scattering. J Am Chem Soc 130(9):2780–2782
19. Coverley D et al. (2017) A quantitative immunoassay for lung cancer biomarker CIZ1b in patient plasma. Clin Biochem 50:336–343
20. Savukoski T et al (2014) Novel sensitive cardiac troponin I immunoassay free from troponin I-specific autoantibody interference. In: Clinical chemistry and laboratory medicine (CCLM), vol 52, pp 1041–1048
21. Guirgis BSS et al (2012) Gold nanoparticle-based fluorescence immunoassay for malaria antigen detection. Anal Bioanal Chem 402(3):1019–1027
22. Popp J et al (2017) Label-free molecular imaging of biological cells and tissues by linear and non-linear Raman spectroscopic approaches. Angew Chem Int. Ed. 56:4392–4430
23. Li Y-S, Church JS (2014) Raman spectroscopy in the analysis of food and pharmaceutical nanomaterials. J Food Drug Anal 22(1):29–48
24. Dietzek B et al (2011) Introduction to the Fundamentals of Raman Spectroscopy. In: Dieing T, Hollricher O, Toporski J (eds) Confocal Raman Microscopy. Springer Berlin Heidelberg, Berlin/Heidelberg, pp 21–42
25. Schlücker S (2014) Surface-enhanced Raman spectroscopy: concepts and chemical applications. Angew Chem Int Ed 53(19):4756–4795
26. Etchegoin PG, Le Ru EC (2010) Basic electromagnetic theory of SERS. In: Surface enhanced Raman spectroscopy. Wiley-VCH Verlag GmbH & Co. KGaA, Weinheim, pp 1–37
27. Campion A, Kambhampati P (1998) Surface-enhanced Raman scattering. Chem Soc Rev 27(4):241–250
28. Cialla D et al (2012) Surface-enhanced Raman spectroscopy (SERS): progress and trends. Anal Bioanal Chem 403(1):27–54
29. Moskovits M (2005) Surface-enhanced Raman spectroscopy: a brief retrospective. J Raman Spectrosc 36(6–7):485–496
30. Xu H et al (2000) Electromagnetic contributions to single-molecule sensitivity in surface-enhanced Raman scattering. Phys Rev E 62(3):4318–4324
31. Lee HM et al (2013) Single-molecule surface-enhanced Raman spectroscopy: a perspective on the current status. Phys Chem Chem Phys 15(15):5276–5287
32. Kneipp K et al (1997) Single molecule detection using surface-enhanced Raman scattering (SERS). Phys Rev Lett 78(9):1667–1670
33. Le Ru EC, Etchegoin PG (2009) Introduction to plasmons and plasmonics, Chapter 3. In: Principles of surface-enhanced Raman spectroscopy. Elsevier, Amsterdam, pp 121–183
34. Le Ru EC, Etchegoin PG (2009) SERS enhancement factors and related topics, Chapter 4. In: Principles of surface-enhanced Raman spectroscopy. Elsevier, Amsterdam, pp 185–264
35. Lin J et al (2013) Photosensitizer-loaded gold vesicles with strong plasmonic coupling effect for imaging-guided Photothermal/photodynamic therapy. ACS Nano 7(6):5320–5329

36. Dinish US et al (2014) Actively targeted in vivo multiplex detection of intrinsic cancer biomarkers using biocompatible SERS nanotags. Sci Rep 4:4075
37. Zeng L et al (2015) Raman reporter-coupled Agcore@Aushell nanostars for in vivo improved surface enhanced Raman scattering imaging and near-infrared-triggered photothermal therapy in breast cancers. ACS Appl Mater Interfaces 7(30):16781–16791
38. Hollricher O (2011) Raman instrumentation for confocal Raman microscopy. In: Dieing T, Hollricher O, Toporski J (eds) Confocal Raman microscopy. Springer Berlin Heidelberg, Berlin/Heidelberg, pp 43–60
39. Griffiths PR (2009) Infrared and Raman instrumentation for mapping and imaging. In: Infrared and Raman spectroscopic imaging. Wiley-VCH Verlag GmbH & Co. KGaA, Weinheim, pp 1–64
40. Delhaye M et al (1996) Instrumentation A2 – Turrell, George, Chapter 3. In: Corset J (ed) Raman microscopy. Academic, London, pp 51–173
41. Rong Z et al (2016) Magnetic immunoassay for cancer biomarker detection based on surface-enhanced resonance Raman scattering from coupled plasmonic nanostructures. Biosens Bioelectron 84:15–21
42. Hidi IJ et al (2016) Toward levofloxacin monitoring in human urine samples by employing the LoC-SERS technique. J Phys Chem C 120(37):20613–20623
43. Chen YS et al (2016) Breath analysis based on surface-enhanced Raman scattering sensors distinguishes early and advanced gastric cancer patients from healthy persons. ACS Nano 10(9):8169–8179
44. Fu X et al (2016) A SERS-based lateral flow assay biosensor for highly sensitive detection of HIV-1 DNA. Biosens Bioelectron 78:530–537
45. Jahn M et al (2016) Plasmonic nanostructures for surface enhanced spectroscopic methods. Analyst 141(3):756–793
46. Lin X-M et al (2009) Surface-enhanced Raman spectroscopy: substrate-related issues. Anal Bioanal Chem 394(7):1729–1745
47. Stewart ME et al (2008) Nanostructured plasmonic sensors. Chem Rev 108(2):494–521
48. Wei X, Sebastian S (2014) Rationally designed multifunctional plasmonic nanostructures for surface-enhanced Raman spectroscopy: a review. Rep Prog Phys 77(11):116502
49. Hidi IJ et al (2015) Droplet based microfluidics: spectroscopic characterization of levofloxacin and its SERS detection. Phys Chem Chem Phys 17(33):21236–21242
50. Leopold N, Lendl B (2003) A new method for fast preparation of highly surface-enhanced Raman scattering (SERS) active silver colloids at room temperature by reduction of silver nitrate with hydroxylamine hydrochloride. J Phys Chem B 107(24):5723–5727
51. Garai E et al (2015) A real-time clinical endoscopic system for intraluminal, multiplexed imaging of surface-enhanced Raman scattering nanoparticles. PLoS One 10(4):e0123185
52. Premasiri WR et al (2005) Characterization of the surface enhanced Raman scattering (SERS) of bacteria. J Phys Chem B 109(1):312–320
53. Kang Y et al (2013) Surface-enhanced Raman scattering (SERS) spectra of hemoglobin of mouse and rabbit with self-assembled nano-silver film. Spectrochim Acta A Mol Biomol Spectrosc 108:177–180
54. Baia L et al (2006) Gold films deposited over regular arrays of polystyrene nanospheres as highly effective SERS substrates from visible to NIR. J Phys Chem B 110(47):23982–23986
55. Yüksel S et al (2015) Background-free bottom-up plasmonic arrays with increased sensitivity, specificity and shelf life for SERS detection schemes. J Phys Chem C 119(24):13791–13798
56. Huebner U et al (2011) Fabrication and characterization of silver deposited micro fabricated quartz arrays for surface enhanced Raman spectroscopy (SERS). Microelectron Eng 88(8):1761–1763
57. Radu AI et al (2016) Toward food analytics: fast estimation of lycopene and [small beta]-carotene content in tomatoes based on surface enhanced Raman spectroscopy (SERS). Analyst 141(14):4447–4455

58. Srichan C et al (2016) Highly-sensitive surface-enhanced Raman spectroscopy (SERS)-based chemical sensor using 3D graphene foam decorated with silver nanoparticles as SERS substrate. Sci Rep 6:23733
59. Jiang T-T et al (2014) Enhanced photoluminescence of CdSe quantum dots by the coupling of Ag nanocube and Ag film. Chin Phys B 23(8):086102
60. Zhou Q, Kim T (2016) Review of microfluidic approaches for surface-enhanced Raman scattering. Sensors Actuators B Chem 227:504–514
61. Chao W, Chenxu Y (2015) Analytical characterization using surface-enhanced Raman scattering (SERS) and microfluidic sampling. Nanotechnology 26(9):092001
62. Alharbi O, Xu Y, Goodacre R (2015) Detection and quantification of the opioid tramadol in urine using surface enhanced Raman scattering. Analyst 140(17):5965–5970
63. Amendola G, Pelosi P, Barbini DA (2015) Determination of pesticide residues in animal origin baby foods by gas chromatography coupled with triple quadrupole mass spectrometry. J Environ Sci Health Part B 50(2):109–120
64. Andreou C et al (2013) Rapid detection of drugs of abuse in saliva using surface enhanced Raman spectroscopy and microfluidics. ACS Nano 7(8):7157–7164
65. Bazylak G, Nagels LJ (2002) Integrated acquisition of analytical and biopharmaceutical screening data for beta-adrenergic-drugs employing diversified macrocycle supported potentiometric detection in HPLC systems. Curr Med Chem 9(16):1547–1566
66. Chung E et al (2013) Trace analysis of mercury(II) ions using aptamer-modified Au/Ag core-shell nanoparticles and SERS spectroscopy in a microdroplet channel. Lab Chip 13(2):260–266
67. Gao R et al (2014) Real-time analysis of diaquat dibromide monohydrate in water with a SERS-based integrated microdroplet sensor. Nanoscale 6(15):8781–8786
68. Gao RK et al (2016) Wash-free magnetic immunoassay of the PSA cancer marker using SERS and droplet microfluidics. Lab Chip 16(6):1022–1029
69. Yazdi SH, White IM (2012) Optofluidic surface enhanced Raman spectroscopy microsystem for sensitive and repeatable on-site detection of chemical contaminants. Anal Chem 84(18):7992–7998
70. Zhou JH et al (2012) Convenient formation of nanoparticle aggregates on microfluidic chips for highly sensitive SERS detection of biomolecules. Anal Bioanal Chem 402(4):1601–1609
71. Qi N et al (2014) Surface-enhanced Raman scattering on a zigzag microfluidic chip: towards high-sensitivity detection of As(iii) ions. Anal Methods 6(12):4077–4082
72. Yazdi SH, Giles KL, White IM (2013) Multiplexed detection of DNA sequences using a competitive displacement assay in a microfluidic SERRS-based device. Anal Chem 85(21):10605–10611
73. Yazdi SH, White IM (2012) A nanoporous optofluidic microsystem for highly sensitive and repeatable surface enhanced Raman spectroscopy detection. Biomicrofluidics 6(1):014105
74. Hwang H et al (2011) In situ dynamic measurements of the enhanced SERS signal using an optoelectrofluidic SERS platform. Lab Chip 11(15):2518–2525
75. Kim KB et al (2012) Dynamic preconcentration of gold nanoparticles for surface-enhanced Raman scattering in a microfluidic system. Small 8(3):378–383
76. Mungroo NA, Oliveira G, Neethirajan S (2016) SERS based point-of-care detection of food-borne pathogens. Microchim Acta 183(2):697–707
77. Guo YB et al (2012) Ultrasensitive optofluidic surface-enhanced Raman scattering detection with flow-through multihole capillaries. ACS Nano 6(1):381–388
78. Gao R et al (2015) Fast and sensitive detection of an anthrax biomarker using SERS-based solenoid microfluidic sensor. Biosens Bioelectron 72:230–236
79. Bailey MR et al (2015) Sheath-flow microfluidic approach for combined surface enhanced Raman scattering and electrochemical detection. Anal Chem 87(8):4347–4355
80. Choi J et al (2015) Integrated real-time optofluidic SERS via a liquid-core/liquid-cladding waveguide. RSC Adv 5(2):922–927

81. Deng Y et al (2015) Optofluidic microsystem with quasi-3 dimensional gold plasmonic nanostructure arrays for online sensitive and reproducible SERS detection. Anal Chim Acta 863:41–48
82. Lamberti A et al (2015) Metal-elastomer nanostructures for tunable SERS and easy microfluidic integration. RSC Adv 5(6):4404–4410
83. Lamberti A et al (2015) Ultrasensitive Ag-coated TiO2 nanotube arrays for flexible SERS-based optofluidic devices. J Mater Chem C 3(26):6868–6875
84. Patze S et al (2017) SERS as an analytical tool in environmental science: the detection of sulfamethoxazole in the nanomolar range by applying a microfluidic cartridge setup. Anal Chim Acta 949:1–7
85. Uusitalo S et al (2015) Performance and flow dynamics studies of polymeric optofluidic SERS sensors. J Eur Opt Soc-Rapid Publ 10:15043
86. Zhao YQ et al (2015) Plasmonic nanopillar array embedded microfluidic chips: an in situ SERS monitoring platform. J Mater Chem A 3(12):6408–6413
87. Yamaguchi A et al (2016) Dielectrophoresis-enabled surface enhanced Raman scattering on gold-decorated polystyrene microparticle in micro-optofluidic devices for high-sensitive detection. Sens Actuators B-Chem 230:94–100
88. Yüksel S et al (2016) Trace detection of tetrahydrocannabinol (THC) with a SERS-based capillary platform prepared by the in situ microwave synthesis of AgNPs. Anal Chim Acta 939:93–100
89. Hidi IJ et al (2016) Lab-on-a-chip-surface enhanced Raman scattering combined with the standard addition method: toward the quantification of nitroxoline in spiked human urine samples. Anal Chem 88(18):9173–9180
90. Muhlig A et al (2016) LOC-SERS: a promising closed system for the identification of mycobacteria. Anal Chem 88(16):7998–8004
91. Kammer E et al (2015) Quantitative SERS studies by combining LOC-SERS with the standard addition method. Anal Bioanal Chem 407(29):8925–8929
92. Piorek BD et al (2014) Discrete free-surface millifluidics for rapid capture and analysis of airborne molecules using surface-enhanced Raman spectroscopy. Anal Chem 86(2):1061–1066
93. Wu L et al (2014) Rapid and reproducible analysis of thiocyanate in real human serum and saliva using a droplet SERS-microfluidic chip. Biosens Bioelectron 62:13–18
94. Hidi IJ et al (2014) LOC-SERS: towards point-of-care diagnostic of methotrexate. Anal Methods 6(12):3943–3947
95. Kammer E et al (2014) A new calibration concept for a reproducible quantitative detection based on SERS measurements in a microfluidic device demonstrated on the model analyte adenine. Phys Chem Chem Phys 16(19):9056–9063
96. Cheng IF et al (2013) Rapid (<5 min) identification of pathogen in human blood by electrokinetic concentration and surface-enhanced Raman spectroscopy. Sci Rep 3:2365
97. Negri P et al (2013) Ultrasensitive surface-enhanced Raman scattering flow detector using hydrodynamic focusing. Anal Chem 85(21):10159–10166
98. Wu AHB (2006) A selected history and future of immunoassay development and applications in clinical chemistry. Clin Chim Acta 369(2):119–124
99. Wild D (2013) Immunoassay for beginners, Chapter 1.2. In: The Immunoassay handbook (fourth edition). Elsevier, Oxford, pp 7–10
100. Rubenstein KE, Schneider RS, Ullman EF (1972) "Homogeneous" enzyme immunoassay. A new immunochemical technique. Biochem Biophys Res Commun 47(4):846–851
101. Darwish IA (2006) Immunoassay methods and their applications in pharmaceutical analysis: basic methodology and recent advances. Int J Biomed Sci IJBS 2(3):217–235
102. Fleischmann M, Hendra PJ, McQuillan AJ (1974) Raman spectra of pyridine adsorbed at a silver electrode. Chem Phys Lett 26(2):163–166
103. Le Ru EC, Etchegoin PG (2009) Metallic colloids and other SERS substrates, Chapter 7. In: Principles of surface-enhanced Raman spectroscopy. Elsevier, Amsterdam, pp 367–413

104. Selkoe DJ (2001) Alzheimer's disease: genes, proteins, and therapy. Physiol Rev 81(2):741–766
105. Jack CR Jr et al (2010) Hypothetical model of dynamic biomarkers of the Alzheimer's pathological cascade. Lancet Neurol 9(1):119–128
106. Karran E, Mercken M, Strooper BD (2011) The amyloid cascade hypothesis for Alzheimer's disease: an appraisal for the development of therapeutics. Nat Rev Drug Discov 10(9):698–712
107. Huang Y, Mucke L (2012) Alzheimer mechanisms and therapeutic strategies. Cell 148(6):1204–1222
108. Mangialasche F et al (2010) Alzheimer's disease: clinical trials and drug development. Lancet Neurol 9(7):702–716
109. Hamley IW (2012) The amyloid beta peptide: a chemist's perspective. Role in Alzheimer's and fibrillization. Chem Rev 112(10):5147–5192
110. Benilova I, Karran E, De Strooper B (2012) The toxic A[beta] oligomer and Alzheimer's disease: an emperor in need of clothes. Nat Neurosci 15(3):349–357
111. Li S et al (2011) Soluble Aβ oligomers inhibit long-term potentiation through a mechanism involving excessive activation of extrasynaptic NR2B-containing NMDA receptors. J Neurosci Off J Soc Neurosci 31(18):6627–6638
112. Palop JJ, Mucke L (2010) Amyloid-β induced neuronal dysfunction in Alzheimer's disease: from synapses toward neural networks. Nat Neurosci 13(7):812–818
113. Grundke-Iqbal I et al (1986) Abnormal phosphorylation of the microtubule-associated protein tau (tau) in Alzheimer cytoskeletal pathology. Proc Natl Acad Sci U S A 83(13):4913–4917
114. Kosik KS, Joachim CL, Selkoe DJ (1986) Microtubule-associated protein tau (tau) is a major antigenic component of paired helical filaments in Alzheimer disease. Proc Natl Acad Sci U S A 83(11):4044–4048
115. Zhou YL et al (2016) Detection of A beta monomers and oligomers: early diagnosis of Alzheimer's disease. Chem Asian J 11(6):805–817
116. Cohen TJ et al (2011) The acetylation of tau inhibits its function and promotes pathological tau aggregation. Nat Commun 2:252–252
117. Iqbal K et al (2010) Tau in Alzheimer disease and related tauopathies. Curr Alzheimer Res 7(8):656–664
118. Hoover BR et al (2010) Tau mislocalization to dendritic spines mediates synaptic dysfunction independently of neurodegeneration. Neuron 68(6):1067–1081
119. Golde TE, Eckman CB, Younkin SG (2000) Biochemical detection of A beta isoforms: implications for pathogenesis, diagnosis, and treatment of Alzheimer's disease. BBA-Mol Basis Dis 1502(1):172–187
120. Lista S et al (2014) CSF A beta 1-42 combined with neuroimaging biomarkers in the early detection, diagnosis and prediction of Alzheimer's disease. Alzheimers Dement 10(3):381–392
121. Blennow K et al (2015) Clinical utility of cerebrospinal fluid biomarkers in the diagnosis of early Alzheimer's disease. Alzheimers Dement 11(1):58–69
122. Galozzi S, Marcus K, Barkovits K (2015) Amyloid- as a biomarker for Alzheimer's disease: quantification methods in body fluids. Expert Rev Proteomics 12(4):343–354
123. El-Said WA et al (2011) Fabrication of gold nanoparticle modified ITO substrate to detect beta-amyloid using surface-enhanced Raman scattering. J Nanosci Nanotechnol 11(1):768–772
124. Zengin A, Tamer U, Caykara T (2013) A SERS-based sandwich assay for ultrasensitive and selective detection of Alzheimer's tau protein. Biomacromolecules 14(9):3001–3009
125. Cherny RA et al (1999) Aqueous dissolution of Alzheimer's disease Aβ amyloid deposits by biometal depletion. J Biol Chem 274(33):23223–23228
126. Yoshiike Y, Akagi T, Takashima A (2007) Surface structure of amyloid-β fibrils contributes to cytotoxicity. Biochemistry 46(34):9805–9812
127. Pesaresi M et al (2006) Plasma levels of beta-amyloid (1–42) in Alzheimer's disease and mild cognitive impairment. Neurobiol Aging 27(6):904–905

128. Zetterberg H et al (2013) Plasma tau levels in Alzheimer's disease. Alzheimers Res Ther 5(2):9
129. Demeritte T et al (2015) Hybrid graphene oxide based plasmonic-magnetic multifunctional nanoplatform for selective separation and label-free identification of Alzheimer's disease biomarkers. ACS Appl Mater Interfaces 7(24):13693–13700
130. Klein WL (2002) Aβ toxicity in Alzheimer's disease: globular oligomers (ADDLs) as new vaccine and drug targets. Neurochem Int 41(5):345–352
131. Haass C, Selkoe DJ (2007) Soluble protein oligomers in neurodegeneration: lessons from the Alzheimer's amyloid [beta]-peptide. Nat Rev Mol Cell Biol 8(2):101–112
132. Wang Q, Wang YM, Lu HP (2013) Revealing the secondary structural changes of amyloid beta peptide by probing the spectral fingerprint characters. J Raman Spectrosc 44(5):670–674
133. Abdolrahim M et al (2015) Development of optical biosensor technologies for cardiac troponin recognition. Anal Biochem 485:1–10
134. Mohammed MI, Desmulliez MPY (2011) Lab-on-a-chip based immunosensor principles and technologies for the detection of cardiac biomarkers: a review. Lab Chip 11(4):569–595
135. Katrukha IA (2013) Human cardiac troponin complex. Structure and functions. Biochem Mosc 78(13):1447–1465
136. Lippi G (2013) Biomarkers of myocardial ischemia in the emergency room: cardiospecific troponin and beyond. Eur J Intern Med 24(2):97–99
137. Fathil MFM et al (2015) Diagnostics on acute myocardial infarction: cardiac troponin biomarkers. Biosens Bioelectron 70:209–220
138. Fathil MFM et al (2016) Progression in sensing cardiac troponin biomarker charge transductions on semiconducting nanomaterials. Anal Chim Acta 935:30–43
139. Han X et al (2016) Recent development of cardiac troponin I detection. ACS Sensors 1(2):106–114
140. Hasanzadeh M et al (2013) Optical immunosensing of effective cardiac biomarkers on acute myocardial infarction. Trac-Trends Anal Chem 51:158–168
141. Qureshi A, Gurbuz Y, Niazi JH (2012) Biosensors for cardiac biomarkers detection: a review. Sensors Actuators B Chem 171:62–76
142. El-Said WA, Fouad DM, El-Safty SA (2016) Ultrasensitive label-free detection of cardiac biomarker myoglobin based on surface-enhanced Raman spectroscopy. Sensors Actuators B Chem 228:401–409
143. Chon H et al (2014) SERS-based competitive immunoassay of troponin I and CK-MB markers for early diagnosis of acute myocardial infarction. Chem Commun 50(9):1058–1060
144. Sacks DB, McDonald JM (1996) The pathogenesis of type II diabetes mellitus: a polygenic disease. Am J Clin Pathol 105(2):149
145. Oliver NS et al (2009) Glucose sensors: a review of current and emerging technology. Diabet Med 26(3):197–210
146. McCrimmon R (2008) The mechanisms that underlie glucose sensing during hypoglycaemia in diabetes. Diabet Med 25(5):513–522
147. Newman JD, Turner APF (2005) Home blood glucose biosensors: a commercial perspective. Biosens Bioelectron 20(12):2435–2453
148. Perez-Mayen L et al (2016) Nanomolar detection of glucose using SERS substrates fabricated with albumin coated gold nanoparticles. Nanoscale 8(23):11862–11869
149. Zhang A et al (2012) Novel molecular specific detection of glucose using a Raman probe molecule with surface enhanced Raman scattering. Sci Adv Mater 4(10):1047–1054
150. Lin JY et al (2014) Label-free optical detection of type II diabetes based on surface-enhanced Raman spectroscopy and multivariate analysis. J Raman Spectrosc 45(10):884–889
151. Yuen JM et al (2010) Transcutaneous glucose sensing by surface-enhanced spatially offset Raman spectroscopy in a rat model. Anal Chem 82(20):8382–8385
152. Ma K et al (2011) In vivo, transcutaneous glucose sensing using surface-enhanced spatially offset Raman spectroscopy: multiple rats, improved hypoglycemic accuracy, low incident power, and continuous monitoring for greater than 17 days. Anal Chem 83(23):9146–9152

153. Sharma B et al (2016) Bisboronic acids for selective, physiologically relevant direct glucose sensing with surface-enhanced Raman spectroscopy. J Am Chem Soc 138(42):13952–13959
154. Lyandres O et al (2008) Progress toward an in vivo surface-enhanced Raman spectroscopy glucose sensor. Diabetes Technol Ther 10(4):257–265
155. Torul H et al (2015) Paper membrane-based SERS platform for the determination of glucose in blood samples. Anal Bioanal Chem 407(27):8243–8251
156. Mei L-P et al (2015) Simple electrodeposition of hierarchical gold-platinum nanothorns and their applications in electrocatalysis and SERS. Electrochim Acta 160:235–243
157. Ceja-Fdez A et al (2014) Glucose detection using SERS with multi-branched gold nanostructures in aqueous medium. RSC Adv 4(103):59233–59241
158. Torul H et al (2014) Glucose determination based on a two component self-assembled monolayer functionalized surface enhanced Raman spectroscopy (SERS) probe. Anal Methods 6(14):5097–5104
159. Dong J et al (2012) Glucose-responsive multifunctional acupuncture needle: a universal SERS detection strategy of small biomolecules in vivo. Anal Methods 4(11):3879–3883
160. Qi GH et al (2015) A highly sensitive SERS sensor for quantitative analysis of glucose based on the chemical etching of silver nanoparticles. J Opt 17(11)
161. Dinish US et al (2011) Development of highly reproducible nanogap SERS substrates: comparative performance analysis and its application for glucose sensing. Biosens Bioelectron 26(5):1987–1992
162. Qi GH et al (2016) Glucose oxidase probe as a surface-enhanced Raman scattering sensor for glucose. Anal Bioanal Chem 408(26):7513–7520
163. Severyukhina AN et al (2015) Nanoplasmonic chitosan nanofibers as effective SERS substrate for detection of small molecules. ACS Appl Mater Interfaces 7(28):15466–15473
164. Quyen TTB et al (2013) Au@SiO2 core/shell nanoparticle assemblage used for highly sensitive SERS-based determination of glucose and uric acid. J Raman Spectrosc 44(12):1671–1677
165. Yuen C, Liu Q (2014) Towards in vivo intradermal surface enhanced Raman scattering (SERS) measurements: silver coated microneedle based SERS probe. J Biophotonics 7(9):683–689
166. Al-Ogaidi I et al (2014) A gold@silica core-shell nanoparticle-based surface-enhanced Raman scattering biosensor for label-free glucose detection. Anal Chim Acta 811:76–80
167. Gupta VK et al (2013) A novel glucose biosensor platform based on Ag@AuNPs modified graphene oxide nanocomposite and SERS application. J Colloid Interface Sci 406:231–237
168. Wang XM et al (2016) A glucose biosensor based on detecting longitudinal surface plasmon resonance of gold nanorods. J Nanosci Nanotechnol 16(7):6925–6929
169. Kong KV et al (2014) Sensitive SERS glucose sensing in biological media using alkyne functionalized boronic acid on planar substrates. Biosens Bioelectron 56:186–191
170. Bi XS et al (2015) Facile and sensitive glucose sandwich assay using in situ-generated Raman reporters. Anal Chem 87(3):2016–2021
171. Sun D et al (2016) Construction of highly sensitive surface-enhanced Raman scattering (SERS) nanosensor aimed for the testing of glucose in urine. RSC Adv 6(59):53800–53803
172. Sun XC et al (2014) Functionalized aligned silver nanorod arrays for glucose sensing through surface enhanced Raman scattering. RSC Adv 4(45):23382–23388
173. Zhang YW et al (2012) One-pot green synthesis of Ag nanoparticles-graphene nanocomposites and their applications in SERS, H2O2, and glucose sensing. RSC Adv 2(2):538–545
174. Güemes M, Rahman SA, Hussain K (2015) What is a normal blood glucose? Arch Dis Child:569–574
175. James TD, Phillips MD, Shinkai S (2006) The molecular recognition of saccharides. Complexation of boronic acids with saccharides. Fluorescent sensors. Modular fluorescent sensors. Other types of sensor. Other systems for saccharide recognition. In: Boronic acids in saccharide recognition. The Royal Society of Chemistry, Cambridge, pp 3–176

176. Wu L, Qu XG (2015) Cancer biomarker detection: recent achievements and challenges. Chem Soc Rev 44(10):2963–2997
177. McAughtrie S, Faulds K, Graham D (2014) Surface enhanced Raman spectroscopy (SERS): potential applications for disease detection and treatment. J Photochem Photobiol C Photochem Rev 21:40–53
178. Ye SJ et al (2014) Enzyme-based signal amplification of surface-enhanced Raman scattering in cancer-biomarker detection. Trac-Trends Anal Chem 55:43–54
179. Bernard CPW, Stewart W (2014) World cancer report 2014. International Agency for Research on Cancer (IARC), Lyon, p 633
180. Gam L-H (2012) Breast cancer and protein biomarkers. World J Exp Med 2(5):86–91
181. Li M et al (2013) Three-dimensional hierarchical plasmonic nano-architecture enhanced surface-enhanced Raman scattering immunosensor for cancer biomarker detection in blood plasma. ACS Nano 7(6):4967–4976
182. Dinish US et al (2014) Sensitive multiplex detection of serological liver cancer biomarkers using SERS-active photonic crystal fiber probe. J Biophotonics 7(11–12):956–965
183. Vaidyanathan R et al (2015) A multiplexed device based on tunable nanoshearing for specific detection of multiple protein biomarkers in serum. Sci Rep 5:9756
184. Wang Y et al (2015) Enabling rapid and specific surface-enhanced Raman scattering immunoassay using nanoscaled surface shear forces. ACS Nano 9(6):6354–6362
185. Mandal S et al (2011) Synthesis and multidisciplinary characterization of polyelectrolyte multilayer-coated nanogold with improved stability toward aggregation. Colloid Polym Sci 289(3):269–280
186. Beqa L et al (2011) Gold nano-popcorn attached SWCNT hybrid nanomaterial for targeted diagnosis and photothermal therapy of human breast cancer cells. ACS Appl Mater Interfaces 3(9):3316–3324
187. Yang J et al (2012) Distinguishing breast cancer cells using surface-enhanced Raman scattering. Anal Bioanal Chem 402(3):1093–1100
188. Zhang P et al (2014) Novel nitrocellulose membrane substrate for efficient analysis of circulating tumor cells coupled with surface-enhanced Raman scattering imaging. ACS Appl Mater Interfaces 6(1):370–376
189. Fales AM, Yuan H, Vo-Dinh T (2013) Cell-penetrating peptide enhanced intracellular Raman imaging and photodynamic therapy. Mol Pharm 10(6):2291–2298
190. Lee S et al (2014) Rapid and sensitive phenotypic marker detection on breast cancer cells using surface-enhanced Raman scattering (SERS) imaging. Biosens Bioelectron 51:238–243
191. Freitag I et al (2016) Recognition of tumor cells by immuno-SERS-markers in a microfluidic chip at continuous flow. Analyst 141(21):5986–5989
192. Jimenez de Aberasturi D et al (2016) Surface enhanced Raman scattering encoded gold nanostars for multiplexed cell discrimination. Chem Mater 28(18):6779–6790
193. Shi ML et al (2016) SERS assay of telomerase activity at single-cell level and colon cancer tissues via quadratic signal amplification. Biosens Bioelectron 77:673–680
194. Lee M et al (2011) Highly reproducible immunoassay of cancer markers on a gold-patterned microarray chip using surface-enhanced Raman scattering imaging. Biosens Bioelectron 26(5):2135–2141
195. Perumal J et al (2015) SERS-based quantitative detection of ovarian cancer prognostic factor haptoglobin. Int J Nanomedicine 10:1831–1840
196. Feng SY et al (2011) Study on gastric cancer blood plasma based on surface-enhanced Raman spectroscopy combined with multivariate analysis. Sci China Life Sci 54(9):828–834
197. Feng SY et al (2010) Nasopharyngeal cancer detection based on blood plasma surface-enhanced Raman spectroscopy and multivariate analysis. Biosens Bioelectron 25(11):2414–2419
198. Xie H-n et al (2012) Tracking bisphosphonates through a 20 mm thick porcine tissue by using surface-enhanced spatially offset Raman spectroscopy. Angew Chem Int Ed 51(34):8509–8511

199. Yang TX et al (2014) Facile and label-free detection of lung cancer biomarker in urine by magnetically assisted surface-enhanced Raman scattering. ACS Appl Mater Interfaces 6(23):20985–20993
200. Wang H-N et al (2016) Multiplexed detection of microRNA biomarkers using SERS-based inverse molecular sentinel (iMS) nanoprobes. J Phys Chem C 120(37):21047–21055
201. Guven B et al (2014) SERS-based direct and sandwich assay methods for mir-21 detection. Analyst 139(5):1141–1147
202. Choi S et al (2015) Biochemical investigations of human papillomavirus-infected cervical fluids. Microsc Res Tech 78(3):200–206
203. Granger JH et al (2013) Toward development of a surface-enhanced Raman scattering (SERS)-based cancer diagnostic immunoassay panel. Analyst 138(2):410–416
204. Domenici F, Bizzarri AR, Cannistraro S (2012) Surface-enhanced Raman scattering detection of wild-type and mutant p53 proteins at very low concentration in human serum. Anal Biochem 421(1):9–15
205. Cepeda-Pérez E et al (2016) SERS-active Au/SiO(2) clouds in powder for rapid ex vivo breast adenocarcinoma diagnosis. Biomed Opt Express 7(6):2407–2418
206. Wang X-P et al (2016) iSERS microscopy guided by wide field immunofluorescence: analysis of HER2 expression on normal and breast cancer FFPE tissue sections. Analyst 141(17):5113–5119
207. Sinha L et al (2015) Quantification of the binding potential of cell-surface receptors in fresh excised specimens via dual-probe modeling of SERS nanoparticles. Sci Rep 5:8582
208. Song J et al (2015) Plasmonic vesicles of amphiphilic nanocrystals: optically active multifunctional platform for cancer diagnosis and therapy. Acc Chem Res 48(9):2506–2515
209. Wood BR et al (2003) Raman imaging of hemozoin within the food vacuole of *Plasmodium falciparum* trophozoites. FEBS Lett 554(3):247–252
210. Garrett NL et al (2015) Bio-sensing with butterfly wings: naturally occurring nano-structures for SERS-based malaria parasite detection. Phys Chem Chem Phys 17(33):21164–21168
211. Chen FN et al (2016) Direct detection of malaria infected red blood cells by surface enhanced Raman spectroscopy. Nanomed Nanotechnol Biol Med 12(6):1445–1451
212. Chen KR et al (2016) Review of surface enhanced Raman spectroscopy for malaria diagnosis and a new approach for the detection of single parasites in the ring stage. IEEE J Sel Top Quantum Electron 22(4)
213. Chen KR et al (2016) Towards ultrasensitive malaria diagnosis using surface enhanced Raman spectroscopy. Sci Rep 6
214. Kaminska A et al (2015) Detection of hepatitis B virus antigen from human blood: SERS immunoassay in a microfluidic system. Biosens Bioelectron 66:461–467
215. Li M et al (2013) Plasmonic nanorice antenna on triangle nanoarray for surface-enhanced Raman scattering detection of hepatitis B virus DNA. Anal Chem 85(4):2072–2078
216. Yao CK et al (2012) Spatially reinforced nano-cavity array as the SERS-active substrate for detecting hepatitis virus core antigen at low concentrations. Sens Actuators B Chem 174:478–484
217. Wu XM et al (2015) Differentiation and classification of bacteria using vancomycin functionalized silver nanorods array based surface-enhanced Raman spectroscopy and chemometric analysis. Talanta 139:96–103
218. Wu X et al (2014) Culture-free diagnostics of *Pseudomonas aeruginosa* infection by silver nanorod array based SERS from clinical sputum samples. Nanomedicine 10(8):1863–1870
219. Avci E et al (2015) Discrimination of urinary tract infection pathogens by means of their growth profiles using surface enhanced Raman scattering. Anal Bioanal Chem 407(27):8233–8241
220. Premasiri WR et al (2016) The biochemical origins of the surface-enhanced Raman spectra of bacteria: a metabolomics profiling by SERS. Anal Bioanal Chem 408(17):4631–4647
221. Marotta NE, Bottomley LA (2010) Surface-enhanced Raman scattering of bacterial cell culture growth media. Appl Spectrosc 64(6):601–606

222. Watson I et al (1997) Therapeutic drug monitoring [Editorial]. Ther Drug Monit 19(2):125
223. Muller DM, Rentsch KM (2010) Therapeutic drug monitoring by LC-MS-MS with special focus on anti-infective drugs. Anal Bioanal Chem 398(6):2573–2594
224. Humble RM et al (2015) Therapeutic drug monitoring of pentobarbital: experience at an Academic Medical Center. Ther Drug Monit 37(6):783–791
225. Carlier M et al (2015) Assays for therapeutic drug monitoring of beta-lactam antibiotics: a structured review. Int J Antimicrob Agents 46(4):367–375
226. Baranowska I, Magiera S, Baranowski J (2013) Clinical applications of fast liquid chromatography: a review on the analysis of cardiovascular drugs and their metabolites. J Chromatogr B Analyt Technol Biomed Life Sci 927:54–79
227. Aucella F et al (2013) Liquid chromatography-tandem mass spectrometry method as the golden standard for therapeutic drug monitoring in renal transplant. J Pharm Biomed Anal 86:123–126
228. Young J et al (2015) A novel immunoassay to measure total serum lymphotoxin-alpha levels in the presence of an anti-LT alpha therapeutic antibody. J Immunol Methods 424:91–99
229. Song ZR et al (2016) A validated chemiluminescence immunoassay for methotrexate (MTX) and its application in a pharmacokinetic study. Anal Methods 8(1):162–170
230. Krieg AK, Gauglitz G (2015) Ultrasensitive label-free immunoassay for optical determination of amitriptyline and related tricyclic antidepressants in human serum. Anal Chem 87(17):8845–8850
231. Guerriero E et al (2014) Unexpected overestimation of methotrexate plasma concentrations: analysis of a single center pediatric population. Ther Drug Monit 36(4):499–504
232. Widemann BC, Adamson PC (2006) Understanding and managing methotrexate nephrotoxicity. Oncologist 11(6):694–703
233. Fornasaro S et al (2016) Toward SERS-based point-of-care approaches for therapeutic drug monitoring: the case of methotrexate. Faraday Discuss 187:485–499
234. Crews KR et al (2004) High-dose methotrexate pharmacokinetics and outcome of children and young adults with osteosarcoma. Cancer 100(8):1724–1733
235. Yuen C, Zheng W, Huang ZW (2010) Low-level detection of anti-cancer drug in blood plasma using microwave-treated gold-polystyrene beads as surface-enhanced Raman scattering substrates. Biosens Bioelectron 26(2):580–584
236. Pletz M, Lipman J (2013) Clinical measures for increased creatinine clearances and suboptimal antibiotic dosing. Intensive Care Med 39(7):1322–1324
237. McKeating KS et al (2016) High throughput LSPR and SERS analysis of aminoglycoside antibiotics. Analyst 141(17):5120–5126
238. Liu SP et al (2015) Raman spectroscopy measurement of levofloxacin lactate in blood using an optical fiber nano-probe. J Raman Spectrosc 46(2):197–201
239. Xia TH et al (2014) Improving the quantitative accuracy of surface-enhanced Raman spectroscopy by the combination of microfluidics with a multiplicative effects model. Anal Methods 6(7):2363–2370
240. Villa JEL, Poppi RJ (2016) A portable SERS method for the determination of uric acid using a paper-based substrate and multivariate curve resolution. Analyst 141(6):1966–1972
241. Mamian-Lopez MB, Poppi RJ (2013) Standard addition method applied to the urinary quantification of nicotine in the presence of cotinine and anabasine using surface enhanced Raman spectroscopy and multivariate curve resolution. Anal Chim Acta 760:53–59
242. Mamian-Lopez MB, Poppi RJ (2013) Quantification of moxifloxacin in urine using surface-enhanced Raman spectroscopy (SERS) and multivariate curve resolution on a nanostructured gold surface. Anal Bioanal Chem 405(24):7671–7677
243. Subaihi A et al (2016) Rapid, accurate, and quantitative detection of propranolol in multiple human biofluids via surface-enhanced Raman scattering. Anal Chem 88 (22):10884–10892
244. Berger AG, Restaino SM, White IM (2017) Vertical-flow paper SERS system for therapeutic drug monitoring of flucytosine in serum. Anal Chim Acta 949:59–66

245. Sun F et al (2016) Hierarchical zwitterionic modification of a SERS substrate enables real-time drug monitoring in blood plasma. Nat Commun 7:9
246. Ma YM et al (2016) Surface-enhanced Raman spectroscopy on liquid interfacial nanoparticle arrays for multiplex detecting drugs in urine. Anal Chem 88(16):8145–8151
247. Robinson AM et al (2015) The development of "fab-chips" as low-cost, sensitive surface-enhanced Raman spectroscopy (SERS) substrates for analytical applications. Analyst 140(3):779–785
248. Dong RL et al (2015) Detection and direct readout of drugs in human urine using dynamic surface-enhanced Raman spectroscopy and support vector machines. Anal Chem 87(5):2937–2944
249. Han Z et al (2015) Portable kit for identification and detection of drugs in human urine using surface-enhanced Raman spectroscopy. Anal Chem 87(18):9500–9506
250. Bisswanger H (2014) Enzyme assays. Perspect Sci 1(1–6):41–55
251. Zong SF et al (2014) Colorimetry and SERS dual-mode detection of telomerase activity: combining rapid screening with high sensitivity. Nanoscale 6(3):1808–1816
252. Zong S et al (2014) Assessing telomere length using surface enhanced Raman scattering. Sci Rep 4:1–8
253. Zong S et al (2013) Ultrasensitive telomerase activity detection by telomeric elongation controlled surface enhanced Raman scattering. Small 9(24):4215–4220
254. März A et al (2011) Detection of thiopurine methyltransferase activity in lysed red blood cells by means of lab-on-a-chip surface enhanced Raman spectroscopy (LOC-SERS). Anal Bioanal Chem 400(9):2755–2761
255. Wang Y et al (2015) A SERS protocol as a potential tool to access 6-mercaptopurine release accelerated by glutathione-S-transferase. Analyst 140(22):7578–7585
256. Han GM et al (2014) Label-free surface-enhanced Raman scattering imaging to monitor the metabolism of antitumor drug 6-mercaptopurine in living cells. Anal Chem 86(23):11503–11507
257. Wu ZT et al (2015) A simple and universal "turn-on" detection platform for proteases based on surface enhanced Raman scattering (SERS). Biosens Bioelectron 65:375–381
258. Yazgan NN et al (2010) A high sensitive assay platform based on surface-enhanced Raman scattering for quantification of protease activity. Talanta 82(2):631–639
259. Yang L et al (2016) SERS determination of protease through a particle-on-a-film configuration constructed by electrostatic assembly in an enzymatic hydrolysis reaction. RSC Adv 6(93):90120–90125
260. Chen LX, Fu XL, Li JH (2013) Ultrasensitive surface-enhanced Raman scattering detection of trypsin based on anti-aggregation of 4-mercaptopyridine-functionalized silver nanoparticles: an optical sensing platform toward proteases. Nanoscale 5(13):5905–5911
261. Wu ZT et al (2013) A "turn-off" SERS-based detection platform for ultrasensitive detection of thrombin based on, enzymatic assays. Biosens Bioelectron 44:10–15
262. Cong Y-S, Wright WE, Shay JW (2002) Human telomerase and its regulation. Microbiol Mol Biol Rev 66(3):407–425
263. Dhaene K, Van Marck E, Parwaresch R (2000) Telomeres, telomerase and cancer: an up-date. Virchows Arch Int J Pathol 437(1):1–16
264. Klingelhutz AJ (1997) Telomerase activation and cancer. J Mol Med JMM 75(1):45–49
265. Smekalova EM et al (2012) Telomerase RNA biosynthesis and processing. Biochem Mosc 77(10):1120–1128
266. Lopez-Otin C, Matrisian LM (2007) Emerging roles of proteases in tumour suppression. Nat Rev Cancer 7(10):800–808
267. Duffy MJ (1992) The role of proteolytic enzymes in cancer invasion and metastasis. Clin Exp Metastasis 10(3):145–155
268. Anastasopoulos JA, Beobide AS, Voyiatzis GA (2013) Quantitative surface enhanced Raman scattering measurements at the early stage of active agent release processes. J Raman Spectrosc 44(3):401–405

269. Chen H et al (2014) SERS-fluorescence monitored drug release of a redox-responsive nanocarrier based on graphene oxide in tumor cells. ACS Appl Mater Interfaces 6(20):17526–17533
270. El-Said WA, Choi JW (2014) In-situ detection of neurotransmitter release from PC12 cells using surface enhanced Raman spectroscopy. Biotechnol Bioprocess Eng 19(6):1069–1076
271. Fang W et al (2014) pH-controllable drug carrier with SERS activity for targeting cancer cells. Biosens Bioelectron 57:10–15
272. Ganbold EO et al (2013) Raman spectroscopy of combinatory anticancer drug release from gold nanoparticles inside a single leukemia cell. J Raman Spectrosc 44(5):675–679
273. Gautier J et al (2013) SERS spectroscopic approach to study doxorubicin complexes with Fe2 + ions and drug release from SPION-based nanocarriers. Analyst 138(24):7354–7361
274. Huang J et al (2013) Tracking the intracellular drug release from graphene oxide using surface-enhanced Raman spectroscopy. Nanoscale 5(21):10591–10598
275. Ilkhani H et al (2016) Nanostructured SERS-electrochemical biosensors for testing of anticancer drug interactions with DNA. Biosens Bioelectron 80:257–264
276. Liang LJ et al (2015) In situ surface-enhanced Raman scattering spectroscopy exploring molecular changes of drug-treated cancer cell nucleus. Anal Chem 87(4):2504–2510
277. Liu L et al (2016) Smart surface-enhanced Raman scattering traceable drug delivery systems. Nanoscale 8(25):12803–12811
278. Masetti M et al (2015) Revealing DNA interactions with exogenous agents by surface-enhanced Raman scattering. J Am Chem Soc 137(1):469–476
279. Nieciecka D, Krolikowska A, Krysinski P (2015) Probing the interactions of mitoxantrone with biomimetic membranes with electrochemical and spectroscopic techniques. Electrochim Acta 165:430–442
280. Ock K et al (2012) Real-time monitoring of glutathione-triggered thiopurine anticancer drug release in live cells investigated by surface-enhanced Raman scattering. Anal Chem 84(5):2172–2178
281. Ock KS et al (2012) Label-free Raman spectroscopy for accessing intracellular anticancer drug release on gold nanoparticles. Analyst 137(12):2852–2859
282. Tian LM, Gandra N, Singamaneni S (2013) Monitoring controlled release of payload from gold nanocages using surface enhanced Raman scattering. ACS Nano 7(5):4252–4260
283. Yang J et al (2012) Tracking multiplex drugs and their dynamics in living cells using the label-free surface-enhanced Raman scattering technique. Mol Pharm 9(4):842–849
284. Yang J et al (2014) Dual-mode tracking of tumor-cell-specific drug delivery using fluorescence and label-free SERS techniques. Biosens Bioelectron 51:82–89
285. Zong SF et al (2014) Telomerase triggered drug release using a SERS traceable nanocarrier. IEEE Trans Nanobioscience 13(1):55–60